Title	Numerical Simulation of Gas Flow with Electrochemical Reaction in a Polymer Electrolyte Fuel Cell
Author(s)	K.M. Salah Uddin
Citation	北海道大学. 博士(工学) 甲第11126号
Issue Date	2013-09-25
DOI	10.14943/doctoral.k11126
Doc URL	http://hdl.handle.net/2115/53853
Type	theses (doctoral)
File Information	K.M._Salahuddin.pdf

Numerical Simulation of Gas Flow with Electrochemical Reaction in a Polymer Electrolyte Fuel Cell

by

K. M. Salah Uddin

A dissertation presented in partial fulfillment of the
requirements for the degree of

Doctor of Philosophy (PhD)

in the

Division of Mechanical and Space Engineering

Hokkaido University, Japan

September 2013

ABSTRACT

The aim of this dissertation was to investigate the performance of Polymer Electrolyte Fuel Cell (PEFC). The investigation involved understanding the mechanism of cross flow and pressure drop, addressing the contribution of cross flow on the performance, and water transport through the membrane. Computational fluid dynamics was used to study the gas flow behavior in the flow channel and porous media and information learned from the fluid dynamics study is used to design the artificial cross flow in the parallel flow field. At the beginning of the research, it was analyzed the mechanism of pressure drop and cross flow behavior in a single serpentine channel and gas diffusion layer. The dependency of physical parameters (e.g. porosity, permeability) and geometrical parameters such as gas channel pitch length and GDL thickness on the cross flow and pressure drop was studied vastly. It was explained pressure drop characteristics at the straight part of a serpentine channel and at the bend region. The role of cross flow on the pressure distribution in the gas channel also has been identified. Finally we concluded that the cross flow suppressed the pressure gradient in the straight part of serpentine channel and pressure gradient was maximum at the bend region. We also quantify the amount cross flow in terms of volume mass flux. The ratio of cross flow rate through the GDL to the total inlet flow rate increases with decreasing gas channel pitch length. Therefore, cross flow through the GDL can be enhanced by decreasing gas channel pitch length.

The aim of the second part of this work was to identify the contribution of cross flow on the performance individually. For this reason, a three dimensional single phase, isothermal model has been developed with considering the electrochemical reaction occurring in fuel cell. However, to avoid complicated two phase flow phenomena it was considered the constant hydration level in the membrane. The developed model was applied to an operating fuel cell to investigate the coupled flow, species transport and current density distribution. The gas channel pitch length effect on the performance has been evaluated by this developed model. The results show that it can capture all the physics occurring in PEM fuel cell very well. Because, it can capture the physics including activation overpotential, ohmic overpotential and mass transport overpotential very well. Hence, it proofs the applicability of our developed model. The gas channel pitch has marked effect on the performance of polymer electrolyte fuel cell. With decreasing of gas channel pitch it is found that the performance of fuel cell is increased. When cross flow was applied through the GDL and in between two channels of a parallel flow field, it was found that the performance of fuel cell increases in the mass transport region of polarization curve. The cross flow can enhance the oxygen transport towards catalyst layer. The simulation results show that the cross flow can help significantly to overcome the oxygen transport limitation; therefore, more electrochemical reaction occurs and result the performance improved. The convection flow caused by inlet flow rate also can increase the performance of PEFC. The effect of convection flow in current density is larger while using larger gas channel pitch length, whereas the thinner GDL has the larger convection flow effect in current density.

Finally we solve the water transport problem in the membrane of a PEM fuel cell which is one of the critical issues for PEFC performance improvement. Since, in the membrane water is transported from anode side to cathode side by electro osmotic drag flux caused by the proton transport. On the other hand, water is diffuse from cathode to anode side by back diffusion flux. Therefore, a delicate water balance is necessary to attain high proton conductivity of the membrane. In order to predict the water distribution in the different layer of PEFC , a three dimensional water transport model is developed which is able to capture the physics occurs in the membrane for transporting water from anode side to cathode side or vice-versa. To check the feasibility of our developed model validation test was carried out by comparing the simulation result with experimental work. This comparison validated the applicability of our developed model quantitatively for low relative humidity and qualitatively for higher relative humidity. The water content profile through the membrane was observed flat for relative humidity 40%. The water content profile in the membrane under the channel was lower than under the rib. With the increase of relative humidity the water content distribution through the membrane increases.

In this thesis, a complete single phase isothermal model has been developed to investigate coupled flow, species transport and electrochemical reaction occurring in PEFC. The cross flow has been analyzed vastly. The mechanism of cross flow and role of cross flow regarding pressure distribution in the gas channel, oxygen transport through the GDL, fuel cell performance improvement have been discussed in details. The water transport mechanism through the membrane also has been pointed out. Performance improvement of fuel cell has been clarified by a new design parameter cross flow.

Acknowledgements

First and foremost I would like to express my sincere gratitude to my supervisor Prof. Nobuyuki Oshima, Graduate School of Engineering, Hokkaido University for the opportunity to be part of his research group and for his support and encouragement throughout my graduate studies. I would like to thank him for making himself available for lengthy discussions, despite his busy schedule. I would also like to thank him for all the excellent advice throughout the entire process which has made my experience as a graduate student significantly more relaxed than I anticipated. I am truly thankful to Prof. Yuichi Murai, Dr. Yutaka Tabe and Prof. Masao Watanabe, my thesis evaluation committee members, for their support and time to review my thesis. I would like to thanks Dr. Makato Tsubokura, who is an associate professor of our laboratory and member of yearly progress evaluation committee, for evaluating me and encouraging my works in the laboratory meeting. I also would like to express thanks Dr. Akira Nishimura, Assistant Professor, Mie University, Japan for his generosity of time through much discussion that made significant contributions to this work.

A special thanks to Dr. Litan Kumar Saha for inspiring me over the last few years to finish this Ph. D. degree. I want to extend my thanks to Genki Hayashi who is a former student of our laboratory, who taught me everything including debugging of FrontFlow/red, Gridgen, FieldView. I am really grateful to him for his support and assistance. I also would like to thank everyone who helps me throughout my research work in the laboratory of

Computational Fluid Mechanics, especially Mr. Yusuke Nagaoka and Naoki Todate for their valuable time and support.

For financial support, I am deeply thankful and grateful to the Ministry of Education, Culture, Sports, Science and Technology (MEXT), Japan for fully funding the three-year scholarship until September 2013 under the scheme of Monbukagakusho Scholarship.

Last but not least, I would like to express my deeply thank to my wife, Sumaya Nasreen, for her unconditional emotional support, patience and devotion as she gave up great job to come to stay with me in Japan. Thank you very much for your love, support and understanding, especially for your encouragement and hard work in home made my life comfortable. Of course, my little baby K. M Labib Shahan for his smile and fun makes to forget the worse situation in research. Whenever, I feel helpless, boring and continuous failure in research, he was kept me alive. Thanks a lot my dear angel Labib. Lastly, but most importantly, I would like to thank my parents and siblings for their support throughout all my endeavors.

Table of Contents

1 Introduction

2 Fundamentals of Fuel Cell

3 Pressure Drop and Cross Flow Mechanism in a PEFC

4 Oxygen Transport by Cross Flow

5 Water Transport through the Membrane

6 Summary of Concluding Remarks and Directions for Further Research

List of Figures

List of Tables

Nomenclature

Roman Symbols

C	Molar concentration, mol/m^3
D	mass diffusivity, m^{2}s^{-1}
EW	Equivalent weight, kg/mol
F_0	Forchheimer coefficient
F	Faraday constant, 96485 C/mol
$\mathbf{g}$	gravity vector, ms^{-2}
i	current density vector, Am^{-2}
$\mathbf{J_i}$	diffusion flux of chemical species, kg/(m^2/s)
j	transfer current density, Am^{-3}
K	permeability, m^2
k_c	Condensation rate of constant
k_e	Evaporation rate of constant
M	molecular weight, kg/mol
m	stoichiometry coefficient in electrochemical reaction
n	number of electrons in the electrochemical reaction
n_d	Electro osmotic coefficient
P	pressure, Pa
R	universal gas constant, 8.314 J/mol K
S	source term in potential equation
t	time, s
T	temperature, K

$\mathbf{u}$	flow velocity in the flow channel, ms^{-1}
u	velocity in the x direction, ms^{-1}
v	velocity in the y direction, ms^{-1}
V	volume, m^3
V_{ex}	Coefficient of volume expansion
U_0	open-circuit potential, V
w	velocity in the z direction ms^{-1}
$\mathbf{w}$	velocity vector at the interface ms^{-1}
x	molar fraction, %
X	chemical formula of species
Y	mass fraction, %

Greek symbols

ε	porosity of porous media
ε_d	porosity in the dry state
μ	viscosity, $kgm^{-1}\ s^{-1}$
ρ	density, kgm^{-3}
ρ_m^{dry}	Density of membrane in dry state, kg m^{-3}
λ	Water content
θ_c	Contact angle, rad

$\boldsymbol{\tau}$	viscous stress, Nm^{-2}
σ	Surface tension, N
σ^{eff}	electronic conductivity, Ω^{-1}m^{-1}
k^{eff}	proton conductivity, Ω^{-1}m^{-1}
Φ	potential, V
α	transfer coefficient
ω	species generation or consumption rate
η	overpotential, V

Superscripts

eff	effective value in the porous medium
ref	reference value

Subscript

a	Anode
c	Cathode
g	gas phase
i	species index
l	liquid phase

s	Electron
f	Proton
wl	Water in ionmer phase

CHAPTER ONE

Introduction

1.1 Background and motivation

Energy is a fundamental building block of nature and it has a huge influence over the world's economy, power structure, and politics. As the demand for energy grows year by year, it has become an immense challenge to meet this requirement, especially among those sectors that are major consumers of energy: the residential sector, the commercial sector, the industrial sector, and the transport sector. Most of the current demand for energy is met by fossil fuels such as coal, oil, and natural gas. The bulk of private transportation devices are powered by internal combustion engines running on fossil-fuel derivatives, which has adverse effects in generating environmental pollution. In recent years, global warming as a result of emissions of greenhouse gases has become a critical issue that is being addressed by scientist all over the world. Some greenhouse gases, such as carbon dioxide, occur naturally and are emitted to the atmosphere through natural process as well as by human activities. Of the human activities that are responsible for the emission of greenhouse gases, the use of automobiles powered by internal combustion engines is among the most significant.

As a result of rising concern regarding global warming and projections of shortages of fossil fuels within the next century, there is a growing interest in the development of alternative renewable sources of clean energy. Both batteries and fuel cells produce electricity through electrochemical reactions and therefore offer the significant benefit of zero emissions at the point of use and, potentially, higher efficiencies.

The fundamental difference between fuel cells and batteries is that a fuel cell is simply an energy-conversion device, whereas a battery is combines the functions of energy conversion and energy storage. Energy is stored in a battery in the form of substances that are consumed in electrochemical reactions. The depletion of the reacting substances or the accumulation of reaction products eventually causes the battery to stop delivering energy, whereupon it must be recharged or replaced. In a fuel cell energy system, on the other hand, the conversion and storage functions are decoupled, and therefore, the power and energy capacities can be separately optimized. Furthermore, a fuel cell system can be rapidly refueled, in contrast to the slow process entailed in recharging a battery.

The classification of fuel cells is based on the type of material that is used as the electrolyte. Some common types of electrolytes include polymer electrolyte membranes (PEMs), solid oxides, molten carbonates, potassium hydroxide (alkaline fuel cells), and phosphoric acid. Of these, PEM and solid-oxide fuel cells have emerged as the most promising candidates for commercial applications. PEM fuel cells are the focus of this thesis. Among the advantages of PEM fuel cells are simplicity, versatility, and low operating temperatures.

Many of the processes that occur in PEM fuel cells are still not well understood. One approach to studying fuel cell involves the use of experimental techniques such as the ac impedance method, in which the impedance characteristics of the fuel cell are investigated or its modes of failure are assessed. Other types of measurements that produce polarization curves are also very useful in providing details of the operating characteristics of fuel cell systems. However, the transport phenomena of chemical species in PEM fuel cells remain difficult to observe and measure by experiments. In this regard, computational fluid dynamics (CFD) modeling is complementary to experimental techniques in that it permits physical transport phenomena and electrode kinetics inside the fuel cell to be modeled and solved by using numerical methods.

1.2 Literature review

There has been remarkable progress in the technology of the PEM fuel cell during the last two decades, and the device might one day be capable of replacing the internal combustion engine as the source of energy in automobiles. A review of research efforts and their achievements in this regard will show that it is impossible to deny the considerable contribution made by mathematical modeling. Extensive modeling of the PEM fuel cell has greatly helped scientists and engineers to achieve a better understanding of the functioning of the device and to improve its performance.

Several modeling approaches have been described in the literature. These can be categorized into one-dimensional (1D) to multidimensional models, steady state or transient models, isothermal or nonisothermal models, and single-phase or multiphase models. The modeling process itself can also be classified as empirical, analytical, or mathematical. In this section, I will discuss several attempts at mathematical modeling and performance optimization that are related to the subject of the research described elsewhere in this dissertation.

Parthasarathy et al. (1992) examined the temperature dependence of the kinetics of the reduction of oxygen kinetics at the platinum/Nafion interface and they derived empirical relationships between the exchange current densities and the transfer coefficients as a function of temperature. Amphlett et al. (1995a, 1995b) developed a generalized steady-state electrochemical model of the PEM fuel cell and investigated the polarization curve empirically. Their empirical relationship permits the prediction of cell voltage, so that it is possible to avoid complicated numerical computations in the estimation of activation and ohmic overpotential. However, the empirical model is inadequate in capturing the internal resistance of the membrane and the proportion of water in the cathode catalyst layer, since the latter is a function of the temperature and the results calculated by using Amphlett’s model are valid only for the isothermal situation. Kim et al. (1995) developed an empirical model that fits the entire polarization curve of the PEM fuel cell. The inclusion of an exponential term provides compensation for the mass-transport region at high current densities.

Most mathematical models of PEM fuel cells are derived from those of Bernardi and Verbrugge (1991, 1992) and Springer et al. (1991, 1993). The Bernardi–Verbrugge model is a one-dimensional steady-state isothermal model in which it is assumed that the membrane is fully hydrated, that ion transport is governed by the Nernst–Plank equation, that liquid water transport is governed by Schogl's equation, and that gas transport by diffusion is described by Stefan–Maxwell equations. Furthermore, the gas pressure in the channel portion is assumed to be constant, so that only conservation of species is applied to the gas in the gas-flow channels. Because they assumed that the membrane is full hydrated, Bernardi and Verbrugge did not consider the water content profile in the membrane. However, the water content is not constant during production of current, and the protonic conductivity is strongly dependent on the water content.

The other pioneering fuel cell model, that of Springer et al. (1991, 1993), is similar but includes modeling of the state of hydration of the membrane. This model accounts for the effects of the water content of the membrane (especially that of Nafion 117 membranes) on diffusion of water, electroosmotic drag, and membrane conductivity. The modeling of the membrane water content is based on its relationship with the water activity in the fuel cell, as described by Zawodzinski et al. (1991). The gas flow channels and the gas diffusion layer were modeled in a similar manner to that adopted in the model of Bernardi and Verbrugge.

Convective models of the fuel cell have been developed on the basis of the approaches adopted by Bernardi and Verbrugge (1991, 1992) and by Springer et al. (1991, 1993). However, unlike the Bernardi–Verbrugge and Springer models, the convective model incorporates the interaction of the gas flows in the gas flow channels and the gas diffusion layer. Fuller and Newmann (1993) modeled this interaction between gas flow channels and the membrane electrode assembly. Nguyen and White (1993) incorporated variations in temperature and reactant concentration along the gas flow channels into the model of Springer et al.

Three-dimensional models can predict the approximate behavior of the PEM fuel cell, but the processes involved in the fuel cell are very complicated, so some assumptions have to be made to simplify the modeling process. Dutta et al. (2000) developed a three-dimensional numerical model based on the commercial CFD software FLUENT (Ansys Inc., Pittsburgh, PA) to aid in understanding of gas flow, species transport, and electrochemical aspects of a fuel cell. Berning et al. (2002) developed a nonisothermal three-dimensional, single-phase model using the CFD program CFX (version 4.3; Ansys Inc.). This model included the gas flow channels, gas diffusion layers, and polymer electrolyte membrane; the catalyst layers were treated as interfaces. Meng and Wang (2004a, 2004b) developed an isothermal, three-dimensional, finite-element model based on Star-CD software (CD-adapco, Melville, NY).

In single-phase models, the fuel, reactants, and water vapor are all assumed to be transported either by pure diffusion [Song et al. (2004), You et al (2001), West and Fuller (1996), Hum and Li (2004)] or by diffusion and pressure-driven convection [Siegel et al. (2003), Gurau et al. (1998), Berning et al. (2002)].Pressure-driven effects can be considered negligible for one- and two-dimensional through-the-channel models that consider only one flow channel. However, they can be important in two-dimensional along-the-channel models and they are critical in three-dimensional simulations of fuel cells with interdigitated flow channels, since the pressures between channels can be quite different (Hu et al. 2004)

It is widely known that flooding by water can limit the performance of PEM fuel cells, and therefore it is vital to understand the two-phase transport characteristics of the fuel cell and their effects on the cell's performance. Wang and Cheng (1996) developed a two-phase transport model based on the multiphase mixture theory for use in PEM fuel cell research. The mixture model is a variant on the single-fluid model and it involves solving a single set of conservation equations for the phase mixture under the assumption that the phases are in equilibrium. By incorporating a microporous layer into their simulation of the PEM fuel cell, Pasaogullari and Wang (2004) derived a two-phase model based on the multiphase mixture model of Wang and Cheng (1996). Later, You and Liu (2006) investigated the effects of operating parameters on the two-phase transport variables. Mazumder and Cole (2003) also derived a multiphase mixture model and they calculated the distribution of liquid distribution in various components of the PEM fuel cell.

Considerable attention has been paid for the design and development of the flow fields in essential components of the fuel cell. Many types of flow design have been introduced as means of improving the performance of the fuel cell (Li and Sabir, 2005). Spurrier et al. (1986) patented a continuous design of flow channel, referred as the serpentine channel design. Some improved versions of the serpentine channel have been described in the recent literature [Xu and Zhao (2007), Nam et al. (2009), Suresh et al. (2011) and Choi et al. (2011a, 2011b)]. However, the identity of the element that is the key to improving the performance of the fuel cell is not yet clear. The power density of a PEM fuel cell is limited mainly by the supply of oxygen to the reactive sites of the catalyst layer. This supply is driven by convective transport from the compressor to the stack and to the single cell. In the single cell, the transport of reactant gas is dominated by diffusion flow and cross-convection flow through the porous media if a serpentine channel is used. Water produced by the electrochemical reaction tends to accumulate in the pores of the porous media and provides an additional impediment to oxygen transport. It is therefore of prime importance to understand the transport of oxygen to the catalyst layer and the transport of water through the membrane.

Convection is often an effective mode of reactant transport, and its influence varies depending on the channel configuration. In a serpentine channel, a large portion of the flow passes beneath the ribs between the two adjacent channels (Saha, 2010). Therefore, in this dissertation, I will examine the mechanism of cross-convection flow in the case of a serpentine channel and the role of convective flow with respect to oxygen transport through the gas-diffusion layer towards the catalyst layer. Finally, I will also focus on the transport process of water through the membrane caused by current density and gas humidity.

1.3 The aims of the research

The objectives of the work described in this thesis are to investigate gas flow phenomena in a separator channel and the ways that gas transport affect the electrochemical reaction in a PEM fuel cell, with emphasis on cross flow through the gas diffusion layer and water transport through the membrane. Attainment of these goals requires three steps:

1. A study of the mechanism of the pressure drop and cross flow in a serpentine channel.
2. Investigations of the effects of convective flow on the performance of the fuel cell.
3. Investigations of water transport phenomena in the membrane as a result of the flow of reactants.

A comprehensive three-dimensional computational model will be developed for analyzing flow phenomena and electrochemical reactions in PEM fuel cells, with particular attention to improving performance by modifying the cross flow. To predict the performance of fuel cell accurately, it is necessary to calculate the mass conservation strictly. A numerical method for predicting the flow-field phenomena correctly has been developed previously by a former student at the Laboratory of Computational Fluid Mechanics (Saha, 2010); the developed method is very useful for maintaining strict mass conservation. This developed method will be incorporated into the three-dimensional, isothermal, single-phase models of Mazumder and Cole (2003) and Meng and Wang (2004a, 2004b). Finally, the effects of hydration of the membrane on the performance of the fuel cell will be taken into account by adding a detailed water-transport model to our newly developed model.

The most widely used gas flow channel configuration for PEM fuel cells is the serpentine channel. The flow behavior of gases in microchannels, especially serpentine channels, is very complex as a result of the appearance of cross flow through the gas diffusion layer. However, the presence of this cross flow may be helpful in relation to the transport of reactant gases and the removal of liquid water from the cell, thereby improving the performance of the cell, and it will therefore be investigated in detail. Understanding the mechanism of cross flow and the pressure drop in the serpentine channel is therefore very helpful in relation to the design of the PEM fuel cell. Moreover, investigations will be carried out to permit the prediction of the contribution of cross flow to the performance of fuel cell; the performance of the fuel cell will be discussed in relation to cross flow as a new design parameter.

The applicability of the computational model in full-scale design calculations and its usefulness in capturing flow phenomena in the serpentine channel and the electrochemical reactions occurring in the fuel cell will be illustrated. Moreover, water transport in the membrane will be discussed. The factors dominating the transport of water through the membrane will be clarified in relation to cross flow through the gas diffusion layer.

1.4 Structure of the dissertation

This dissertation focuses on gas-transport phenomena and the electrochemical reactions that occur in PEM fuel cells and it is therefore divided into several chapters that discuss each of the topics individually and carefully.

- Chapter 2 briefly presents basic knowledge regarding the PEM fuel cell, discusses its fundamental principles, and describes its various components.

- Chapter 3 describes research on the understanding of cross flow and the mechanism of pressure drop in the serpentine channels of PEM fuel cells.

- Chapter 4 examines how cross flow can help to facilitate oxygen transport through the gas diffusion layer towards the catalyst layer. The role of cross flow in improving the performance of the cell is clarified.

- Chapter 5 presents results of research on the problem of water transport in the membrane. The mechanism of water transport in the polymer membrane is analyzed for various operating conditions and gas channel configurations, and the concept of artificial cross flow in the parallel flow field is introduced.

- Chapter 6 provides a summary the rest of the dissertation and its conclusions and it presents indications of future directions for research to follow on from the present study.

1.5 References

Amphlett J., Baumert R., Mann R., Peppley B., Roberge P., Harris T. (1995a), Performance modeling of the Ballard–Mark-IV solid polymer electrolyte fuel cell. 1. Mechanistic model development. *J. Electrochem. Soc.* **142**, 1–8.

Amphlett J., Baumert R., Mann R., Peppley B., Roberge P., Harris T. (1995b), Performance modeling of the Ballard–Mark-IV solid polymer electrolyte fuel cell. 2. Empirical model development. *J. Electrochem. Soc.* **142**, 9–15.

Bernardi D. M., Verbrugge M. W. (1991), A mathematical model of a gas diffusion electrode bonded to a polymer electrolyte. *AIChE J.* **37**, 1151–1163.

Bernardi D. M., Verbrugge M. W. (1992), A mathematical model of the solid-polymer-electrolyte fuel cell. *J. Electrochem. Soc.* **139**, 2477–2491.

Berning T., Lu D. M., Djilali N. (2002), Three-dimensional computational analysis of transport phenomena in a PEM fuel cell. *J. Power Sources*, **106** 284–294.

Berning T., Lu D. M., Djilali N. (2002), Three-dimensional computational analysis of transport phenomena in a PEM fuel cell. *J. Power Sources* **106**, 284–294.

Choi K. S., Kim H. M., Moon S. M. (2011b), An experimental study on the enhancement of the water balance, electrochemical reaction and power density of the polymer electrolyte fuel cell by under-rib convection. *Electrochem. Commun.* **13**, 1387–1390.

Choi P. V., Jayanti S., Deshpande A. P., Haridoss P. (2011a), An improved flow field with enhanced cross flow for fuel cell applications. *Int. J. Hydrogen Energy*, **35**, 6067–6072.

Dutta S., Shimpalee S., Van Zee J. W. (2000), Three-dimensional numerical simulation of straight channel PEM fuel cells. *J. Appl. Electrochem.* **30**, 135–146.

Dutta S., Shimpalee S., Van Zee J. W. (2001), Numerical prediction of mass exchange between cathode and anode channels in a PEM fuel cell. *Int. J. Heat Mass Transfer* **44**, 2029–2042.

Fuller T. F., Newmann J. (1993), Water and thermal management in solid polymer electrolyte fuel cells. *J. Electrochem. Soc.*, **140**, 1218–1225.

Gurau V., Liu H., Kakaç S. (1998), Two-dimensional model for proton exchange membrane fuel cells. *AIChE J.* **44**, 2410–2422.

Hu G., Fan J., Chen S., Liu Y., Cen K. (2004), Three-dimensional numerical analysis of proton exchange membrane fuel cells (PEMFCs) with conventional and interdigitated flow fields. *J. Power Sources*, **136**, 1–9.

Hum B., Li X. (2004), Two-dimensional analysis of PEM fuel cells. *J. Appl. Electrochem.*, **34**, 205–215.

Kim J., Lee S., Srinivasan S., Chamberlin C. (1995), Modeling of proton exchange membrane fuel cell performance with an empirical equation. *J. Electrochem. Soc.* **142**, 2670–2674.

Li X., Sabir I. (2005), Review of bipolar plates in PEM fuel cells: Flow field designs *Int. J. Hydrogen Energy* **30**, 359–371.

Mazumder S., Cole V. (2003), Rigorous 3-D mathematical modeling of PEM fuel cells. *J. Electrochem. Soc.* **150**, A1589–A1598.

Meng H., Wang C. Y. (2004a), Large-scale simulation of polymer electrolyte fuel cells by parallel computing. *Chem. Eng. Sci.* **59**, 3331–3343.

Meng H., Wang C. Y. (2004b), Electron Transport in PEFCs, *J. Electrochem. Soc.* **151**, A358–A367.

Nam J. H. , Lee K. J., Sohn S., Kim C. H. (2009), Multi-pass serpentine flow fields to enhance under rib convection in polymer electrolyte membrane fuel cells: design and geometrical characterization. *J. Power Sources*, **188**, 14–23.

Nguyen P. T., Berning T. Djilali N. (2004), Computational model of a PEM fuel cell with serpentine gas flow channels. *J. Power Sources*, **130**, 149–157.

Nguyen T. V., White R. E. (1993), A water and heat management model for proton-exchange membrane fuel cells. *J. Electrochem. Soc.* **140**, 2178–2186.

Parthasarathy A., Srinivasan S., Appleby A., Martin C. (1992), Temperature dependence of the electrode-kinetics of oxygen reduction at the platinum/Nafion interface: A microelectrode investigation. *J. Electrochem. Soc.* **139**, 2530–2537.

Pasaogullari U., Wang C.-Y. (2004), Two-phase transport and the role of the micro-porous layer in polymer electrolyte fuel cells. *Electrochim. Acta*, **49**, 4359–4369.

Saha L. K. (2010), *Numerical Simulation of Gas Flow in Polymer Electrolyte Fuel Cell*. Ph.D. dissertation, Division of Mechanical Engineering, Hokkaido University.

Siegel N. P., Ellis M. W., Nelson D. J., Von Spakovsky M. R. (2003), Single domain PEMFC model based on agglomerate catalyst geometry. *J. Power Sources*, **115**, 81–89.

Song D., Wang Q., Liu Z., Navessin T., Eikerling M., Holdcroft S. (2004), Numerical optimization study of the catalyst layer of PEM fuel cell cathode. *J. Power Sources*, **126**, 104–111.

Springer T. E, Wilson M., Gottesfeld S. (1993), Modeling and experimental diagnostics in polymer electrolyte fuel cells. *J. Electrochem. Soc.* **140**, 3513–3526.

Springer T. E., Zawodzinski T. A., Gottesfeld S. (1991), Polymer electrolyte fuel cell model. *J. Electrochem. Soc.* **138**, 2334–2342.

Spurrier F. R., Pierce B. E., Wright M. K. (1986), *Fuel Cell Plates with Improved Arrangement of Process Channels for Enhanced Pressure Drop Across the Plates*. US Patent No. 4631239.

Wang C. Y., Cheng P. (1996), A multiphase mixture model for mutiphase, multicomponent transport in capillary porous media. I. Model development. *Int. J. Heat Mass Transfer,* **39**, 3607–3618.

West A. C., Fuller T. F. (1996), Influence of rib spacing in proton-exchange membrane electrode assemblies. *J. Power Sources*, **26**, 557–565.

Xu C., Zhao T. S. (2007), A new flow field design for polymer electrolyte-based fuel cells. *Electrochem. Commun.* **9**, 497–503.

You L., Liu H. (2001). A parametric study of the cathode catalyst layer of PEM fuel cells using a pseudo-homogeneous model. *Int. J. Hydrogen Energy*, **26**, 991–999.

You L., Liu H. (2006), A two-phase flow and transport model for PEM fuel cells. *J. Power Sources* **155**, 219–230.

Zawodzinski T. A., Neeman M., Sillerud L. O., Gottesfeld S. (1991), Determination of water diffusion coefficient in perfluorosulfonate ionomeric membranes. *J. Phys. Chem.* **95**, 6040–6044.

CHAPTER TWO

Fundamentals of Fuel Cell

2.1 Fuel Cell

Fuel cells are electrochemical device that act as a factory which receive fuel as an input and produce electricity, heat and water as an output without any intermediate combustion step. In principle, a fuel cell operates like a battery in the sense that it uses an electrochemical reaction to produce direct current electricity. However, unlike a battery, it does not require long-time recharging. The energy will be generated in the form of electricity and heat as long as fuel is supplied.

Fuel cells are mainly classified as their kind of electrolyte employed. There several types of fuel cell exists in the literature among them most common fuel cell types are

① Polymer Electrolyte Membrane Fuel Cells (PEMFC),

② Alkaline Fuel Cells (AFC),

③ Phosphoric Acid Fuel Cells (PAFC),

④ Molten Carbonate Fuel Cells (MCFC),

⑤ Solid Oxide Fuel Cells (SOFC) and

⑥ Direct Methanol Fuel Cell (DMFC)

The detailed description of each type of fuel cell have been discussed by the book of Gregor Hoogers (1)

2.2 History of Fuel Cell

In 1839, Sir William Grove invents the basic operating principle of fuel cells by reversing water electrolysis to generate electricity from hydrogen and oxygen. In 1842, Grove developed a stack of 50 fuel cells, which he called a "gaseous voltaic battery". However, for almost a century after Grove's invention the fuel cell did not make any practical progress, remaining only a scientific curiosity. In 1937, Francis T. Bacon, an Englishman, began to work on practical fuel cell. By the end of the 1950s (Barbir (2005)) he had developed a 40-cell stack capable of 5 kW.

In the early 1960s Thomas Grubb and Leonard Niedrach developed a fuel cell with solid ion-exchange membrane electrolyte. Initially, sulfonated polystyrene membranes were used as the solid electrolytes, but very soon these were replaces by Nafion membranes in 1966. The Nafion has proved to be superior in performance and durability, and still the most popular membrane in use. This type of fuel cell is generally termed as polymer electrolyte membrane fuel cell or the proton exchange membrane fuel cell.

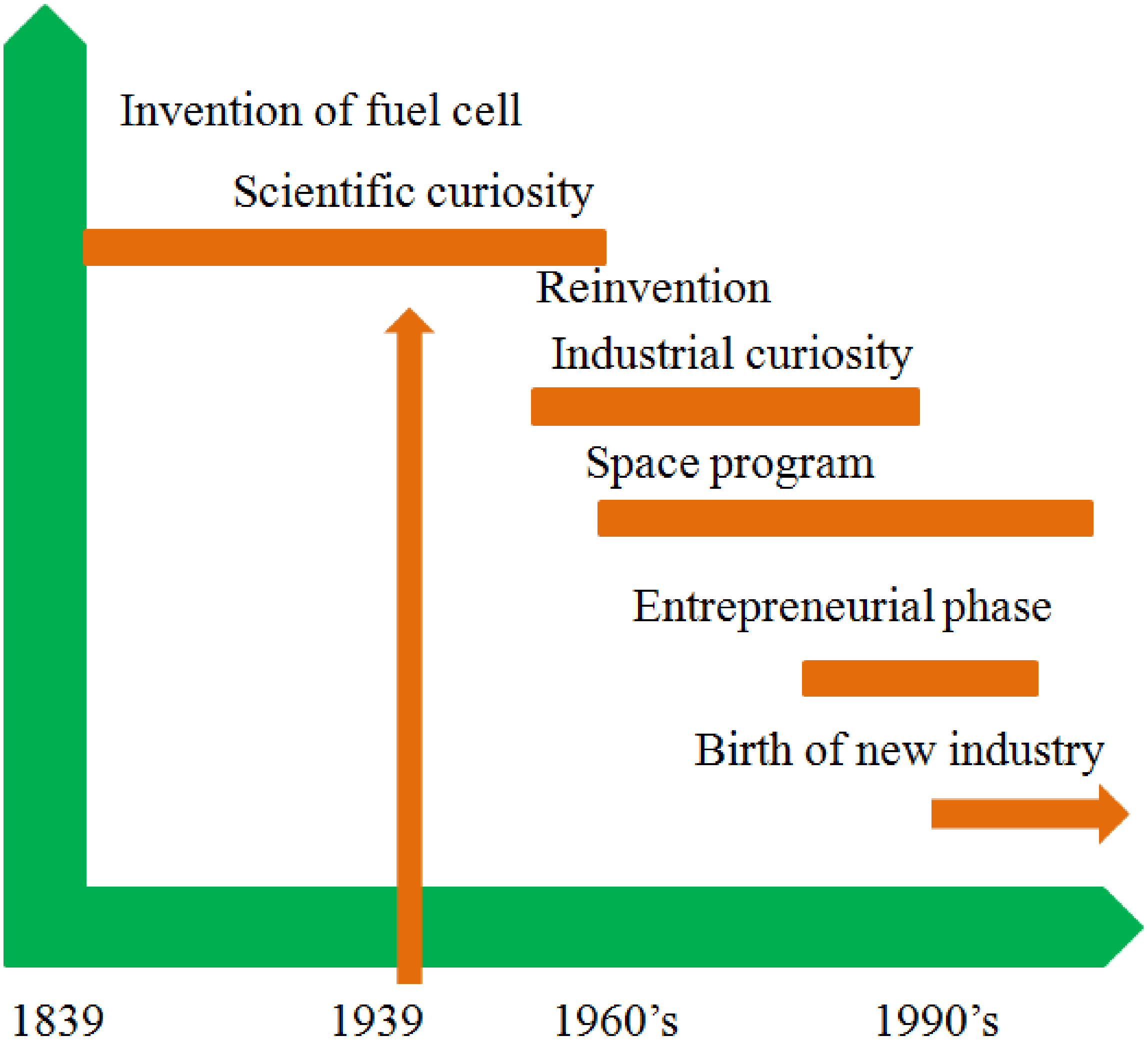

Fig. 2.1: Timeline of Fuel cell history

In the early 1960, polymer membrane fuel cell was first used in the Gemini program, that fuel cell was developed by General Electric based on the work of Grubb and Niedrach.

Following the Gemini Program the fuel was also used in the Apollo program, which used the fuel cells to generate electricity for life support, guidance, and communications. These fuel cells were made by Pratt and Whitney based on the Bacon's patents.

Due to their high cost, fuel cell systems were limited in space missions and in some special applications. In 1990 Ballard Power systems began development of polymer electrolyte membrane fuel cell (PEMFC). The strategy of Ballard was to lower the cost of the fuel cell by using less expensive materials and fabrication techniques, that fuel cell became a real option for wider applications. In 1993, Ballard Power Systems manifested fuel cell-powered buses.

The first passenger car running on PEM fuel cells was demonstrated by Energy Partners in 1993.At the end of the century almost every car manufacturer picked up on this activity and had built and manifested a fuel cell-powered vehicle. A new industry was born.

The timeline of fuel cell development history is shown in Fig 2.1

2.3 Polymer Electrolyte Membrane Fuel Cell

2.3.1 Electrochemical Reaction in a PEM Fuel Cell

Consider a PEM fuel cell consists of two platinum plate catalyst layers (CL) separated by a thin polymer electrolyte membrane (PEM) (Figure 2.2). In the PEFC, the supplied hydrogen (H_2) fuel is oxidized at the anode catalyst layer grant freedom to electrons and producing protons. On the anode side, each hydrogen molecule splits into two protons and two electrons

Anode: $2H_2 \rightarrow 4H^+ + 4e^-$ (2.1)

Four protons move to the polymer electrolyte membrane, while four protons stay in the anode catalyst layer. As a result, on the anode side we get a charged capacitor.

On the cathode side, the oxygen molecule captures four protons from the electrolyte membrane and four electrons from the anode catalyst particles. When all these species come together on the cathode catalyst surface, results two water molecules:

Cathode: $O_2 + 4H^+ + 4e^- \rightarrow 2H_2O$ (2.2)

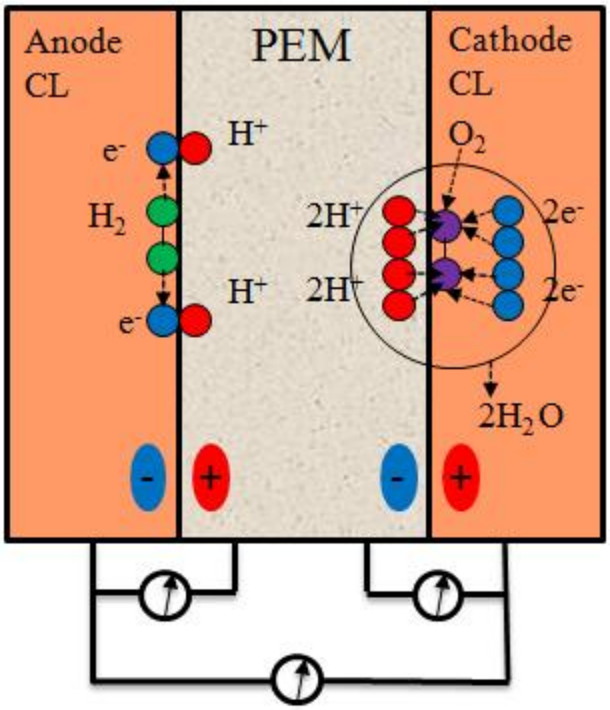

Fig. 2.2 : Schematic of anode and cathode separator in fuel cell which determine the cell open-circuit voltage.

Depletion of protons in the electrolyte induces in a negative charge on the polymer electrolyte membrane side, whereas removal of four electrons charges from cathode platinum catalyst induces positive charge. Thus on the cathode side we also get a charged capacitor (which is shown in Fig. 2.2). The three layer sandwich in Fig. 2.2 transforms to the tow charged capacitors connected in series, which results in a voltage drop between anode catalyst layer and cathode catalyst layer. The anode and cathode capacitors determine the cell open circuit voltage. We can use this voltage to generate electric power. According to thermodynamics theory, for any reaction running under constant pressure and temperature the following relation holds

$$\Delta H = T\Delta S + \Delta G$$

where ΔH is the enthalpy change in the reaction, T is the absolute temperature, ΔS is the entropy change and ΔG is the change in the Gibs free energy. This ΔG can be converted into useful work by the thermodynamics system.

Consider direct hydrogen-oxygen combustion:

$$2\mathrm{H}_2 + \mathrm{O}_2 \rightarrow 2\mathrm{H}_2\mathrm{O} \tag{2.3}$$

In this reaction temperature and /or pressure increases and ΔH ultimately transform into heat:

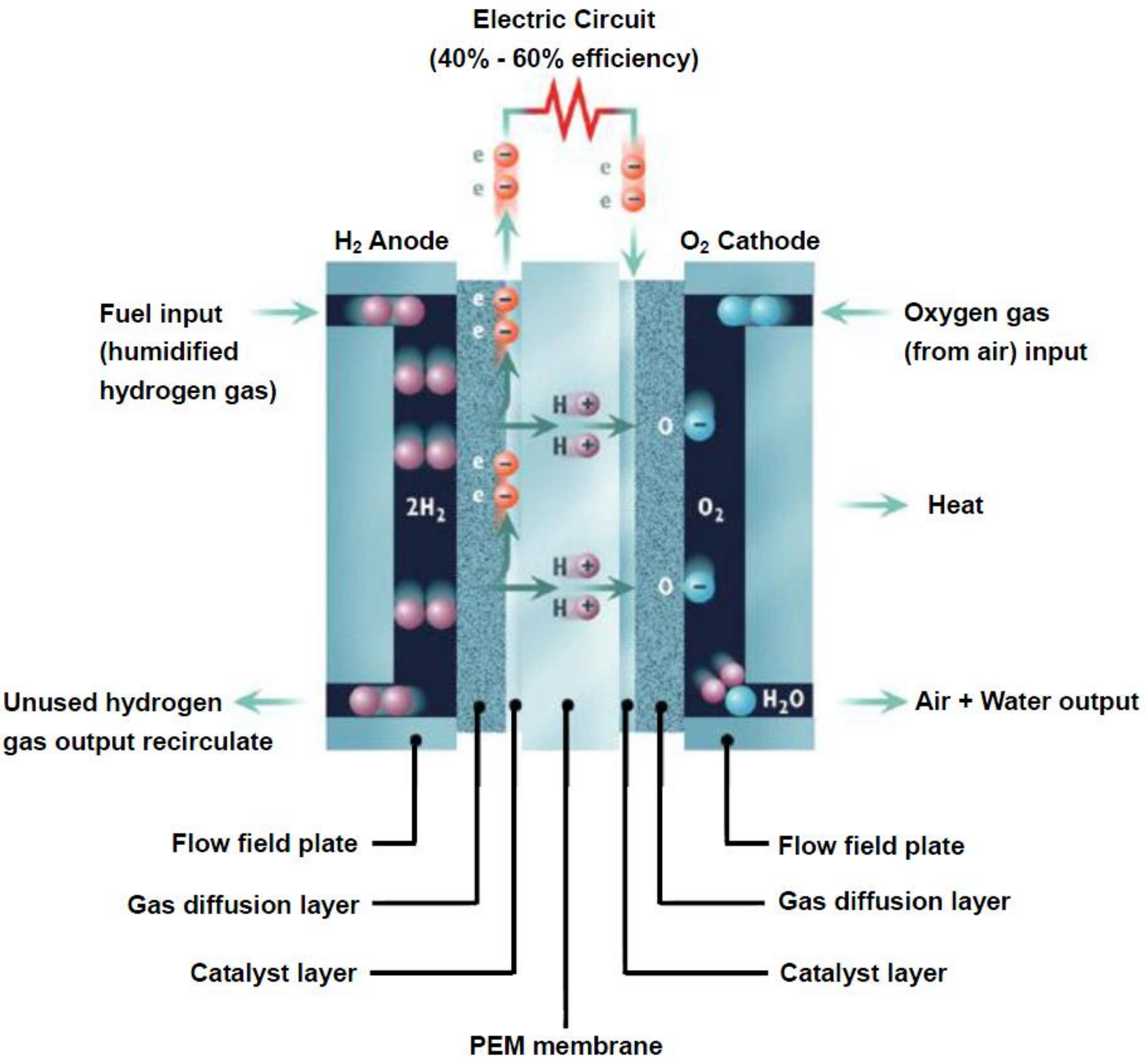

Fig. 2.3 : Schematic view of the operating principle of a typical PEMFC [Mengbo,[2]]

Thus, in a PEM fuel cell the purely chemical combustion of natural molecules (2.3) is split into two electrochemical reactions (2.1) and (2.2), which run with the participation of charged particles. Basically, any combustion reaction can be split up into a pair of electrochemical half reactions and hence any fuel can be utilized in a fuel cell for direct conversion of ΔG into electric energy.

2.4 Component of PEM Fuel Cell

The Major components of PEM fuel cell are polymer electrolyte membrane, catalyst layer, gas diffusion layer and bipolar plate (gas channel is grooved into the bipolar plate). The schematic of fuel cell component is described in the Fig. 2.4. The detail discussion of every component in the following section:

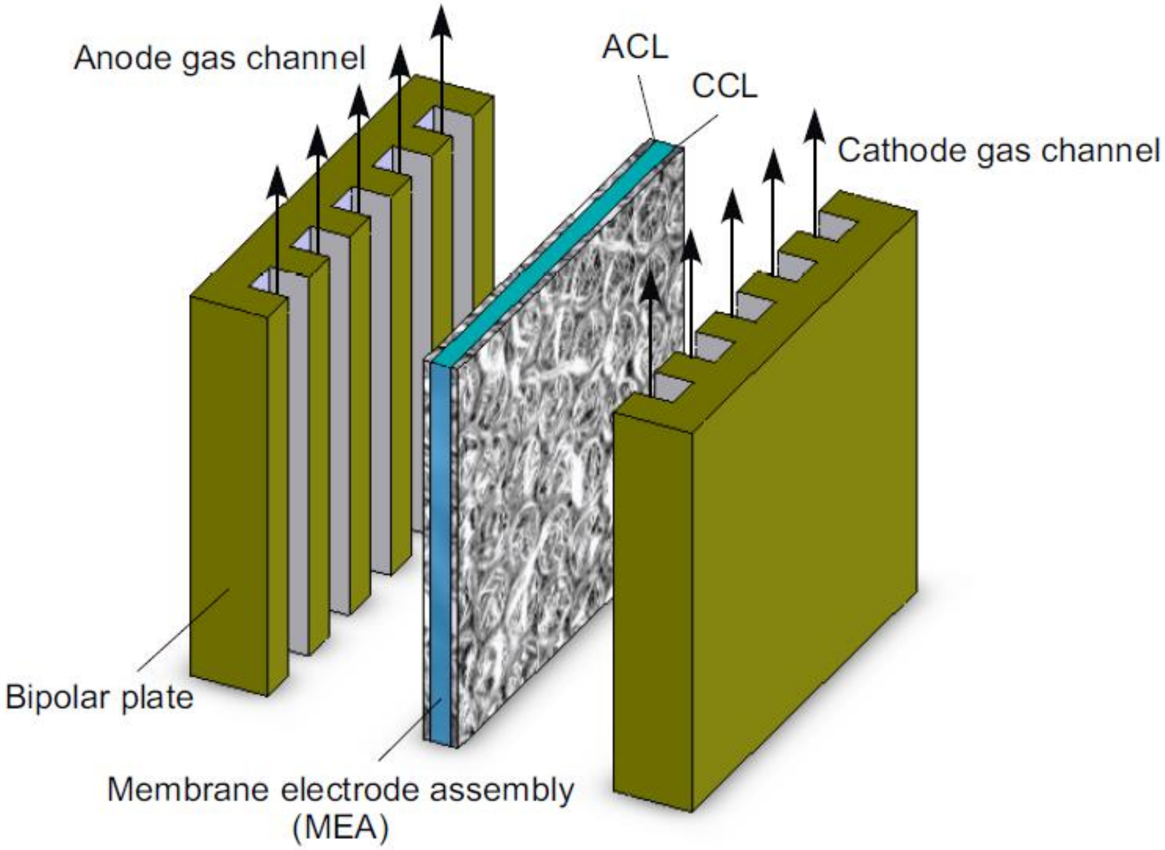

Fig. 2.4 : Schematic of PEM fuel cell components

2.4.1 Polymer Electrolyte Membrane

The polymer electrolyte is a thin membrane with a typical thickness between 25 and 200μm. Polymer electrolyte membrane is placed at the heart of a PEMFC that separates the anode from the cathode. Polymer electrolyte membrane is an essential component (heart) in PEFC where it plays a crucial role engaging preventing the mixing of H_2 and O_2**.** It allows transporting protons produced by dissociation of the hydrogen at the anode to the cathode and preventing the associated electrons flow through the membrane and forcing them to flow in the external circuit to cathode leading to production of electricity. In current PEFC technologies, most modern electrolytes are perflourinated ionomers with a fixed side chain of sulfonic acid bonded covalently to the inert, but chemically stable, polymer polytetrafluoroethylene structure*ref {fuel cell engines}. acid membranes, water content of the membrane has a large effect on membrane performance and durability. Sufficient water content is required to maintain the high proton conductivity of the membrane, which affects the efficiency of the electrochemical reaction.

When the structure is hydrated, H_3O^+-SO_3^- groups enable motion of H^+ ions. Dry perflourinated ionomers are almost completely non-conductive, so PEFCs typically operate with humidified reactant flow to boost conductivity and reduce ohmic losses.

2.4.2 Catalyst Layer

In low temperature fuel cells like PEFCs, due the high activation energy need to induce the electrochemical reaction, a catalyst, such as platinum is required to speed up the reactions. Cathode and anode catalyst layers (CLs) are major elements of any fuel cell. Any catalyst layer is a combination of three ingredients: electronic and ionic conductors and voids for gas/liquid supply. . High active surface area is obtained with highly dispersed catalyst particles (3-10 nm diameters). However, the catalyst area can only be considered active if the catalyst particles are electronically and ionically connected and diffusion path for reactant gases are not too stringent.

To ensure the close contact of the three phases (electric, ionic, gas) catalyst particles are deposited from a solution of the corresponding metal salt onto carbon particles as shown in SEM image in Fig. 2.5.

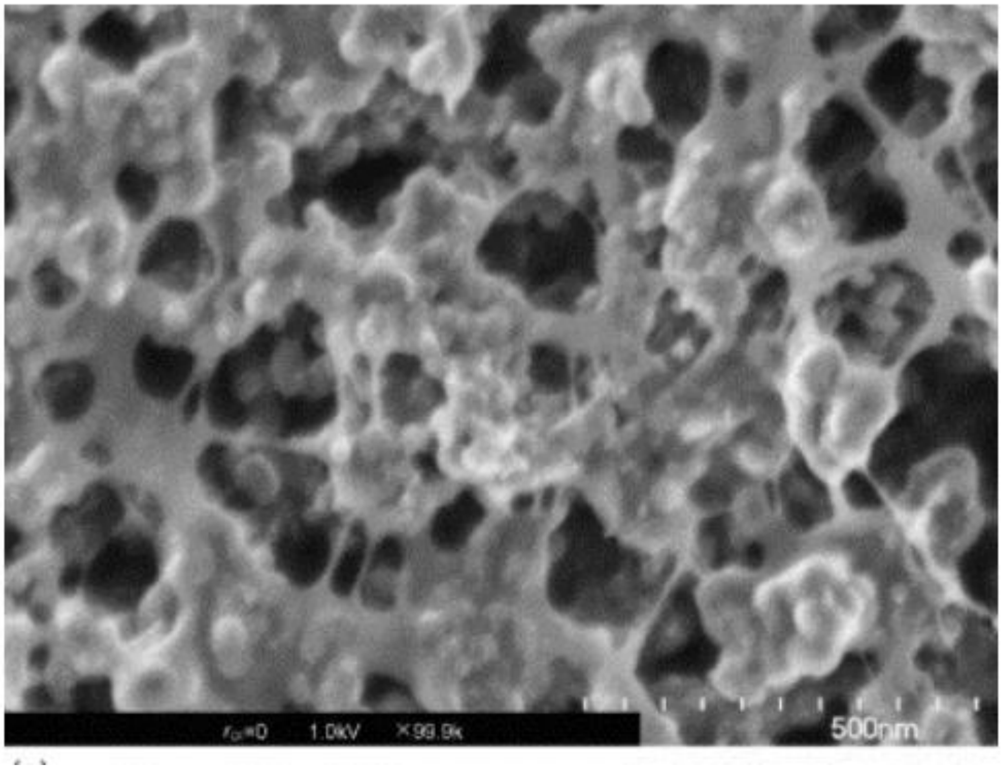

Fig. 2.5: FE-SEM images of catalyst layer fabricated from catalyst (adapted from Chisaka and Daiguji, 2006)

The thickness of cathode catalyst layer in low temperature fuel cells varies from ten micrometers in modern PEFCs to hundred of micrometers in direct methanol fuel cells.

2.4.3 Gas Diffusion Layer (GDL)

Either carbonized cloth or carbon-paper serve as gas diffusion media, employed with intention to ensure a homogeneous distribution over the active area. Further on, they conduct the electron produced/ consumed by the reactions from the electrode to bipolar plate or vice versa. A microscopic image of carbon paper is depicted in Fig. 2.6. The thickness of gas diffusion layer between 100 to 400 μm is mainly characterized by their porosity, which is usually 70%.

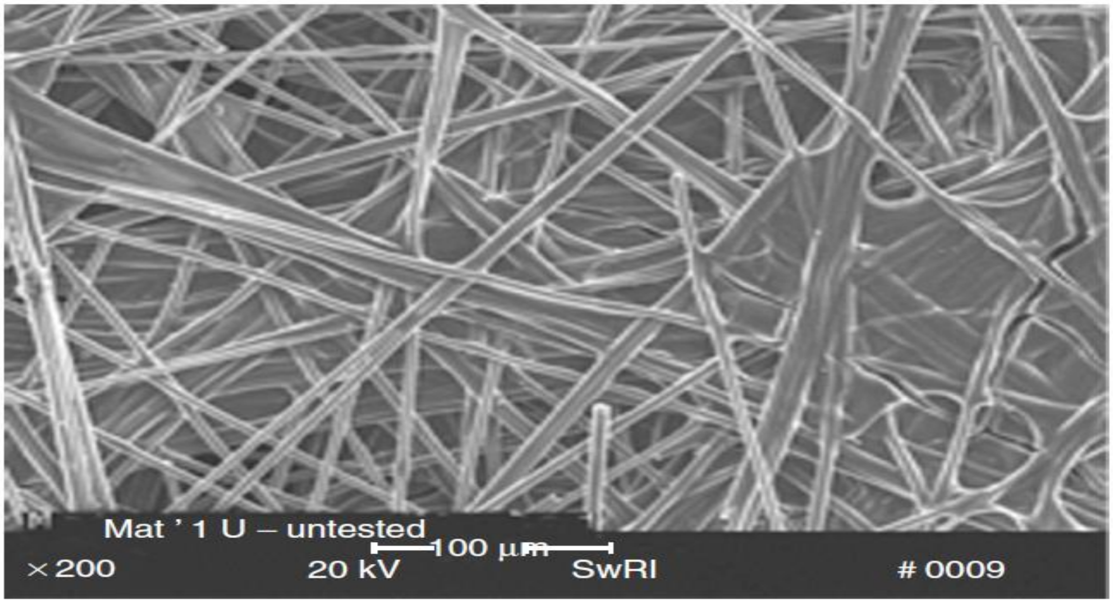

(a)

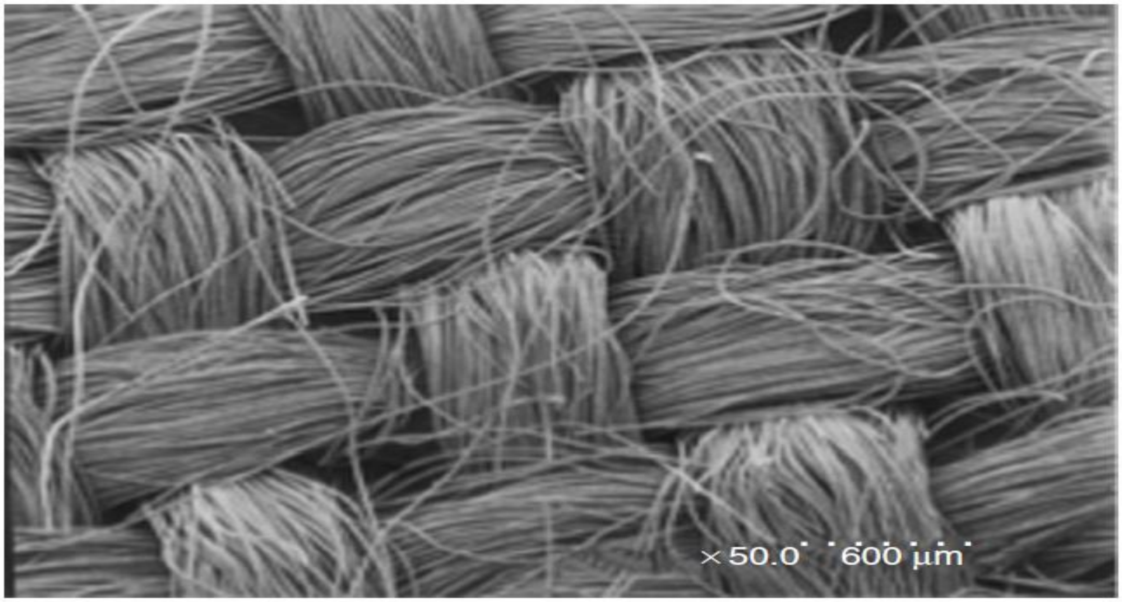

(b)

Fig. 2.6: SEM Micrographs of two gas diffusion layer (a) Carbon fiber paper and (b) Carbon cloth (Adapted from Mathias et al. 2003)

The gas diffusion layer (GDL) or electrode backing is placed between the catalysts layer and the flow field plates. The GDL accomplishes various tasks are schematically shown in Fig. 2.7 and explained in the following:

1. The functions of the gas diffusion layers are to provide structural support for the catalyst layers

2. Passages for reactant gases to reach the catalyst layer and transport of water to or from the catalyst layers

3. To transport electron from the catalyst layer to the bipolar plate in the anode side and from the bipolar plate to the catalyst layer in the cathode side

4. To remove the heat from the catalyst layer

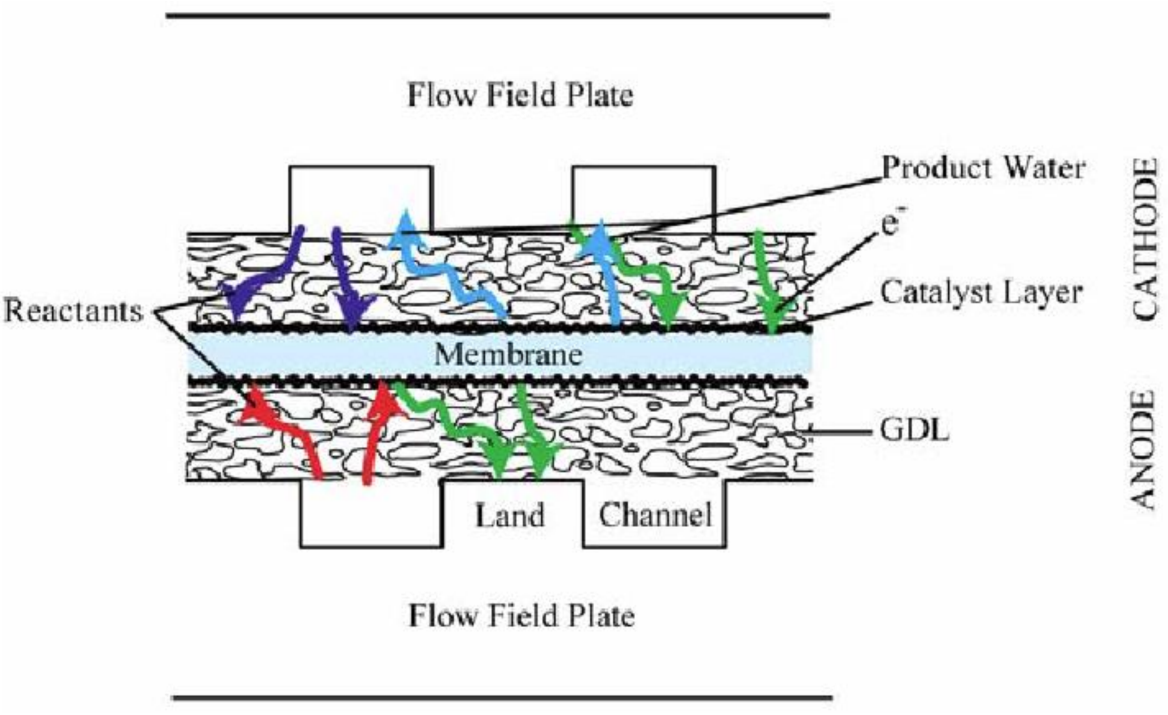

Fig. 2.7: Schematic of Gas diffusion layer (GDL), Catalyst layer, Membrane, and Flow field plates

Gas diffusion layers are usually coated with Teflon to reduce flooding can significantly reduce fuel cell performance due to poor reactant gas transport.

2.4.4 Bipolar Plate

Bipolar plate is one of the most important components in PEFCs must perform a number of functions in order to achieve a good fuel cell stack performance and lifetime. The bipolar plates distribute the fuel gas and air uniformly over the active areas. These plates also provide structural support for the thin and mechanically weak MEA.

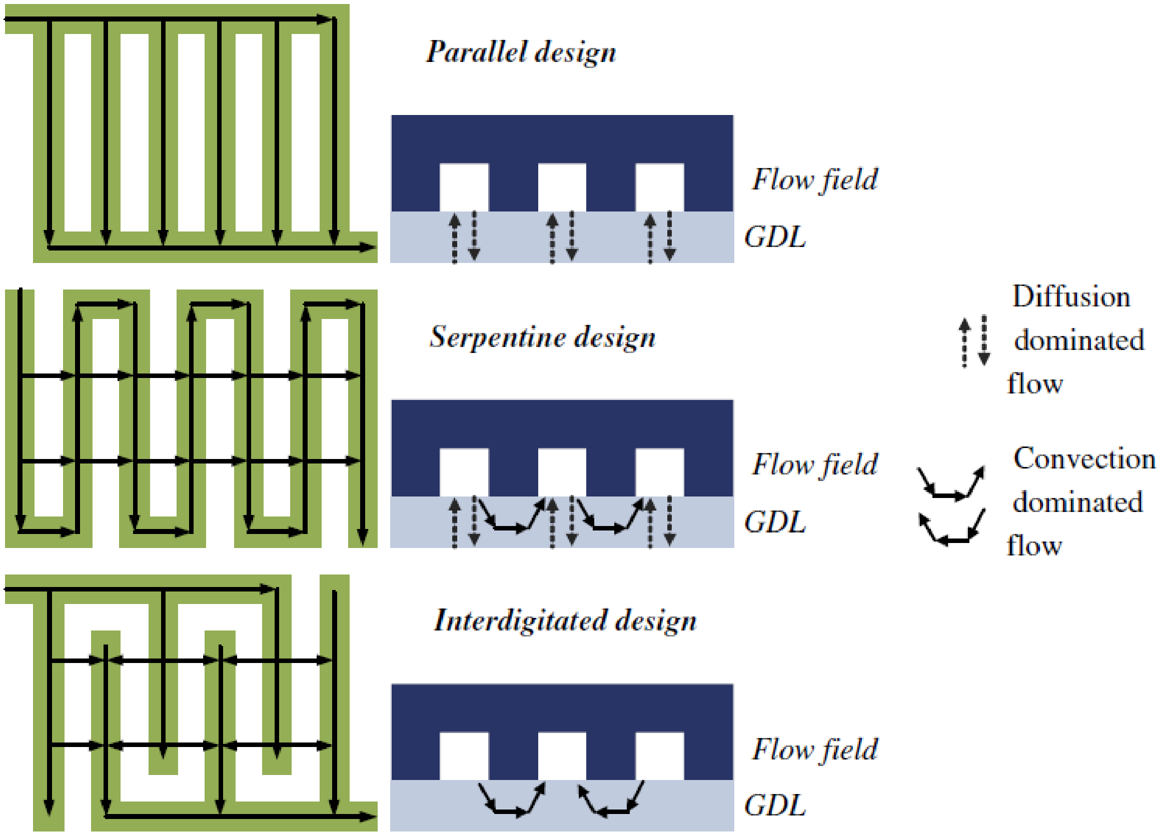

Fig. 2.8: Basic flow field designs for PEFCs

Bipolar plates facilitate heat removal from the active area and serve the purpose of electronically connecting one cell to another cell in the electrochemical cell stack. The bipolar plates also serve as current conductor from cell to cell. Gas channel is grooved into bipolar plate. Several types of materials are being used in bipolar plates. The main materials are electro graphite; carbon-carbon composite; sheet metal; flexible graphite foil; graphite polymer composite.

One of the most obstacles to large commercialization of fuel cell is gas flow field designs, including the development of low-cost materials, construction of materials, optimal design, fabrication methods and their impact on PEFCs performance. The basic flow field design-types can be categorized in parallel, interdigitated and serpentine flow field is shown in Fig. 2.8.

In the parallel flow field designs flow field plate includes a number of separate parallel flow channels (Pellegri et al. (1980)). The parallel design is made of a number of straight channels connected to common inlet and outlet headers. One issue associated with this design is that the pressure drop is too low to remove the water, and water tends to accumulate in the channels (Barbir, 2005, pp. 119-121). This issue leads to the misdistribution of the reactant gases in the flow field, causing the starvation is some channels and excess of reactant in other channels.

Interdigitated flow fields, there are a number of parallel discontinuous channels (i. e., the channels are discontinuous from the inlet header to the outlet header). The reactant gases are forced to flow through the porous GDL in order to reach the channels connected to the outlet manifolds. Since the gases are forced along a short path through the GDL catalyst layer, the liquid water is removed more efficiently, resulting in better performance at higher current densities. However, these flow fields don not remove the water located at the inlet of the channels properly, and the voltage stability at low current densities are very poor (Nguyen and He 2003). In general, this flow field is the most ideal for high current densities, but it increases the parasitic losses due to larger pressure drops.

The serpentine type flow field is the most commonly used flow field type in PEFCs. It composed of a series of parallel channels in a meander like structure which extends from gas channel inlet to the outlet covering the MEA area (Spurrier et al. 1986). Serpentine flow fields have one or more continuous channels connected to an inlet and outlet and typically follow a path with several bends. These flow fields generally have longer channel lengths and greater pressure drop along the channels due to the bends, which facilitates water removal. Multiple parallel serpentine channels are used for large active areas in order to avoid excessive high pressure drop.

2.5 Fuel Cell Performance

The performance of the fuel cell is directly dependent on the overall reaction rate and is usually expressed in terms of the polarization curve, which is the relation between the cell voltages versus its current density as given in Fig. 2.9

The performance of the fuel cell is characterized by three different regions; activation polarization area, ohmic polarization area and concentration polarization area.

Activation losses are highly non-linear with current and manifest as a sharp initial drop in cell voltage. Physically, the activation polarization characterizes the voltage loss required to initiate the electrochemical reaction. Activation losses are attributed to the sluggish of reaction occurring in the fuel cell at high voltages.

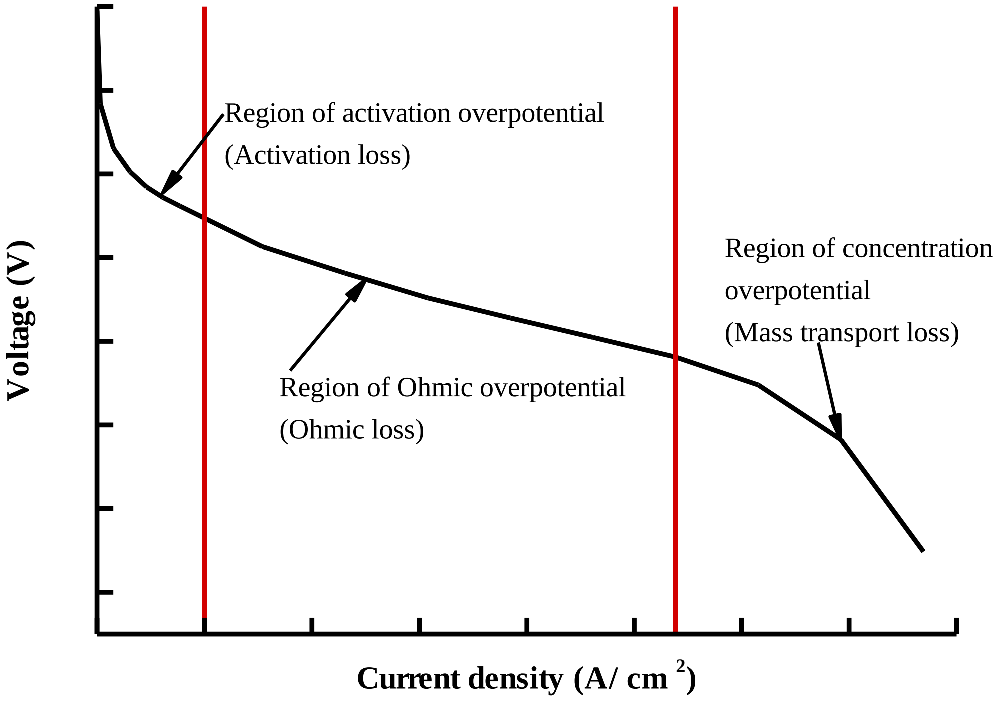

Fig. 2.9: Typical performance curve of a PEM fuel cell

Ohmic loss

When the electrical current load increases, activation overpotential is less of a factor and ohmic losses increase at a greater rate, then the curves enters the region characterized by ohmic potential. This voltage loss is mainly caused by the resistance to the flow of electrons through the material of the electrodes and various connections in the current collection pathway, as well as the resistance to the flow of protons though the electrolyte membrane. These losses are proportional to current density, and are essentially linear

Mass transport losses occur when there is a disparity in relation to the rate at which reactants are supplied and the rate at which they are consumed. During the cell operation, the hydrogen oxidation and oxygen reduction process give rise to the release of electrical energy, heat energy and water.

At the limiting current density, oxygen at the catalyst layer is depleted and no more current can be obtained from the fuel cell. This is responsible for the sharp decline in potential at high current densities. To reduce the mass transport loss, the cathode is usually run at high pressure.

2.6 References:

１. Gregor Hoogers, FUEL CELL TECHNOLOGY HANDBOOK, CRC PRESS, Boca Raton London New York Washington , D.C.

２. Mengbo Ji and Zidong Wei, A Review of Water Management in Polymer Electrolyte Membrane Fuel Cells, Energies 2 (2009) 1057-1106

３. Pellegri A., Spaziante P. M., Bipolar separator for electrochemical cells and method of preparation thereof, US Patent No. 4197178, April 8, 1980

４. Spurrier F. R., Pierce B. E., Wright M. K., Fuel cell plates with improved arrangement of process channels for enhanced pressure drop across the plates, US Patent No. 4631239, December 23, 1986

５. Mathias M., Roth J., Fleming J., and Lehnert W., Diffusion media materials and characterisation, Chapter 46, Handbook of Fuel Cells-Fundamentals, Technology and Applications, edited by wolf Vielstich, Hubert A. GAsteiger, Arnold Lamm. Volume 3: Fuel Cell Technology and Applications, John Wiley & Sons, Ltd, 2003

６. Chisaka M., Daiguji H., effect of glycerol on micro/nano structures of catalyst layers in polymer electrolyte membrane fuel cells, Electrochimica Acta, 51 (2006) 4828-4833

７. Barbir F., PEM fuel cells : theory and practice, New York: Elsevier Academic Press, 2005

８. Nguyen T. V., He W. Vielstich, Gasteiger H. A., and Lamm A., Handbook of Fuel Cells: Fundamentals Technology and Applications, vol. 3, John Wiley & Sons Ltd., 2003, pp. 325-336

CHAPTER THREE

Pressure Drop and Cross Flow Mechanism in a PEFC

3.1 Introduction:

The polymer electrolyte membrane fuel cell (PEMFC) is an electrochemical device that converts the chemical energy of a fuel directly into electricity. This direct conversion of energy has a profound impact on the maximum theoretical efficiency of electrical devices. PEMFCs are promising and worthy candidates for use as high-efficiency/low-emission energy-conversion devices for stationary or portable applications, and even for use in small items of mobile equipment such as cellular phones.

The flow field plays a major role in distributing reactant towards the catalyst layer. Several types of flow field such as parallel, serpentine, interdigitated are commonly used in the fuel cells [1]. The interdigitated flow field, in which reactant gas flows directly into the electrodes, was proposed by Nguyen [2] as a means of solving the problem of mass transport limitation at high current density operation. Nishimura et al. [3] measured in-plane temperature distribution for various shapes of serpentine channel, and they identified the optimal design for the separator. However, in designing the flow field, pressure drop is of paramount importance as this is considered to be main design parameter [4]. Barbir et al. [5] investigated the relationship between pressure drop and cell resistance as a diagnostic tool for PEM fuel cells. They monitored the pressure drop in fuel cell and confirmed that the pressure drop increase is the reliable indicator of fuel cell flooding, while an increase of cell resistance is reliable indicator of fuel cell drying. Ma et al. [6] measured the pressure drop between the inlet and outlet of the channel to monitor liquid water accumulation and removal. Pressure drop characteristics and visualization study of liquid water has been conducted by Liu et al. [7]. In their study, the total pressure drop increased with the increase of current density, but pressure drop decreasing was found with the increasing of cell temperature. The effects of depth of separator channel on current density have been investigated by Inoue et al. [8]. The simulation results confirmed that the current density and pressure drop both is increased using smaller depth of gas channel.

The gas diffusion layer (GDL) is a porous material inside which the flow distribution is very complex. The effect of the gas diffusion layer parameter on the performance of PEMFC has a great influence, which is investigated by several authors [9-15]. Influence of GDL thickness on the cell performance was investigated by Lee et al. [9] and Inoue et al. [10]. The GDL properties such as porosity, permeability [9, 11, and 15], morphology of GDL and Polytetrafluoroethylene (PTFE) [12-14] loading were also investigated in the experimental as well as numerical simulation.

PEMFCs use specially designed channels machined into the bipolar plates to distribute reactant gases and to remove the by-products. The most widely used configuration of gas flow channel in a PEMFC is a serpentine channel. In this design, the gas flow channels are groove into the bipolar plate and GDL is placed beneath the channel and bipolar plate. The area where bipolar plate is in direct contact with the GDL is known as the land or rib. This serpentine flow channel layout has relatively long flow path, and therefore produces substantial pressure drop; as a result there is a significant parasitic power loss associated with the supply of gas to the cathode. In ordinary gas flow situations, the gaseous reactants reach the catalyst layer through gas diffusion layer. The gas diffusion layer (GDL) plays an important role in distributing the reactants to the catalyst layer by diffusion process. However, in the case of large calculation, it is thought that there is an in the differential pressure between adjoining channels that causes the supplied gas to flow through the GDL. By this process, the reactant gases flow through the GDL under the rib from one part of the channel to another; this process is referred to as cross flow.

The cross leakage flow through the GDL as a direct result of the pressure difference has been investigated by Kanezaki et al. [16]. The effect of cross flow on the performance of fuel cell with a serpentine flow channel design with assembly compression has been investigated by Shi and Wang [17]. They found that the cross flow through the GDL from one channel to another channel decreases when assembly compression is considered; the performance of fuel cell, especially in the high current density region, also decreases. The gas diffusion thickness effect on the cross flow has been investigated by Park and Li [11]. The pressure drop and flow cross-over through the GDL of a PEMFC with a serpentine channel has been investigated by Sun et al. [18], who used a channel cross section with a trapezoidal shape. Their results indicate that the trapezoidal cross-sectional shape ratio has a significant effect on the pressure variation in the flow field in both the presence and absence of cross over. The cross convection under the rib can significantly improve the performance and consequently the power density of PEFCs [19]. Experimental investigations on liquid water removal from gas diffusion layer by the cross flow have been carried out by Jiao et al. [20]. The visualization of liquid water under the rib area was confirmed that the cross flow was effective to remove the liquid water, even at low flow rates. The characteristics of liquid water behavior in the GDL under pressure gradient have been investigated numerically by Park et al. [21]. The simulation results indicated that liquid water can be removed effectively from the gas diffusion layer by the pressure gradient caused by the reactant flow in the flow channel and gas diffusion layer. Recently Bachman et al. [22] experimentally induced cross flow in a parallel flow field experimentally and they showed that cross flow produced a 24% improvement in current density.

In order to estimate the pressure drop accurately it is necessary to calculate the conservation of mass precisely which is strictly maintained in our present simulation, since a numerical method was developed previously by our group to calculate the coupling of velocity and pressure with an attention of mass conservation strictly. The details of this developed method and advantage was discussed in the previous paper by Saha et al. [28] and it is used to carry out our present simulation. It is obviously important to notice that the error level change from 0.05% to 0.1% causes the change in the pressure drop which cannot be allowed as sometimes comparable the pressure drop obtained for two different order of permeability was reported in the study of Saha et al. Using this improved method, the pressure drop mechanism was predicted with considering the complex situation of GDL deformation and validated the results with experimental work by Saha et al. [29]. Furthermore, Saha and Oshima [30] also predicted pressure drop using multiple serpentine channels and the solution was validated again with experimental results by this developed numerical method. So, therefore, we maintained the maximum error level of mass conservation 0.05% throughout our present simulation.

Many researchers have investigated the cross flow which is limited on the fuel cell performance evaluation. A very few of them have discussed the flow field phenomena. However, there is no research where the variation of serpentine channel width / rib width is considered to investigate the cross flow behavior.

Therefore, the objective of this study is to investigate the cross flow behavior based on the pitch length (pitch length is defined as the distance between the centre of channel width and rib width) of a serpentine channel, GDL thickness and physical properties of GDL, and to investigate the role of cross flow on the pressure distribution in the gas channel.

3.2 Numerical procedure

3.2.1 Physical and Mathematical Model

To understand the pressure drop mechanism and cross flow behavior, we examined three different cross-sectional areas of a single serpentine channel grooved into the bipolar plate for four different thickness of GDL placed under the channel and bipolar plate. The GDLs had a wide range of permeability and porosity values. The gas-channel pitch length has a marked effect on the uniformity of the temperature distribution and hence on the performance of the PEMFC [3]. The pitch length is defined as the distance between center of channel and center of rib width. In the present study, we designed our computational domain based on the experimental setup used by Nishimura et al. [3]. However, to simplify matters and to reduce the computational cost, we modified the computational domain to a single serpentine channel. Figure 3.1 shows an example of numerical grid that we used in our present simulation. The dimension of the computational domain are listed Table 3.1. For the sake of simplification, we made the following assumptions: (1) the gas mixture is assumed as an ideal gas; (2) the flow is incompressible and laminar flow with low Reynolds number; (3) the GDL consists of an isotropic and homogeneous porous medium. We examined the gas flow only in the cathode side which including the cathode separator, single serpentine and cathode GDL. The gas flow behavior in the gas channel and GDL can be obtained by solving the continuity equation (Eq. 1) and momentum equation (Eq. 2). The governing equations corresponding to the various region (i) gas channel and (ii) porous media GDL are given below.

$$\frac{\partial(\varepsilon\rho)}{\partial t} + \nabla\cdot(\varepsilon\rho\,\mathbf{u}) = 0 \tag{1}$$

$$\frac{\partial}{\partial t}(\varepsilon\,\rho\mathbf{u}) + \nabla\cdot(\varepsilon\rho\,\mathbf{u}\mathbf{u}) = -\varepsilon\nabla p + \nabla\cdot\left(\mu^{*}\,\nabla\mathbf{u}\right) + \varepsilon\rho\,\mathbf{g} - \frac{\varepsilon\mu^{*}\,\mathbf{u}}{K} \tag{2}$$

Here, **u** is the velocity vector, ρ is the density, μ^* is the effective viscosity approximated by the model of $\mu^* = \varepsilon\mu$, where μ is the intrinsic viscosity, ε is the porosity of the GDL, and *K* is the permeability of the GDL. The porosity ε is defined as the ratio of the volume occupied by the pores to the total volume of the porous medium, whereas the permeability *K* is defined as the ratio of the square of the effective volume to the surface area of the porous matrix [23].The last term of equation (2) represents the Darcy's drag force in the porous media. In the gas channel, $\varepsilon \rightarrow 1$ and $K \rightarrow \infty$, so equation (2) becomes the original Navier-Stokes equation.

3.2.2 Boundary conditions

A no-slip boundary condition is applied to all wall boundaries. The velocity at the inlet of the channel is assumed to be constant. Ambient pressure is maintained at the outlet of the gas channel.

3.2.3 Numerical Method

The governing equations, together with appropriate boundary conditions, were implemented and solved by using FrontFlow/red which is non-commercial software and open to use as free for all [24]. The computational code FrontFlow/red (FFR),which was originally developed under the project of "Frontier Simulation Software for Industrial Science" and optimized for vehicles aerodynamics simulation by Tsubokura et al. [25-26]. Later on, this software was developed by Computational Fluid Mechanics laboratory of

Hokkaido University with the support of the Adaptable and Seamless Technology Transfer Program through Target-Driven R & D of Japan Science and Technology Agency [27].

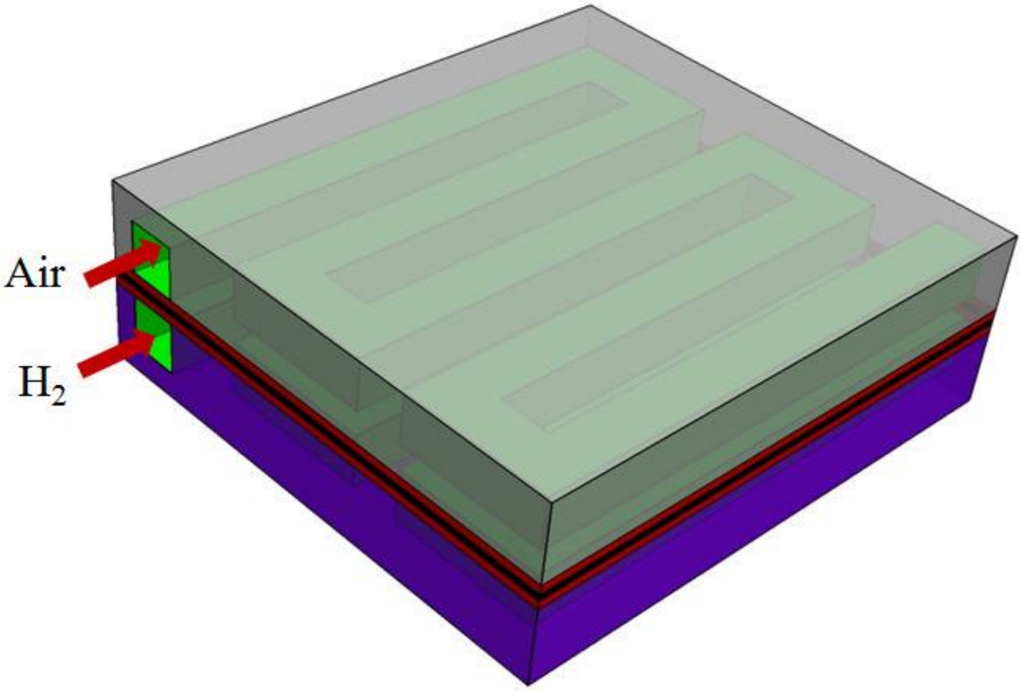

(a)

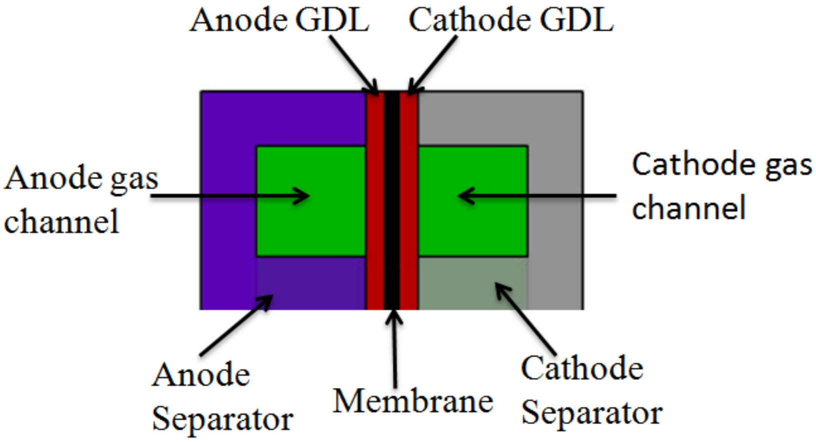

(b)

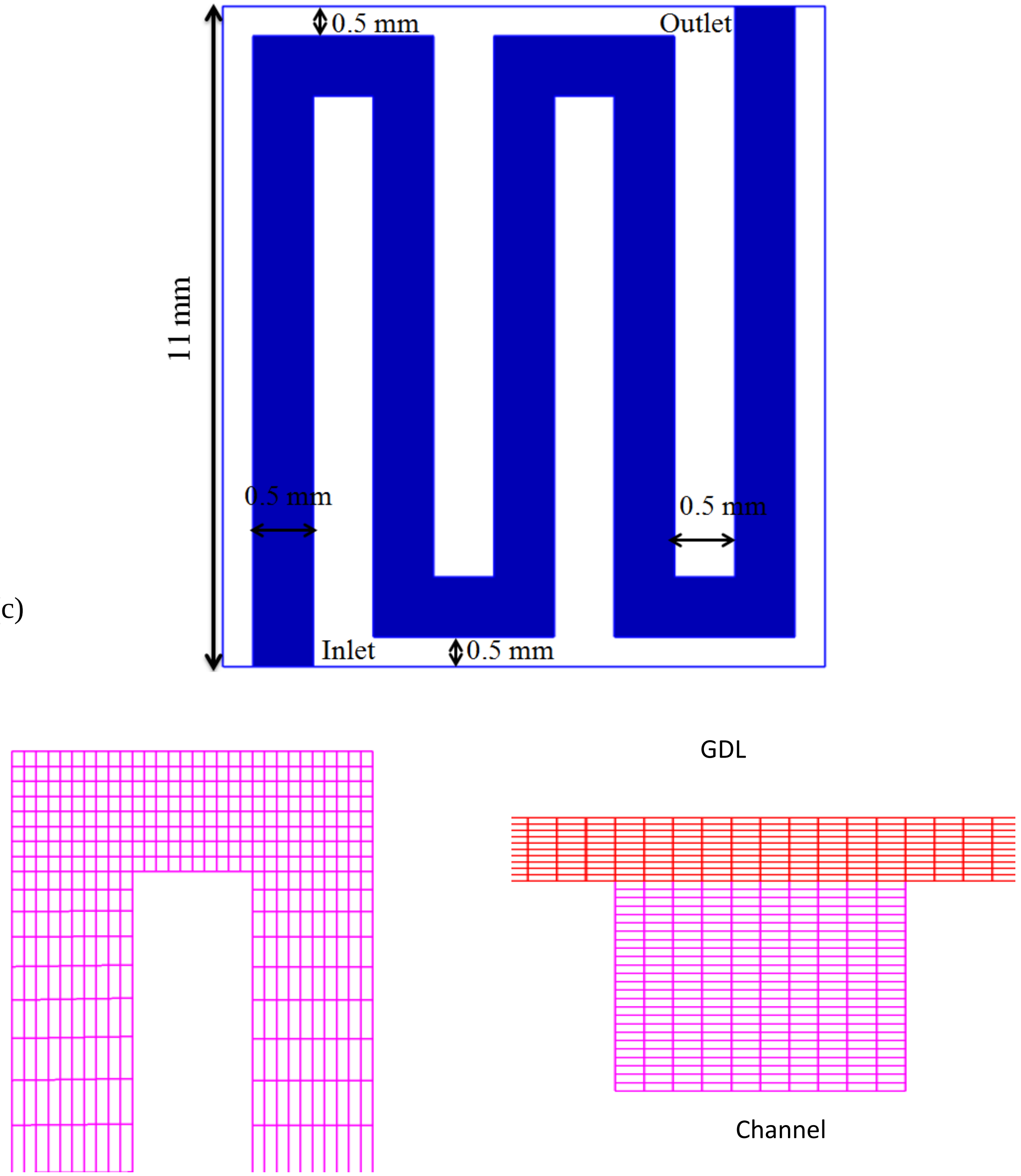

(c)

(d)

Fig. 3.1: (a) Schematic view of a PEMFC (b) Section view of PEMFC (c) Serpentine channel layout with separator (d) Grid arrangement of the numerical domain

The software employs the finite-volume method, and the equations for mass and momentum conservation and the boundary conditions are discretized by a finite-volume scheme. The software also takes into account the electrical field, the nature of the porous medium, electrochemical reactions, and water transport in a PEMFC.

The Euler implicit scheme was used for time integration, and the first-order upwind scheme was used to discretize the convection terms in the governing equations. The fractional-step algorithm was used to update the pressure and velocity fields from solutions of the pressure Poisson equations. The fractional-step algorithm was developed by considering an implicit treatment of the Darcy drag term with attention to strict mass conservation. Details of the advantages of this algorithm have been described previously [28], and the algorithm is incorporated in our simulation code FrontFlow/Red PEFC version. This simulation code already has been validated by means of small- scale calculations on deformation of the GDL [29]. Furthermore, our group recently derived numerical predictions of the amount of flow crossover through the GDL for five multiple serpentine channels and obtained results that were in good agreement with experimental measurements [30], thereby providing additional validation of our numerical scheme.

3.3 Grid Independent Study

The convergence characteristics and accuracy of the numerical solution depends on the discretization scheme, equation solver algorithm and grid quality. The grid generation of our simulation is carried out by the commercial grid generation software GRIDGEN.

Table 3.1: Details of Computational Geometry

Dimension	Value
Channel width (m)	0.0005, 0.001, 0.0025
Land width (m)	0.0005, 0.001, 0.0025
Channel height (m)	0.001
GDL thickness (m)	0.0003,0.0002, 0.00017, 0.000128
Ratio of channel width and land width	1:1
Number of channels	1
Number of U-turns	4

Table 3.2. Physical properties and operational parameters.

Physical Quantity	**Value**
GDL porosity	0.1–0.9
GDL permeability, K (m^2)	1.76×10^{-5}–1.76×10^{-14}
Density, ρ (kg/m^3)	1.2
Viscosity, μ ($kg/m \cdot s$)	1.83×10^{-5}

Operational temperature (K)	333
Operational pressure (Pa)	101325
Gas flow rate, (m^3/s)	2.0×10^{-6}
Gas composition	O_2: 21% N_2: 79%

Table 3. 3. Grid independence test with three grid arrangements.

Resolution	Length direction	Width direction	Height direction (channel)	GDL thickness
Coarse grid	200-400 μm	125 μm	66.7 μm	37.5 μm
Base grid	125-320 μm	100 μm	40 μm	30 μm
Fine grid	125-250 μm	62.5 μm	25 μm	20 μm

To investigate the influence of grid resolution, three different grid arrangements is taken into account namely coarse grid, base grid and fine grid. Variation of grid resolution is considered along the channel length, height and width direction and also to GDL thickness direction is shown in the Table 3.3.In grid independency test we have carried out simulation for computational domain with a pitch length of 1.0 mm and a GDL thickness of 0.3 mm. The total number of cell in the base grid is more than two times larger than coarse while the number of cell in the fine grid is six times larger than coarse and two times larger than base grid.

From Fig. 3.2 it is evident that base grid can capture the physics accurately, since there is no significant difference between the solution of base grid and fine grid at the steady state situation.

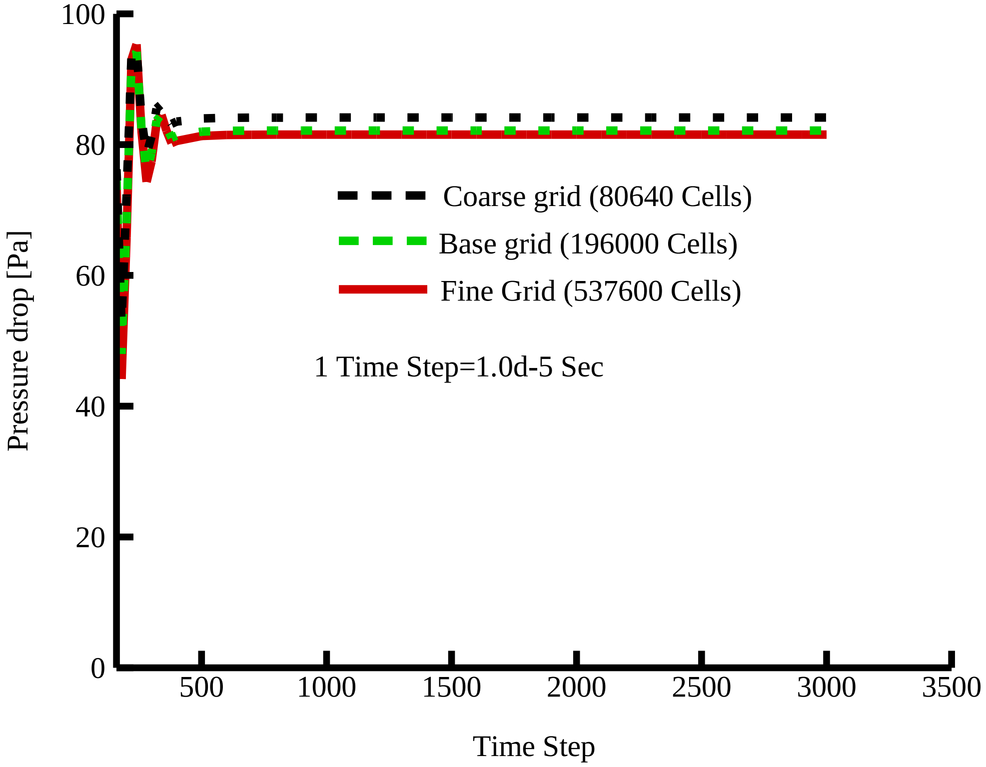

Fig.3. 2: Convergence history of pressure drop with different grid sizes

Table 3.4**:** The quantitative comparison of grid independency test

Solution at the steady state	Coarse grid	Base grid	Fine grid
Pressure drop [Pa]	84.14	81.94	81.52

We decided therefore to use the concept of base grid to the others computational domain. The quantitative comparison among three cases is given in the Table 3.4.

3.3 Results and Discussions

The results presented in this section were obtained by using the numerical procedure described above and the physical and operational parameters listed in Table 3.2. Figures 3.3 (a)–3(c) show the calculated velocity distribution in the channel. The velocity profile in the gas channel becomes laminar and is fully developed in the downstream direction. The maximum velocity is found at the center of gas channel. As the flow approaches a bend region, the symmetric velocity profile becomes asymmetric and it remains so until the flow leaves region of bend. A small recirculation zone can be observed near the beginning of each bend. The velocities in these zones are very high, which contributes to an increase in friction, leading to greater pressure drop around the bend region. Further downstream from each bend, velocity profile becomes fully developed once more and remains so until the flow of reactant gas approaches the next bend region.

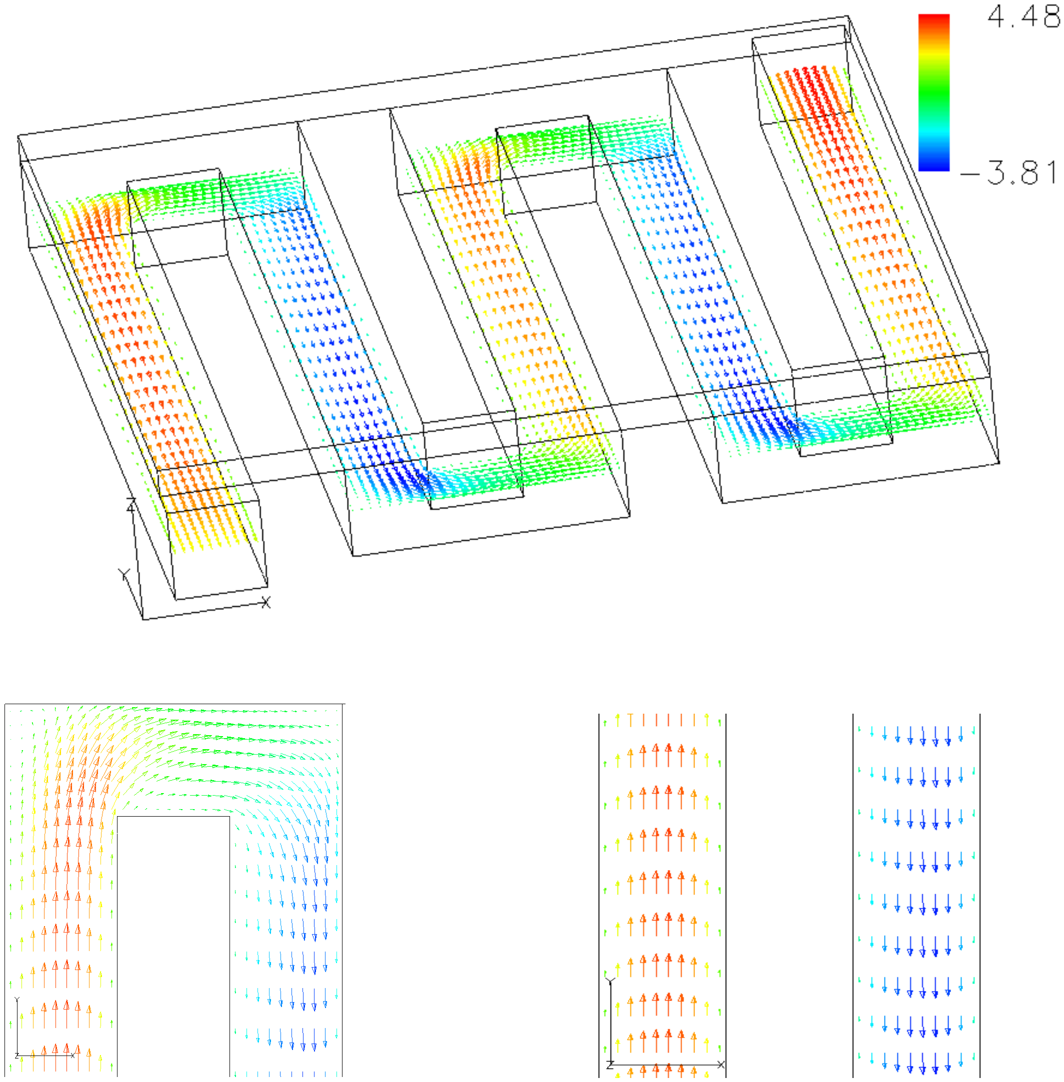

(a)

(b)

(c)

Fig. 3.3: (a) Velocity (m s^{-1}) distribution at the mid-plane of the gas channel (b) Velocity (m s^{-1}) at the corner of U-turn (c) at the middle of the channel

The pressure distribution in the channel and GDL are shown in Fig. 3.4. The pressure distribution decreases along the flow channel from inlet to outlet. Fig. 3.4 confirms that pressure gradient across the GDL under the rib area is much larger than that under the channel. As a result a significant amount of flow crosses through the GDL under the rib area, as shown in Fig. 3.5.

On the other hand, pressure gradient across the GDL under the channel (especially under the area of bend) is much lower than under the rib.

The Fig. 3.6(a) shows the total pressure drop from inlet to outlet for various pitch length with wide range of permeability values. Here the porosity value was used fixed at 0.7. The effect of porosity on the total pressure drop at permeability 1.76×10^{-11} m^2 is depicted in Fig. 3.6(b). In this numerical simulation, three distinct pitch length of gas channel were considered. In this calculation constant flow rate is used since there are some experiment available in the literature was done using constant flow rate. The flow rate is expressed as: Cross sectional area of channel inlet × Inlet velocity. The flow rate $Q = 2.0 \times 10^{-6} m^3$ /s remained constant in all cases. Therefore, the increase in estimated pressure arises from an increase in the flow velocity. The velocity increases as the inlet cross-sectional area decreases, as a result of a decrease in the pitch length. Hence, the total pressure drop increases with decreasing of pitch length.

Moreover, an additional simulation has been carried out for all pitch length with constant velocity (stoichiometry A and 5 A) given at the channel inlet, and then obtained results are shown in Fig. 3.6 (a). Under the assumption of stoichiometry and current density is constant for all pitch lengths, then the consumption rate is proportional to the reaction area occupied by pitch length. Hence, the constant stoichiometry provides the constant velocity for every pitch length.

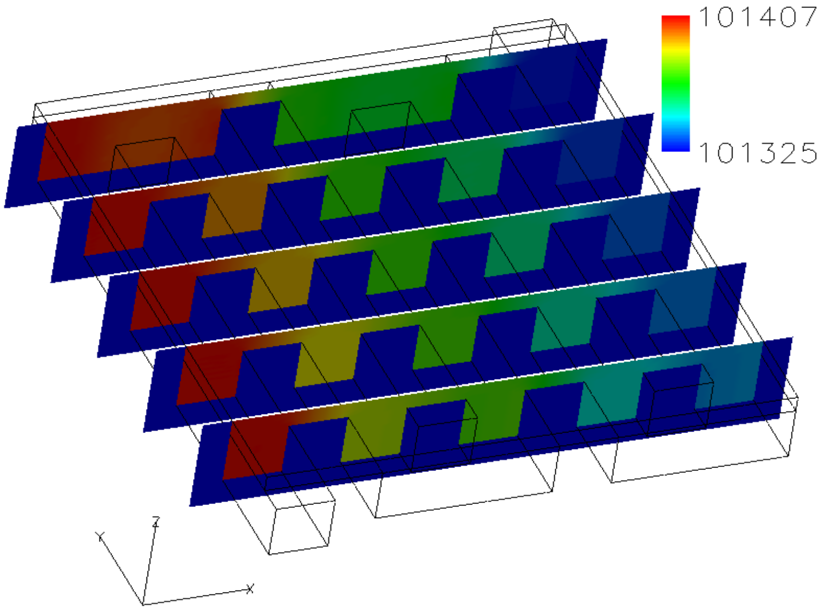

Fig. 3.4: Pressure (Pa) distribution in the channel and GDL at several axial positions (*y*=2, 4, 6, 8 mm from inlet)

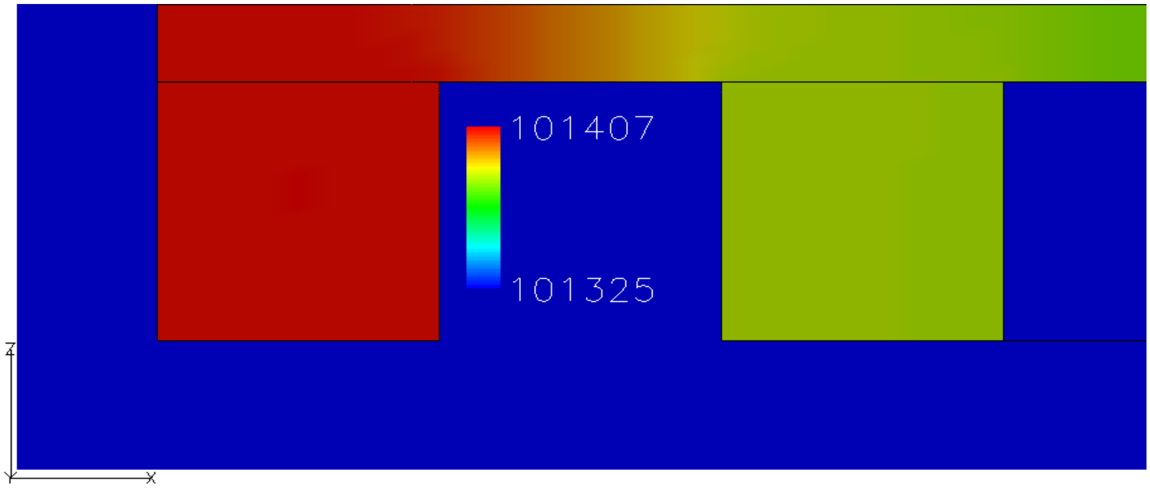

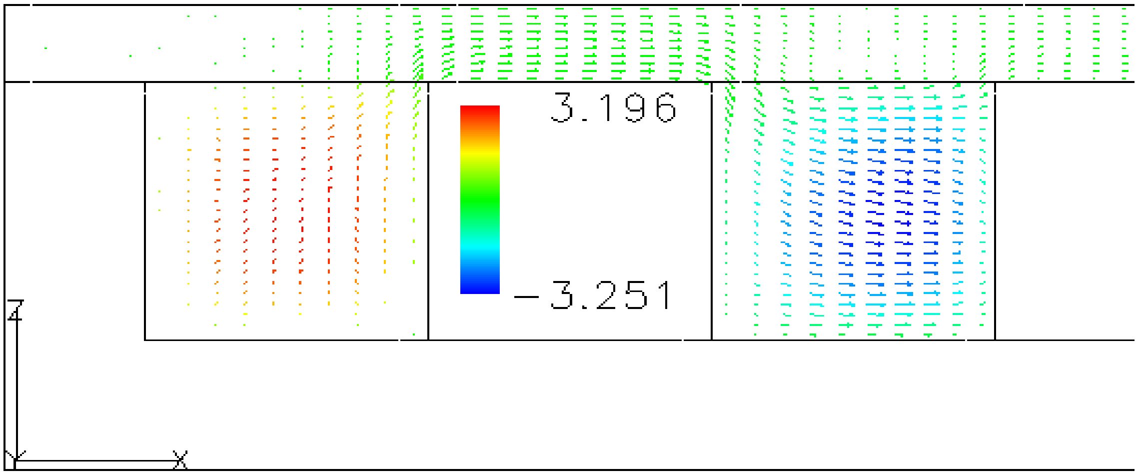

Fig. 3.5:Pressure (Pa) and velocity (m s^{-1}) distribution in the channel and GDL on the *x-z* plane at *y=2* mm with *x=0 to x=4* mm

(a)

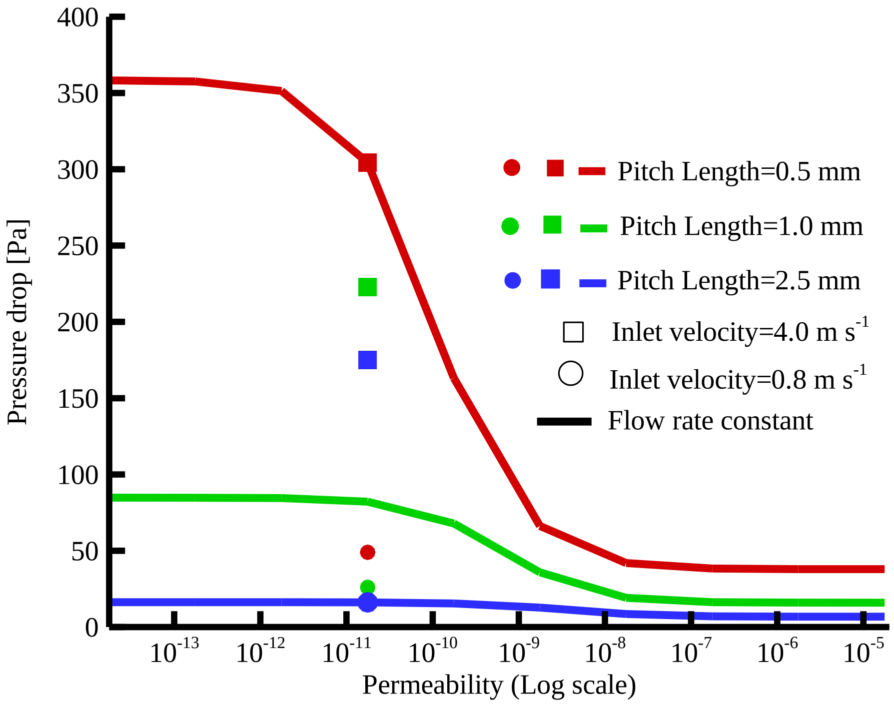

(b)

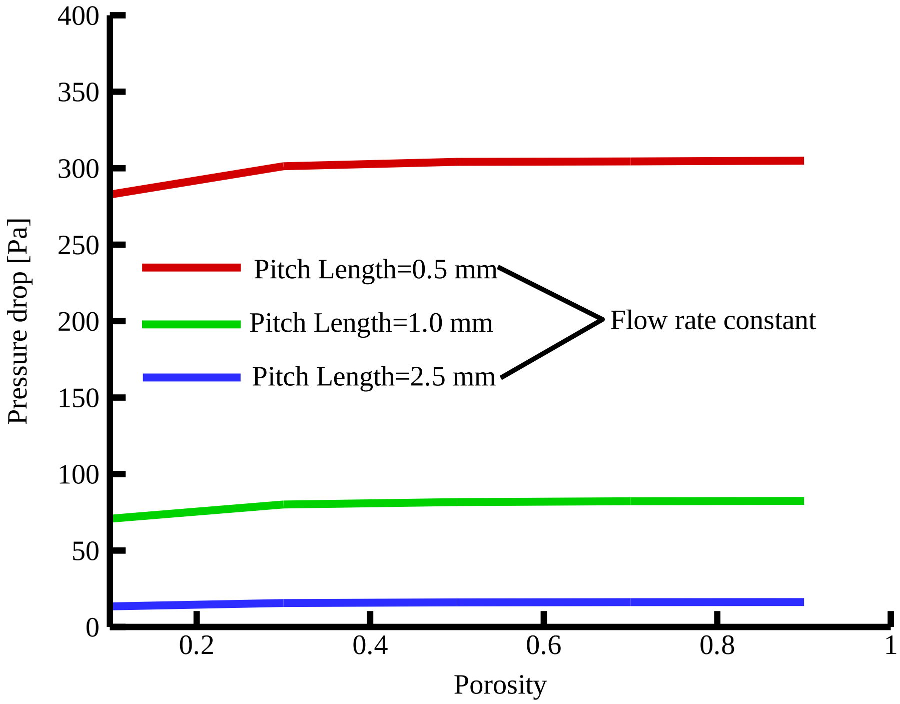

Fig. 3.6: The effect of gas channel pitch length on the total pressure drop varying with (a) wide range of permeability (b) various values of porosity

Let suppose that the stoichiometry *A*, provided the velocity 0.8 m s^{-1} which is the same value as constant flow rate of pitch length 2.5 mm, and when the stoichiometry is 5*A*, provided the velocity 4.0 m s^{-1} which is the same value as constant flow rate of pitch length 0.5 mm. The Fig. 3.6(a) shows that under the constant velocity 0.8 ms^{-1} and 4.0 m s^{-1} (stoichiometry *A* and 5 *A*) the pressure drop increases with decreasing pitch length. For the increase of inlet velocity (stoichiometry) the pressure drop increases for any values of pitch lengths. The pressure drop obtained with different pitch length in our simulation shows the similar tendency either setting the stoichiometry or flow rate at the channel inlet given as a constant value which concluded that the pressure drop increases with decreasing pitch length. Since the conclusion remains the same with constant stoichiometry and constant

flow rate cases, hence the further calculation has been done in the following section keeping the flow rate constant.

On the other hand, for any values of pitch length the total pressure drop decreases with the increasing of permeability values. This phenomenon can be explained in two ways. The first explanation is that by increasing the permeability, the ability to transmit reactant gas to the gas diffusion layer is increased. The second explanation is that transfer of the reactant gas by flow cross-over through the GDL also increases. This phenomenon can be clarified by considering the conservation of momentum in Eq. (2). In the momentum equation, the final term is known as Darcy drag term. The influence of Darcy drag term becomes larger than that of convection term at low values of the permeability. In these cases, the Darcy drag term is balanced by pressure gradient term. Basically, one-order decreases in permeability results in almost one-order increase in the Darcy drag term. This explains why a decrease in permeability produces in the total pressure drop. On the other hand, increasing porosity doesn't produce a large increase in the Darcy drag term. From Fig. 3.6(b) it is evident that the variation of pressure drop for various values of porosity is very small.

Moreover, from figure 3.6(a) it can be seen that the pressure drop remains unchanged when permeability values larger than 10^{-8} m^2 and smaller than 10^{-12} m^2. This result indicate that when GDL permeability is less than 10^{-12} m^2 or larger than 10^{-8} m^2 it behaves almost

(a)

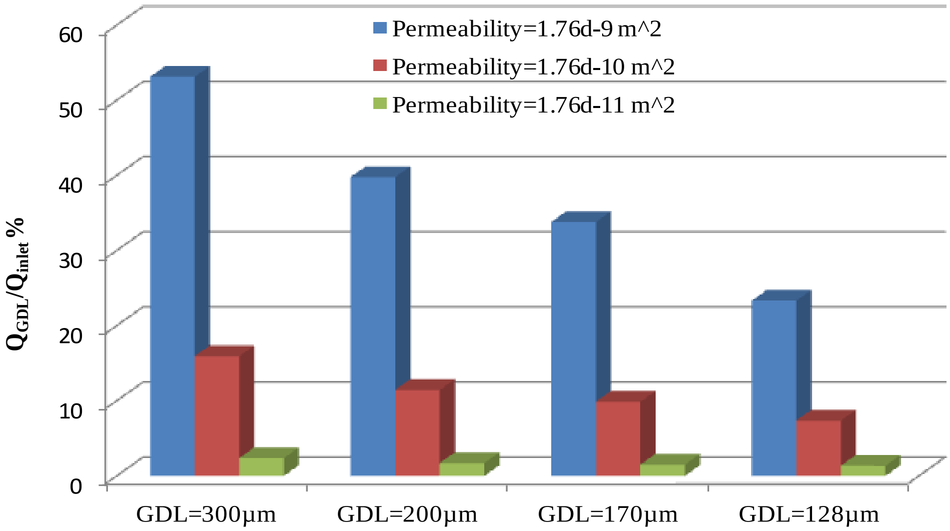

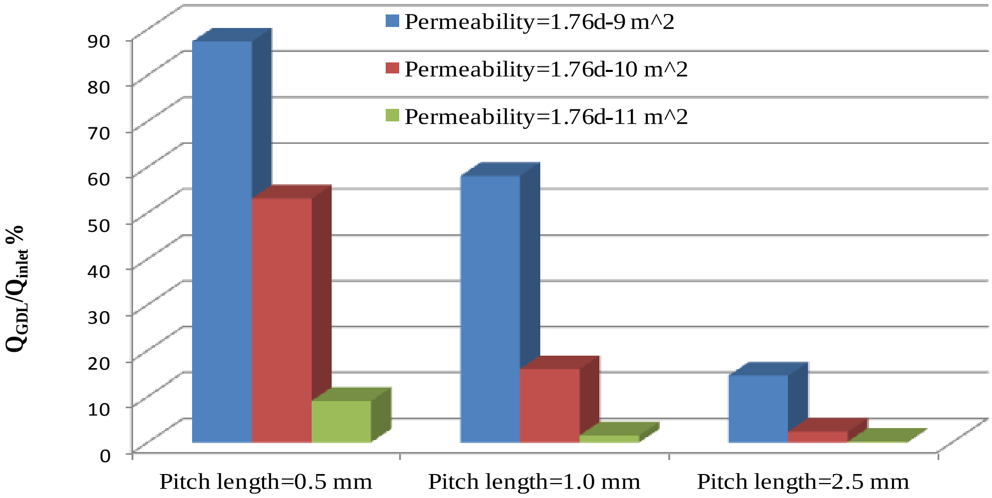

(b)

Fig. 3.7: The ratio of cross flow rate through the GDL to the total inlet flow rate (a) various GDL thickness with gas channel pitch length=1.0 mm (b) various pitch length with GDL thickness=300µm

like solid or fluid, respectively. Therefore, the range of permeability 10^{-12} m^2 to 10^{-8} m^2 is the representative values of porous medium.

The cross flow rate through the GDL under the rib is quantified as volume mass flux. The volume mass flux is calculated over the surface through the GDL under the rib near to the outlet section.

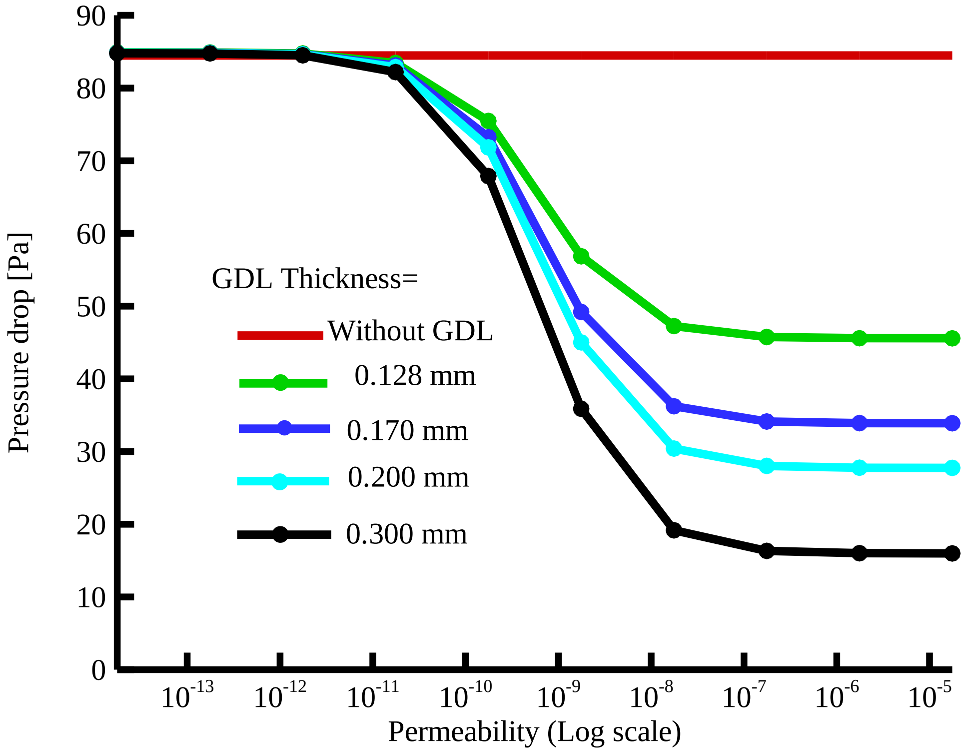

Fig. 3.8: The effect of GDL thickness on total pressure drop from inlet to outlet with wide range of permeability values

Fig. 3.7 (a) shows the ratio of cross flow rate to the total inlet flow rate for various thickness of GDL with varying permeability values. Fig. 3.7(b) shows the same ratio for different pitch lengths. It can be seen that decreasing the thickness of GDL decreases the cross flow rate through the GDL, whereas decreasing the pitch length increases the cross flow rate through the GDL.

Fig. 3.8 shows the effect of thickness of the GDL on the total pressure drop with a pitch length of 1.0 mm. The highest pressure drop is obtained in the case of without GDL. The total pressure drop decreases on increasing the thickness of GDL. It is thought that placing GDL on the channel permits the gas to flow from the channel through the GDL by convective flow as well as by diffusion process.

Also, as the thickness of the GDL gradually increased, cross flow in the serpentine channel increases resulting in a decrease in the total pressure drop. It is mentioned that in our previous work [30], the pressure drop was predicted and compared with experimental work for more practical serpentine channel. It was found a very good agreement with the experimental work. The total pressure drop from inlet to outlet was obtained approximately1675 Pa and 1850 Pa for with GDL and without GDL respectively in Fig 3.5 of Saha et al. [30]. Now if we compare our present result in Fig. 8 with the result in Fig. 3.5 of Saha et al., we can see that the result obtained in our present simulation shows the similar tendency as the result of Saha et al. although we consider the simplified single serpentine channel.

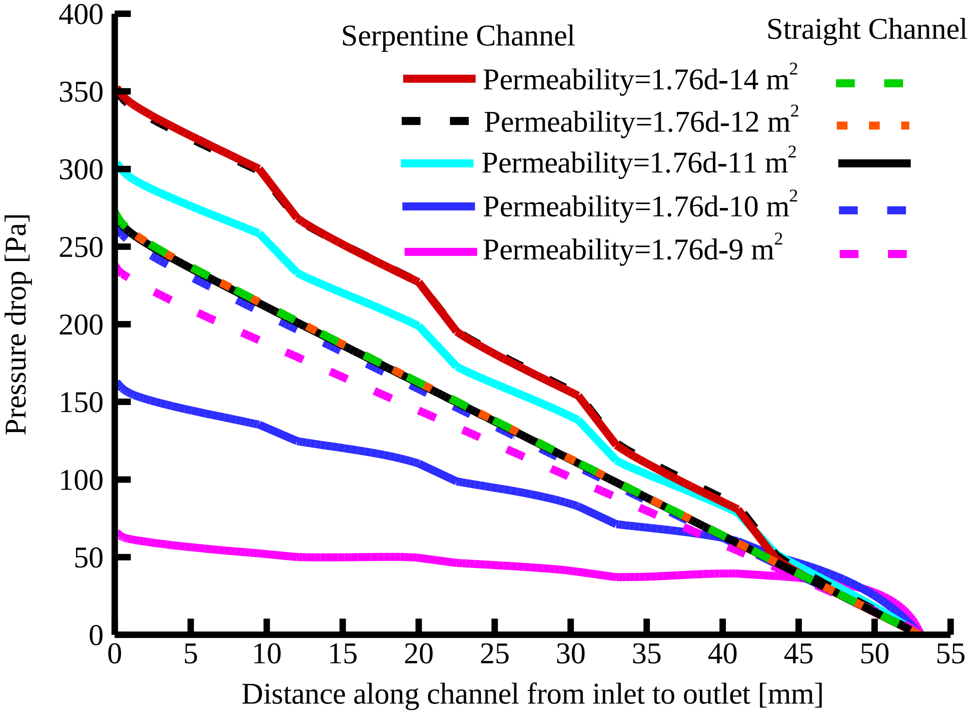

Fig. 3.9: The pressure drop distribution from channel inlet to outlet in the straight channel and in the serpentine channel

To clarify the effects of cross flow and bend regions on pressure drop in a serpentine channel, we considered a straight channel 53 mm long, which is the same length as the serpentine channel with a pitch length of 0.5 mm. From Fig. 3.9, it is clear that cross flow has a significant effect on the pressure drop. Because there is no cross flow in the case of the straight channel, in comparison with the change observed with the serpentine channel, the pressure drop distribution from channel inlet to outlet shows little change when the permeability is increased. However, in the case of serpentine channel, the pressure drop decreases with increasing permeability values.

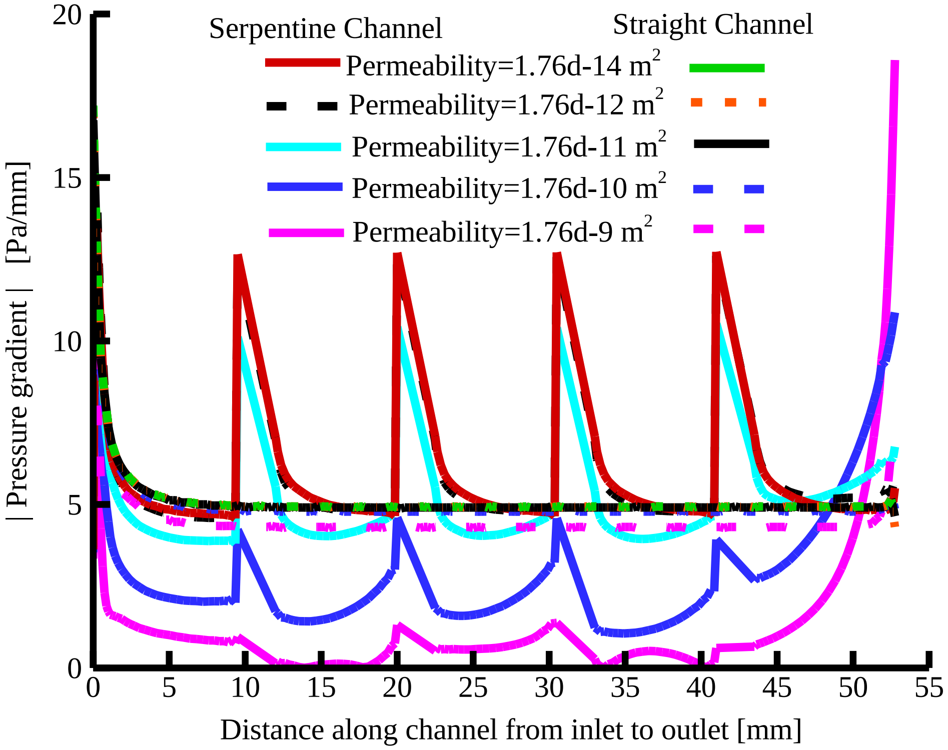

Fig. 3.10: Slope of Fig.3. 9

Because the cross flow rate through the GDL under the rib increases with increasing permeability (Fig. 3.7), the pressure gradient along the channel from inlet to outlet decreases as result of cross flow.

When permeability values is very small, for example 1.76 × 10^{-14} m^2, there is no cross flow in the serpentine channel. In the straight channel, cross flow cannot occur for any value of permeability. Therefore, if we compare the red curve corresponding to the serpentine channel and the green curve corresponding to the straight channel in Fig. 3.9, we can confirm that the gap between two curves is caused by the presence of bends in a serpentine channel.

To understand the effect of the position of bends in the serpentine channel on their pressure drop characteristics, we plotted the slope of the lines in Fig. 3.9 against the distance along the channel. The results are shown in Fig. 3.10. For the straight channel, the plot of the pressure gradient along the channel from the inlet to outlet is a straight line (except near the inlet position).

For the serpentine channel, however, sudden changes in the pressure gradient occur near to the bends. Figure 3.10 also shows that the pressure gradients in the straight parts of the serpentine channel decrease as the value of the permeability is increased because the cross flow increases with increasing permeability (see Fig. 3.7).

Conclusion: In this study, we clarified the effects of geometrical characteristics and physical properties of porous media on the pressure loss mechanism and cross flow behavior in the serpentine channels of a PEMFC. We can summarize our conclusion as follows:

① The pressure gradient through the GDL under the rib is larger than under the channel is observed.

② The pitch length of a serpentine channel has significant effect on the pressure drop and cross flow.

③ The pressure drop increases with decreasing pitch length. Furthermore, the permeability has a strong effect on pressure drop. The pressure drop remains unchanged when permeability is lower than 10^{-12} m^2 or larger than 10^{-8} m^2. The GDL therefore behaves as a porous medium when it values lies in the range 10^{-12} m^2 to 10^{-8} m^2. However, the effect of porosity on pressure drop and cross flow is indistinguishable.

Decreasing the thickness of GDL results in a increase in the pressure drop and decrease in the amount of cross flow.

④ The cross flow rate through the GDL under the rib increases with decreasing of pitch length. Therefore, the cross flow rate through the GDL under the rib can be enhanced by reducing gas channel pitch length of a serpentine channel.

⑤ The pressure drop characteristics at the bend region of serpentine channel are identified. Pressure gradient is higher at the bend region than that of straight part of a serpentine channel. The pressure gradient at the straight part of serpentine channel decrease with increasing permeability values. Therefore, pressure gradient at the straight part of serpentine channel suppressed by the cross flow.

In the flow dynamics point of view, the numerical simulation has been carried out under a simplified serpentine channel where length of the channel was made shortened. The simulation results obtained by present numerical method were found reasonable under different shape of the serpentine channel, different thickness of GDL and various operating conditions. However, the cross flow rate through the GDL would be higher under longer length of practical serpentine channel used in the real application of PEM fuel cell. Since the cross flow is mainly depends on the pressure difference between adjacent channels, so the accurate estimation of pressure is necessary which can be obtained by the present numerical method. Therefore, this numerical method can also be applicable in the case of complex flow situation (e.g. cross flow) might appear in the micro channel and porous media in the various engineering disciplines.

In the PEM fuel cell flow field design point of view, the results indicate that the cross flow rate through the GDL can be enhanced by decreasing pitch length, suggesting the proper optimization is required between pitch length and cross flow. It is expected that cross flow may increase the performance of fuel cell by facilitating the oxygen transport towards the catalyst layer and removing the liquid water from the cell which should be investigated together with proper consideration of GDL deformation. Further studies are currently under way to investigate the individual contribution of cross flow on the performance of fuel cell.

3.5 References

[1] X. Li and I. Sabir, Review of bipolar plates in PEM fuel cells: Flow designs, International Journal of Hydrogen Energy, 30 (4) (2005) 359-371

[2] T. V. Nguyen, A gas distributor design for proton-exchange membrane fuel cells, Journal of the Electrochemical Society, 143 (5) (1996) L103-L105

[3] A. Nishimura, K. Shibuya, A. Morimoto, S. Tanaka, M. Hirota, Y. Nakamura, M. Kojima, M. Narita, and E. Hu, Dominant factor and mechanism of coupling phenomena in single cell of polymer electrolyte fuel cell, Applied Energy, 90 (2) (2012) 73-79

[4] X. Li, I. Sabir, and J. Park , A flow Channel design procedure for PEM fuel cells with effective water removal, Journal of Power Sources,163 (1) (2007) 933-942

[5] F. Barbir, H. Gorun, and X. Wang, Relationship between pressure drop and cell resistance as a diagnostic tool for PEM fuel cells, Journal of Power Sources, 141 (2005) 96-101

[6] H. P. Ma, H. M. Zhang, J. Hu, Y. H. Cai, and B. L. Yi, Diagnostic tool to detect liquid water removal in the cathode channels of proton exchange membrane fuel cells, Journal of Power Sources, 162 (1) (2006) 469-473

[7] X. Liu, H. Go, F. Ye, and C. F. Ma, Water flooding and pressure drop characteristics in flow channels of proton exchange membrane fuel cells, Electrochimica Acta, 52 (11) (2007) 3607-3614

[8] G. Inoue, Y. Matsukuma, and M. Minemoto, Effect of gas channel depth on current density distribution of polymer electrolyte fuel cell by numerical analysis including gas flow through gas diffusion layer, Journal of Power Sources, 157 (1) (2006) 136-152

[9] H. Lee, J. Park, D. Kim, and T. Lee, A study on the characteristics of the diffusion layer thickness and porosity of the PEMFC, Journal of Power Sources, 131(1-2) (2004) 200-206

[10] G. Inoue, Y. Matsukuma, and M. Minemoto, Evaluation of the thickness of membrane and gas diffusion layer with simplified two-dimensional reaction and flow analysis of polymer electrolyte fuel cell, Journal of Power Sources, 154 (1) (2006) 8-17

[11] J. Park and X. Li, An experimental and numerical investigation on the cross flow through gas diffusion layer in a PEM fuel cell with a serpentine flow channel, Journal of Power Sources, 163 (2) (2007) 853-863

[12] L. R. Jordan, A. K. Shukla, T. Behrsing, N. R. Avery, B. C. Muddle, and M. Forsyth, Diffusion layer parameters influencing optimal fuel cell performance, Journal of Power Sources, 86 (1-2) (2000) 250-254

[13] E. Antolini, R. R. Passos, and E. A. Ticianelli, Effects of the carbon powder characteristics in the cathode gas diffusion layer on the performance of polymer electrolyte fuel cells. Journal of Power Sources, 109 (2) (2002) 477-482

[14] E. Antolini, R. R. Passos, and E. A. Ticianelli, Effects of the cathode gas diffusion layer characteristics on the performance of polymer electrolyte fuel cells. Journal of Applied Electrochemistry, 32 (4) (2002) 383-388.

[15] J. P. Owejan, T. A. Trabold, D. L. Jacobson, M. Arif, and S. G. Kandlikar, Effects of flow field and diffusion layer properties on water accumulation in a PEM fuel cell, International Journal of Hydrogen Energy, 32 (17) (2007) 4489-4502

[16] T. Kanezaki, X. Li, and J. J. Baschuk , Cross leakage flow between adjacent channels in PEM fuel cells, Journal of Power sources, 162 (1) (2006) 415-425

[17] Z. Shi, and X. Wang , A numerical study of flow crossover between adjacent channels in a proton exchange membrane fuel cell with serpentine flow field, Journal of Power Sources,185 (2) (2008) 985–992

[18] L. Sun, P. H. Oosthuizen, and K. B. McAuley, A numerical study of channel-to-channel flow cross-over through the gas diffusion layer in a PEM-fuel cell flow system using a serpentine channel with a trapezoidal cross-sectional shape, International Journal of Thermal Sciences, 45 (10) (2006) 1021-1026

[19] D. Tehlar, R. Fluckiger, A. Wokaun, and F. N. Buchi, Investigation of channel-to-channel cross convection in serpentine flow fields, Fuel Cells, 10 (6) (2010) 1040-1049

[20] K. Jiao, J. Park, and X. Li, Experimental investigations on liquid water removal from the gas diffusion layer by reactant flow in a PEM fuel cell, Applied Energy, 87 (9) (2010) 2770-2777

[21] J. W. Park, K. Jiao, and X. Li, Numerical investigations on liquid water removal from the porous diffusion layer by reactant flow, Applied Energy, 87 (7) (2010) 2180-2186

[22] J. Bachman , A. Santamaria, H. Tang, and J. Park, Investigation of polymer electrolyte membrane fuel cell parallel flow field with induced cross flow, Journal of Power

Sources, 198 (15) (2012) 143-148

[23] S. Mazumder and J. V. Cole, Rigorous 3-D ma-thematical modeling of PEM fuel Cells, Journal of the Electrochemical Society, 150 (11) (2003) A1503-1509

[24] http://www.ciss.iis.u-tokyo.ac.jp/english/dl/

[25] https://www.eng.hokudai.ac.jp/labo/fluid/download/download.htm

[26] M. Tsubokura, T. Kobayashi, T. Nakashima, T. Nouwzawa, T. Nakamura, H. Zhang, K. Onishi, N. Oshima, Computational visualization of unsteady flow around vehicles using high performance computing, Computers & Fluids, 38 (5) (2009) 981-990

[27] M. Tsubokura, T. Nakashima, K. Kitoh, Y. Sasaki, N. Oshima, T. Kobayashi, Development of an unsteady aerodynamics simulator using large-Eddy simulation based on high-performance computing technique, SAE International Journal of Passenger Cars-Mechanical Systems, 2(1) (2009) 168-178

[28] L. K. Saha, E. Kurihara, and N. Oshima, Comparative studies of time-steeping schemes for the treatment of the Darcy drag term of the momentum equation, Journal of Fluid Science and Technology, 5 (2) (2010) 259-269

[29] L. K. Saha, Y. Tabe, and N. Oshima, Effect of GDL deformation on the pressure drop of polymer electrolyte fuel cell separator channel, Journal of Power Sources, 202 (1) (2012) 100-107

[30] L. K. Saha and N. Oshima, Prediction of flow crossover in the GDL of PEFC using serpentine flow channel, Journal of Mechanical Science and Technology, 26 (5) (2012) 1315-1320

CHAPTER FOUR

Oxygen Transport by Cross Flow

4.1 Introduction

The polymer electrolyte fuel cell (PEFC) is a promising next-generation power source for vehicles. PEFCs have attracted considerable attention because of advantages such as a low operating temperature, high efficiency, and environmental friendliness. However, for PEFCs to be commercialized, several technological problems must be resolved, including the severe water flooding of the cathode and induced mass-transfer losses [1, 2]. The distribution of reactant on the reaction site is one of most important factors affecting PEFC performance. Transport of the reactant toward the catalyst layer involves both convection-dominated flow in the gas channel and convection–diffusion mixed flow in the gas diffusion layer (GDL). Enhancement of convection flow in the GDL is beneficial because it feeds the reactant to the catalyst layer for the electrochemical reaction and reduces the accumulation of liquid water in a large part of the GDL [3-6].

Using experimental studies and numerical simulations, researchers have investigated flow-field designs to enhance the current density, the homogeneity of the reactants, and the uniformity of temperature and to overcome pressure losses and the removal of water from the cathode side [7-11]. Water flooding in the GDL under ribs is usually more serious than elsewhere at the cathode [12]. Various complex flow-channel layouts such as multiple parallel channels, interdigitated channels, serpentine channels, and other combined versions have been used for PEFCs [2]. The parallel version is the simplest and requires the smallest pressure drop because the reactant is equally distributed in many parallel paths. However, the parallel channel layout has low drainage ability compared to the serpentine channel [11]. An interdigitated flow channel is designed to allow the reactant to go directly through the GDL under the rib [13]. Because it can direct the convection in the GDL under the rib, an interdigitated flow channel can improve the reactant transport of gas to the catalyst layer and more effectively remove liquid water from the GDL to the gas flow channel in PEFCs [14-15] compared to multiple parallel channels.

Recently, studies have focused on the effect of the geometrical configuration of a gas channel on the mass, current, and heat transfer in PEFCs [9, 16-19]. Akhtar et al. [16] investigated the effect of the channel width and rib-width ratio on the cathode transport phenomena of a proton-exchange membrane fuel cell and found that increasing the channel-to-width ratio had no effect on the total liquid saturation; however, this value was significantly affected under the channel and rib regions of porous layers. The effects of cathode channel dimensions (width, depth, and height) on the performance of an air-breathing fuel cell were reported by Kumar et al. [17]. Inoue et al. [18] experimentally investigated the effect of the gas-channel depth on the current density and pressure drop and found an optimum separator. The impact of the gas-channel pitch length on the in-plane temperature distribution was measured [19], and it was found that when the gas-channel pitch length (pitch length is defined as the distance between the center of channel width and the center of rib width) was reduced, the power generation performance was improved and a uniform temperature distribution was maintained. Because the gas-channel pitch length affects uniformity and influences higher power generation, we designed our computational domain using the pitch-length concept of Nishimura et al. [19]. However, to simplify the analysis and reduce the computational cost, we considered a straight channel with various gas-channel pitch lengths instead of a serpentine channel.

A serpentine flow channel layout produces a relatively long flow path, hence, a substantial pressure drop causes a significant pressure gradient through the GDL, and the reactant gas is distributed from one channel to an adjacent channel by crossover flow through the GDL under the rib [18]. Therefore, in a PEFC, the reactant is driven to the reaction site not only by diffusion but also by convection [20]. Williams et al. [21] experimentally showed that higher GDL permeability improves the performance of PEFCs with serpentine channels. Pharoah et al. [22] observed that convection under the rib could not be ignored when the GDL permeability exceeds 10-13 m2. This convection flow has been defined as “channel-to-channel cross over” [23], “bypass flow” [11], and “flow cross over” [27]. In this study, cross flow was used to characterize this phenomenon.

The pressure drop and flow crossover through the GDL of a PEFC with a serpentine channel flow field was investigated by Sun et al. [23] using a trapezoidal channel cross section. They found that the trapezoidal cross-sectional shape ratio has a significant effect on the pressure variation in the flow field for cases with and without crossover. The cross-leakage flow through the electrode with a single serpentine channel was investigated by Kanezaki et al. as a direct result of the pressure difference between two channels [24], it was found that a significant amount of reactant gas flows through the GDL owing to the pressure difference, and enter the next flow channel. The effect of GDL deformation on the flow cross over with a serpentine flow channel design was investigated by Shi and Wang [25]. They found that cross flow decreases through the GDL from one channel to another channel with assembly compression.

Cross flow helps to remove water vapor from the catalyst layer, with serpentine flow fields producing higher current densities than parallel flow fields [26]. Park and Li [27] used numerical analysis to show that cross convection is responsible for 40% of the inlet flux in a serpentine flow field. The effects of the GDL thickness and the reactant flow rate on liquid water removal were investigated experimentally by Jiao et al. [28]. Their visualization confirmed that cross flow has a significant effect on water removal, even at low flow rates.

Improved models of serpentine flow field have been developed in the recent literature to address some of these bypassing by enhancing cross flow [29-32]. However, these do not discuss the mechanism of performance improvement by cross flow individually. In the present paper, we design a parallel flow field by inducing cross flow to isolate the contribution of cross flow on the performance of fuel cell.

On the other hand, a three dimensional, isothermal, single phase model is developed based on the 3D model of Mazumder and Cole [33] and Meng-Wang [35] research work. The present model is developed to investigate the effect of gas flow phenomena on the electrochemical reaction. In order to treat the complex flow situation such as cross flow, it was previously developed a numerical method [40] focusing the mass conservation strictly which is incorporated to their [33, 35] three dimensional single phase model to investigate the coupled flow, species transport and electrochemical aspects in a PEFCs. To check the feasibility of our developed model we intently designed such a complex flow in a polymer electrolyte fuel cell.

Therefore, the objective of this study is to check the feasibility of our developed model and to investigate the effect of cross flow on the performance of a fuel cell by inducing cross flow in a parallel flow field. We also investigated the influence of the gas-channel pitch length on the performance of fuel cell.

In the case of parallel flow field, the cross flow through the GDL under rib can be created by many ways such as: (1) applying different inlet velocities to the adjacent channels, (2) maintaining different outlet gas channel pressure, (3) using different cross sectional area of gas channel to the adjacent channels (4) supplying counter gas flow. In order to investigate the individual contribution of cross flow on the PEM fuel cell performance improvement, we have applied different inlet velocities to the adjacent gas channels.

4.2 Numerical procedures

4.2.1 Computational domain

The computational domain used for the present numerical simulation considered an entire cell consisting of an anode separator, an anode gas channel, an anode GDL, a membrane, a cathode GDL, a cathode gas channel, and a cathode separator. The schematic view of a PEFC is shown in Fig. 4.1(a). In the present study, we designed our computational domain based on the experimental observation of Nishimura et al. [19]. However, to simplify the analysis and reduce the computational cost, we modified the computational domain into a straight channel with 4-mm length; the pitch length was changed by 0.5, 1.0, and 2.5 mm.

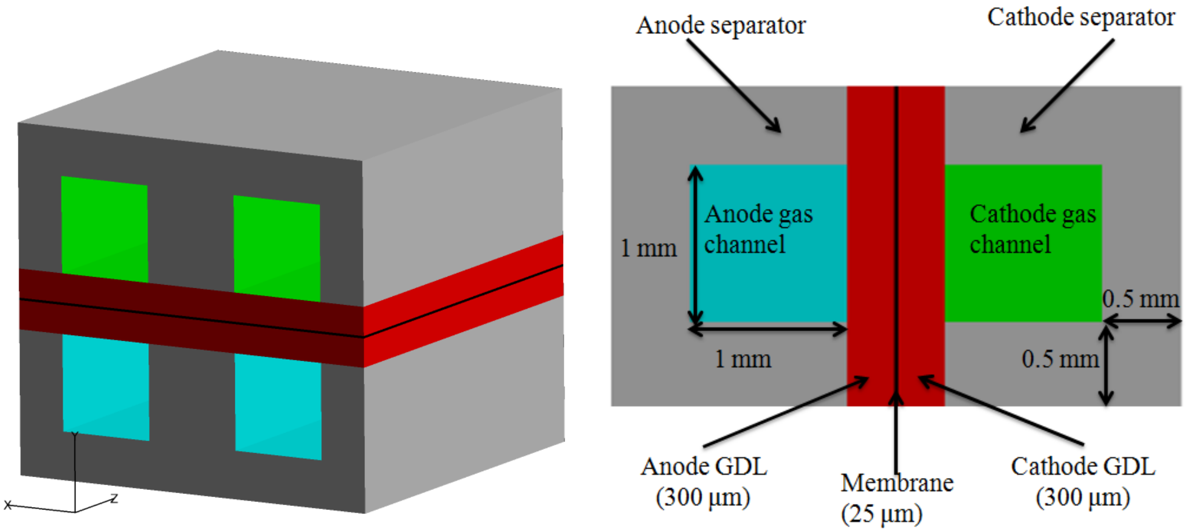

(b)

(a)

Fig. 4.1: (a) Schematic view of a PEFC (b) Half Cross sectional view of a computational domain with a pitch length of 1 mm

The pitch length was defined as the distance between center of gas channel width and the center of the rib width. Half cross sectional view of the computational domain is shown in Fig. 4.1 (b), and the design details of the computational geometry are given in Table 1.

4.2.2 Model assumptions

The fuel cell electrochemical reaction and flow-field phenomena are very complicated. To simplify our model, the following assumptions were made:

1. An ideal gas mixture exists in the gas-flow channel and the gas-diffusion layer.
2. The flow is laminar because of its small Reynolds number.
3. The physical properties of the GDL and the membrane are isotropic and homogeneous.
4. Proton conductivity of the membrane is constant.
5. Temperature is constant within the entire computational domain.
6. The gravity effect is neglected.
7. The water produced is in the vapor phase and there is no condensation or evaporation.

Table 4.1: Dimension of cell geometry

Channel type	Two parallel straight channels
Channel length	4×10^{-3} m
Channel height	1×10^{-3} m
Channel width	0.5×10^{-3} m, 1×10^{-3} m, 2.5×10^{-3} m

Rib width	0.5×10^{-3} m, 1×10^{-3} m, 2.5×10^{-3} m
Channel width: rib width	1:1
GDL thickness	300 μm
Membrane thickness	25 μm

4.2.3 Governing equations

A single set of governing equations was employed for an entire PEFC to investigate the electrochemical and transport phenomena in the fuel cell using finite volume method. The three-dimensional, single-phase, isothermal mathematical model of a PEFC is presented in this section based on previous works (Mazumder and Cole [33-34]; Meng and Wang [35]). Conservation of mass, momentum, species, and charge equations as described in the below, are numerically solved, with proper account of electrochemical kinetics. Superficial velocities are used in the momentum equation in order to automatically ensure flux continuity at the interface between the porous medium and gas channel.

In order to achieve flow field, the mass and momentum equations are numerically solved. In the momentum equation, Darcy drag term is added based on the Darcy's law, illustrating as an additional drag force which is proportional to viscosity and velocity and inversely proportional to the permeability of a porous medium. The conservation of species is solved to obtain hydrogen, oxygen and water distributions, where source terms are included based on the electrochemical reactions. In order to take accounts the proton transport in the membrane an additional charge conservation equation is solved.

Mass conservation:

$$\frac{\partial(\varepsilon\rho)}{\partial t} + \nabla\cdot(\varepsilon\rho\,\mathbf{u}) = 0 \tag{1.1}$$

Momentum conservation:

$$\frac{\partial}{\partial t}(\varepsilon\,\rho\mathbf{u}) + \nabla\cdot(\varepsilon\rho\,\mathbf{uu}) = -\varepsilon\nabla p + \nabla\cdot\left(\mu^{*}\,\nabla\mathbf{u}\right) + \varepsilon\rho\,\mathbf{g} - \frac{\varepsilon\mu^{*}\,\mathbf{u}}{K} \tag{1.2}$$

Here, **u** is the velocity vector, ρ is the density, μ^{*} is the effective viscosity approximated by the model of $\mu^{*} = \varepsilon\mu$, where μ is the intrinsic viscosity, ε is the porosity of the GDL, and *K* is the permeability of the GDL. The porosity ε is defined as the ratio of the volume occupied by the pores to the total volume of the porous medium, whereas the permeability *K* is defined as the ratio of the square of the effective volume to the surface area of the porous matrix [33].The last term of equation (1.2) represents the Darcy's drag force in the porous media. In the gas channel, $\varepsilon \rightarrow 1$ and K→∞, so equation (1.2) becomes the original Navier-Stokes equation.

Species conservation:

$$\frac{\partial}{\partial t}(\varepsilon\rho Y_i) + \nabla\cdot(\varepsilon\rho\,\mathbf{u}Y_i) = \nabla\cdot\mathbf{J}_i + \omega_i \tag{1.3}$$

Charge conservation:

Electrons

$$\nabla \cdot \left(\sigma^{eff} \nabla \Phi_s\right) + S_{\Phi_s} = 0 \tag{1.4}$$

Protons

$$\nabla \cdot \left(k^{eff} \nabla \Phi_{\mathrm{f}}\right) + S_{\Phi} = 0 \tag{1.5}$$

The diffusion flux of species is given by the Stefan–Maxwell equation:

$$\mathbf{J}_i = \rho D_i^{eff} \nabla Y_i + \frac{\rho Y_i}{M} D_i^{eff} \nabla M - \rho Y_i \sum_j D_i^{eff} \nabla Y_j - \frac{\rho \nabla M_i}{M} \sum_j D_i^{eff} Y_j \tag{1.6}$$

Here, M is the molecular weight of the mixture and D_i^{eff} is the effective mass diffusivity given by the following expression [35]:

$$D_i^{eff} = \left[\varepsilon_d (1-s)\right]^{1.5} D_i$$

The last term in Eq. (1.3) represents the generation or consumption of species resulting from electrochemical reactions:

$$\omega_i = -\frac{M_i\, m_i}{n\,F}\, j$$

Here, m_i and n are the stoichiometry coefficient and the number of electrons transferred in the electrochemical reactions, respectively [35], which are expressed as follows:

$$\sum_i m_i\, X_i = n\, e^-$$

Here, X_i denotes chemical formula of species i.

The source terms in Eqs (1.4) and (1.5) are:

$$S_{\Phi_s} = j_a \tag{1.7}$$

$$S_{\Phi} = j_c \tag{1.8}$$

In Eqs. (1.7) and (1.8), j is the exchange current density, which can be expressed as follows [35]:

Anode:

$$j_a = a\, j_{0,a}^{ref} \left(\frac{C_{H_2}}{C_{H_2,ref}} \right)^{1/2} \left(\frac{\alpha_a + \alpha_c}{RT} F \eta_a \right) \tag{1.9}$$

Cathode:

$$j_c = -a\, j_{0,c}^{ref} \left(\frac{C_{O_2}}{C_{O_2,ref}} \right) \exp\left(-\frac{\alpha_c}{RT} F \eta_c \right) \tag{1.10}$$

Here, the surface over-potential η is defined as follows:

Anode:

$$\eta_a = \Phi_s - \Phi_f \tag{1.11}$$

Cathode:

$$\eta_c = \Phi_s - \Phi_f - U_0 \tag{1.12}$$

Here, the open-circuit potential is expressed as follows:

$$U_{OC} = 1.23 - 0.9 \times 10^{-3}(T - 298) + \frac{RT}{2F}\left(\ln(P_{H2}) + \frac{1}{2}\ln(P_{O2})\right) \tag{1.13}$$

Table 4.2: (a) **Cathode inlet operating conditions**

Case	Channel A	Channel B
Case 1	Inlet velocity = 0.1 m s^{-1}	Inlet velocity = 0.1m s^{-1}
Case 2	Inlet velocity = 4.0 m s^{-1}	Inlet velocity = 4.0 m s^{-1}
Case 3	Inlet velocity = 4.0 m s^{-1}	Inlet velocity= 0.1 ms^{-1}

(b) **Anode inlet operating conditions**

Case	Channel A	Channel B
Case 1, Case 2, and Case 3	Inlet velocity = 0.1 m s^{-1}	Inlet velocity= 0.1 m s^{-1}

Table 4.3: Electrochemical and transport properties with operating conditions

Anode exchange current density, $a\,j_0$ (A/m^3)	9.23×10^8

Cathode exchange current density, $a\,j_0$ (A/m^3)	3×10^2
Reference hydrogen current density, c_{H_2}	40 [35]
Reference oxygen current density, c_{O_2}	40 [35]
Anode transfer coefficient, α_a	1 [35]
Cathode transfer coefficient, α_c	1 [35]
Faraday constant, F	96485
Electronic conductivity in solid materials (S/m)	20000 [35]
Electronic conductivity in GDL (S/m)	300 [35]
Protonic conductivity in membrane (S/m)	6.0 [36]
GDL permeability	1.76×10^{-11} m^2 [20]
Porosity	0.7 [20]
Anode/cathode pressure	0.2 M Pa
Temperature	343 K
Relative humidity	60% (anode and cathode both sides)

Cathode gas composition	0.8% O_2 with N_2
Anode gas composition	H_2
Cell operating voltage	0.6 V

4.2.4 Boundary conditions

No-slip boundary was used on all wall boundaries. A constant velocity was applied at the inlet of the gas channel. A constant pressure of 0.2 MPa was maintained at the outlet of the channel.

4.2.5 Solution Procedures

The governing equations described in the previous section were solved for the single phase, isothermal, three dimensional PEFC. A finite volume method was employed to discretize the set of governing equations together with boundary conditions and was solved using the software FrontFlow/red. This is non-commercial software and open to use as free for all [37]. The computational code FrontFlow/red, which was originally developed under the project of "Frontier Simulation Software for industrial Science" and optimized for vehicle aerodynamics simulation by Tsubokura et al.[38-39]. Later on, the PEFC model is implemented into the software FrontFlow/red under the project of "New Energy and Industrial Technology Development Organization" (NEDO). The Euler implicit scheme was used for time integration, and the first-order upwind scheme was used to discretize the convection terms in the governing equations.

The fractional-step algorithm was used to update the pressure and velocity fields from solutions of the pressure Poisson equations. The fractional-step algorithm was developed by considering an implicit treatment of the Darcy drag term with attention to strict mass conservation. Details of the advantages of this algorithm have been described previously [40], and the algorithm was incorporated in our FrontFlow/red (for PEFC) simulation code. This simulation code previously was validated using small-scale calculations on the deformation of the GDL [41]. Furthermore, our group [20] recently derived numerical predictions of the amount of flow crossover through the GDL for five multiple serpentine channels and obtained results that were in good agreement with experimental measurements, thereby providing additional validation of our numerical scheme. The convergence of an iterative solution was determined when the relative residual error between iterations was less than 10^{-7}.

The cathode inlet velocity was kept constant for all of the cases given in Table 2. However, the anode inlet velocity was fixed as Case 1 for all cases simulated in the present calculation

Table 3 lists the physical properties and parameters used in the numerical simulation. The simulation was carried out in such a way so that oxygen transport resistance became much higher. The supplied oxygen concentration was 0.8% with a relative humidity 60% and N_2. Then we explained how to reduce the oxygen transport resistance by the means of convective flow. In this paper, the convective flow has been treated by two ways: (1) Convective flow in the gas channel caused by inlet velocity (2) Convective flow through the GDL under the rib caused by cross flow.

4.3 Results and Discussion

The numerical procedure described above and the operating conditions and physical parameters listed in Table 2 and Table 3 were used to obtain the numerical results presented in the following section. All the results except the polarization curve have been discussed with operating voltage 0.6 V.

4.3.1 Effect of pitch length

4.3.1.1 Oxygen mass fraction distribution

Fig. 4.2 shows the oxygen mass fraction distribution at the middle section of the gas channel for various pitch lengths with a GDL thickness of 300μm for Case 1 and Case 2. In this simulation, three distinct gas-channel pitch lengths were considered. The velocity was kept constant for all values of the gas-channel pitch length.

Left: pitch length = 0.5 mm, middle: pitch length = 1.0 mm, and right: pitch length = 2.5 mm.

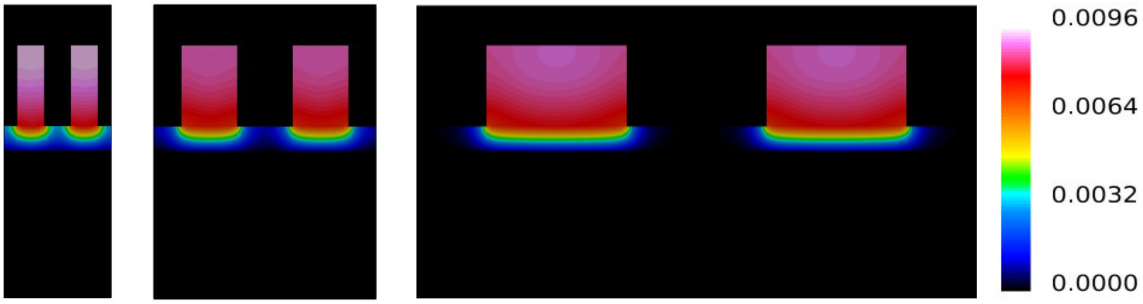

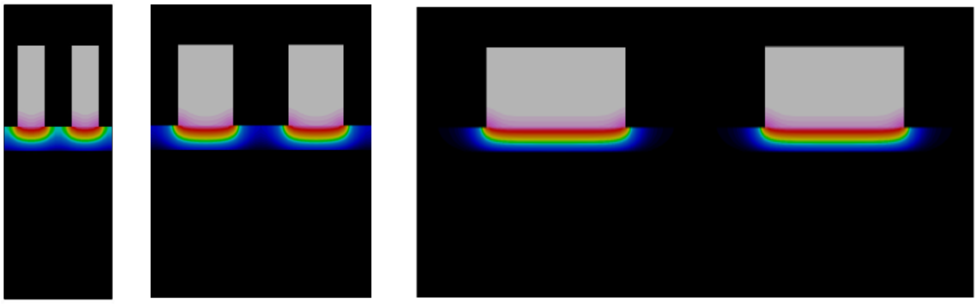

Fig. 4.2: The effect of the gas-channel pitch length on the oxygen mass fraction distribution in the middle cross section of the cell for Case 1 (upper three) and Case 2 (lower three)

Fig. 4.2 shows that the oxygen mass fraction in the gas channel is higher than that of the GDL. The mass fraction of oxygen decreased noticeably inside the GDL, and the effect of oxygen depletion was significant, particularly under the rib areas.

Moreover, the oxygen mass fraction through the GDL under the rib decreased when the gas-channel pitch length increased. As the inlet velocity increases, the oxygen mass fraction in the gas channel would increase regardless of the gas-channel pitch length. With the increase of inlet velocity, the convection flow in the gas channel would increase, causing the oxygen concentration gradient through the GDL to become higher. Therefore, the transfer of oxygen mass flux through the GDL toward the catalyst layer would increase because of the higher concentration gradient in the GDL, causing an enhancement in the electrochemical reactions, which can significantly increase the performance of the fuel cell.

4.3.1.2 Current density distribution

Fig. 4.3 shows the current density distribution on the middle section in the PEM for various gas-channel pitch lengths for Case 1 and Case 2. The current density distribution under the channel was higher than under the rib because the diffusion path for oxygen transport in the catalyst layer under the rib was longer than under the flow channel.

Left: pitch length = 0.5 mm, middle: pitch length = 1.0 mm, and right: pitch length = 2.5 mm.

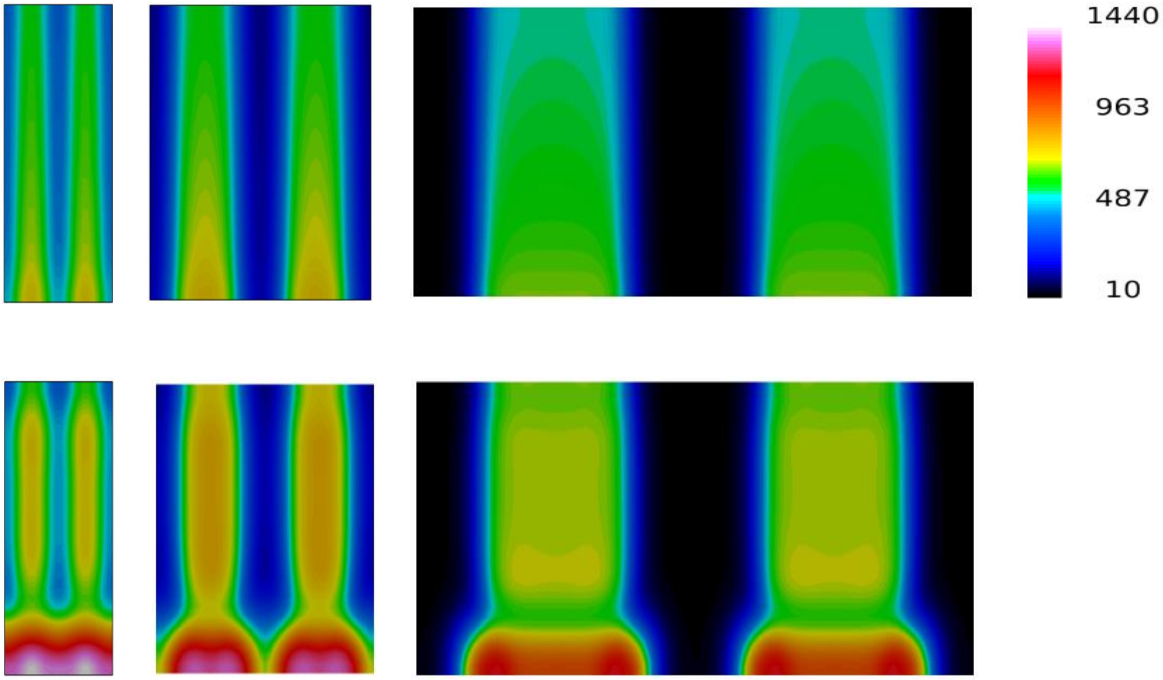

Fig. 4.3: The effect of pitch length on the current density (A/m2) distribution at the middle cross-section in the membrane for Case 1 (upper three) and Case 2 (lower three)

The current density gradually decreased along the flow channel direction from the channel inlet position to the channel outlet position as oxygen was consumed gradually by the electrochemical reaction. As the inlet velocity increased, the current density increased for any value of the gas-channel pitch length. The one-dimensional plot of the current density is drawn at the middle position of Fig. 4.3; this is shown in Fig. 4.4. By comparing the solid and dashed lines for any value of gas channel pitch length in Fig. 4.4, we confirmed that the gap between two curves is the result of increased convective flow in the gas channel as the inlet velocity increases. For example, comparing the two red curves (solid and dashed lines) in Fig. 4.4 shows that the gap between the two lines was caused by increased convective flow in the gas channel, which results from increasing the inlet velocity. In addition, the gas-channel convection flow on the current density was more pronounced under the channel than under the rib.

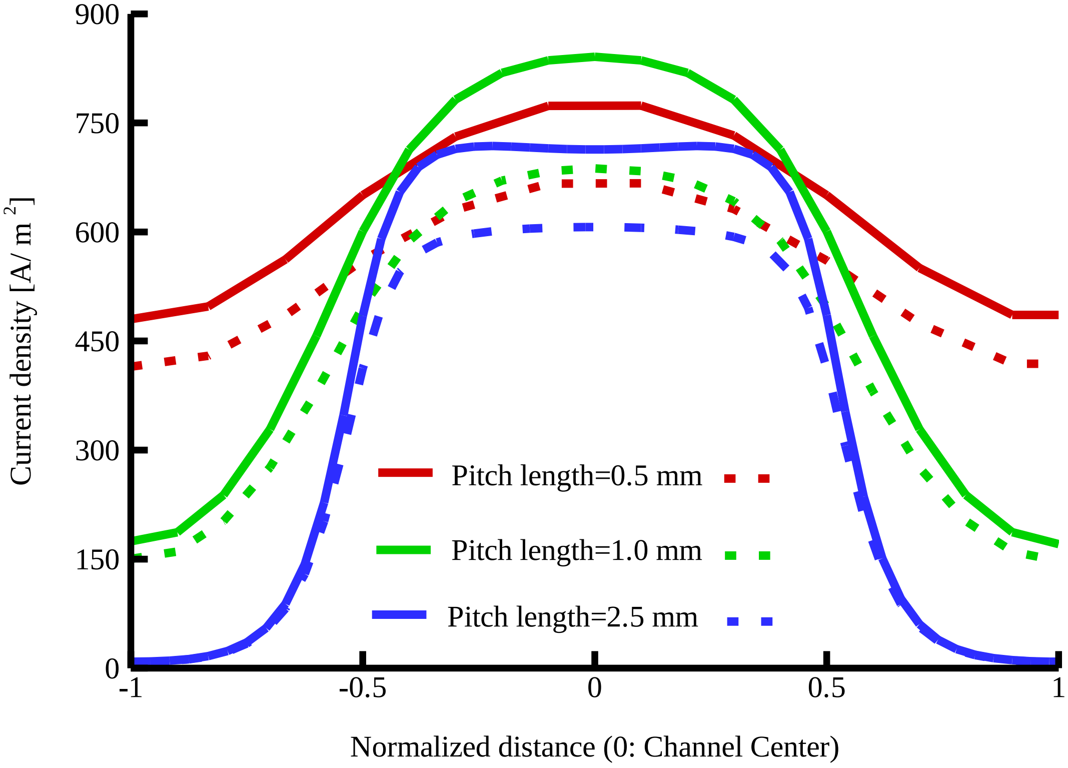

Fig. 4.4:The current density distribution along in-plane direction in the mid-length of the cell for various gas channel pitch lengths for Case 1 (dashed lines) and Case 2 (solid lines)

The maximum current density under the channel was obtained for a pitch length of 1.0 mm, whereas a more uniform current density was maintained by a smaller pitch length (0.5 mm). As the gas-channel pitch length decreased, the current density profile became more uniform. Therefore, improved performance can be achieved by using a gas channel with a smaller pitch length.

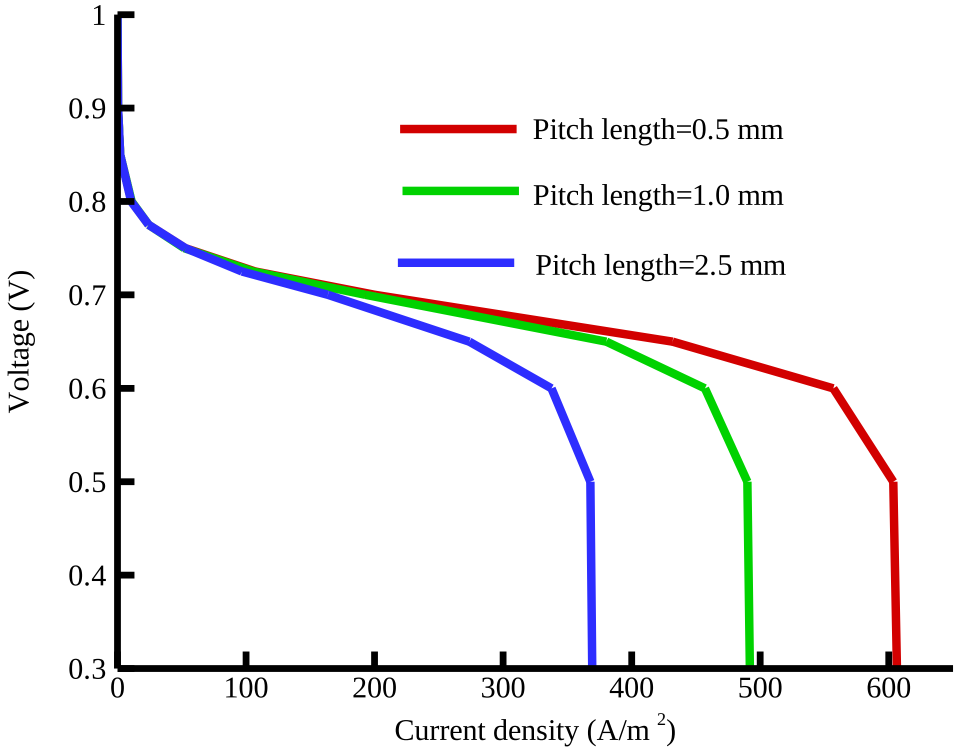

Fig. 4.5: Polarization curve for various gas channel pitch length with Case1

4.3.1.3 Polarization curve by pitch length

The Fig. 4.5 shows the polarization curve for various gas channel pitch length with Case 1.

The polarization curves provided that the effects due to the oxygen exhaustion in the flow field have a variation. With decreasing the gas channel pitch length the limiting current density increases. Since, with the increase of inlet velocity local current density increases in Fig. 4.4, therefore the limiting current density in the polarization would also increase. The sharp declination appears in the mass transport region for all the cases as the oxygen supplied was limited in our present simulation. However, the polarization curve is well predicted by our present developed model as it can capture all the physics including activation loss, ohmic loss and mass transport loss although we used simplified geometry and very special conditions of oxygen transport. Therefore, the newly developed three dimensional computational models was successfully applied to compute gas flow characteristics and to evaluate the performance of fuel cells.

4.3.2 Effect of cross flow

In the above section we have discussed how our present model works with the explanation of species transport phenomena, current density distribution, and polarization curve prediction. With similar manner, the following section the mechanism of fuel cell performance improvement by cross will be discussed. To predict the effect of cross flow on the individual performance of fuel cells, we performed a simulation with three different cases, as summarized in Table 2.

4.3.2.1 Pressure and velocity distribution

To explain the contribution of cross flow to performance, the cross-flow mechanism must first be understood. The cross-flow effect was predicted in a layout with two parallel straight channels with a gas-channel pitch length of 0.5 mm and GDL thickness of 300 μm.

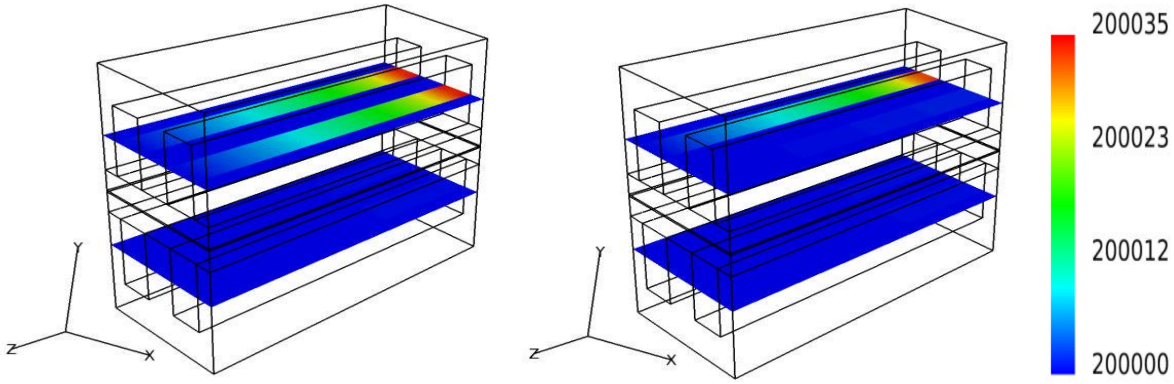

(a) (b)

Fig. 4.6: Pressure distribution (Pa) in the middle section of the gas channel for (a) Case 2 and (b) Case 3

We applied three different velocities to the cathode gas inlet; in the first two cases, an identical inlet velocity was applied to both cathode gas channels. For this reason, the pressure distribution in the two parallel cathode gas channels was essentially the same for each case, as shown in Fig. 4.6. The inlet velocity was larger for Case 2 than for Case 1 prompted a change in the pressure distribution in the cathode gas channel for Case 2; the pressure distributions of both cathode gas channels are shown in Fig. 4.6. Because no pressure difference existed between adjacent channels for Case 1 and Case 2, no cross flow appeared. However, for Case 3, a different gas inlet velocity was applied to the two adjacent gas channels in the cathode side, which caused the pressure distribution to differ between the adjacent gas channels. The significant pressure difference between adjacent channels produced a large pressure gradient through the GDL.

As a result, a significant amount of reactant gas flowed through the GDL and under the rib, from a high-pressure region of the gas channel to a low-pressure region, as shown in Fig. 4.7. In this process, the reactant gas was distributed through the GDL owing to the different pressure of the adjoining channel by the way of cross flow. The cross-flow velocity at the middle of the gas channel is shown in figure 4.7.

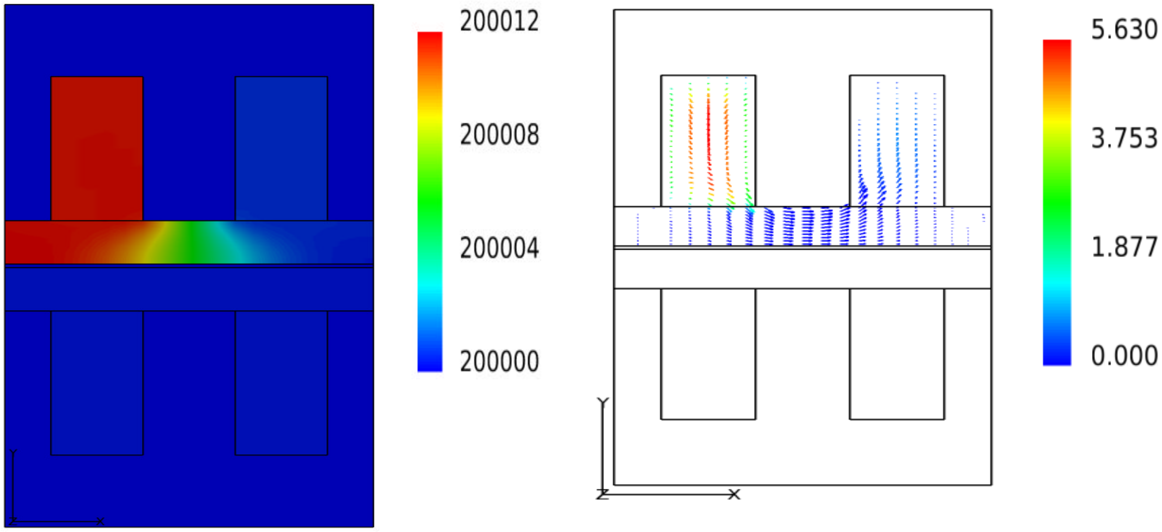

Fig. 4.7: Distribution of pressure (Pa) and velocity (m s^{-1}) in the gas channel and the GDL on the *x*–*y* plane at the middle cross section of the cell (at z = 2 mm).

The relationship between the cross-flow velocity and the pressure difference between adjacent channels is shown in Fig. 4.8. The cross-flow velocity and pressure difference between adjacent channels are linearly proportional, which means that a greater pressure difference between adjacent channels corresponds to a higher cross-flow velocity.

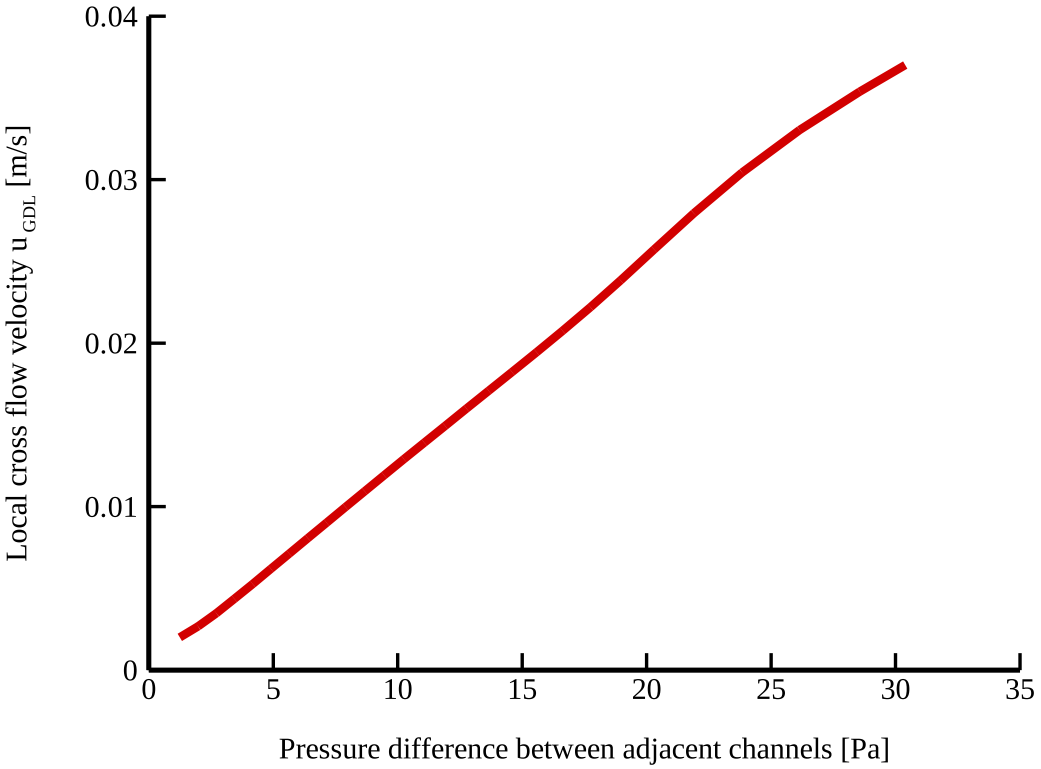

Fig. 4.8: Relationship between cross-flow velocity and pressure difference between adjacent channels

4.3.2.2 Oxygen mass fraction distribution

Fig. 4.9 shows the oxygen mass fraction distribution at the middle section of a single cell for Case 1, Case 2, and Case 3. Because the velocity in Case 2 was higher than in Case 1, the oxygen mass fraction distribution in the gas channel was higher for Case 2. The oxygen concentration gradient through the GDL increased as the inlet velocity increased. Cross flow through the GDL was previously observed for Case 3 (see Fig. 4.7). This cross flow plays an important role in distributing the oxygen mass fraction in the channel and the GDL, as depicted in Fig. 4.9, which shows the transport of a large amount of oxygen through the GDL, especially under the rib. The oxygen mass fraction distribution is enhanced through the GDL under the rib. Therefore, cross flow through the GDL under the rib significantly facilitate the oxygen transport towards the catalyst layer. Hence, cross flow can reduce the depletion of oxygen through the GDL, particularly under the rib. The enhancement of oxygen transport can also improve the local current density distribution of a PEFC.

4.3.2.3 Current density distribution

Fig. 4.10 shows the current density distributions for Case 1, Case 2, and Case 3. The current density increases when the inlet velocity increases.

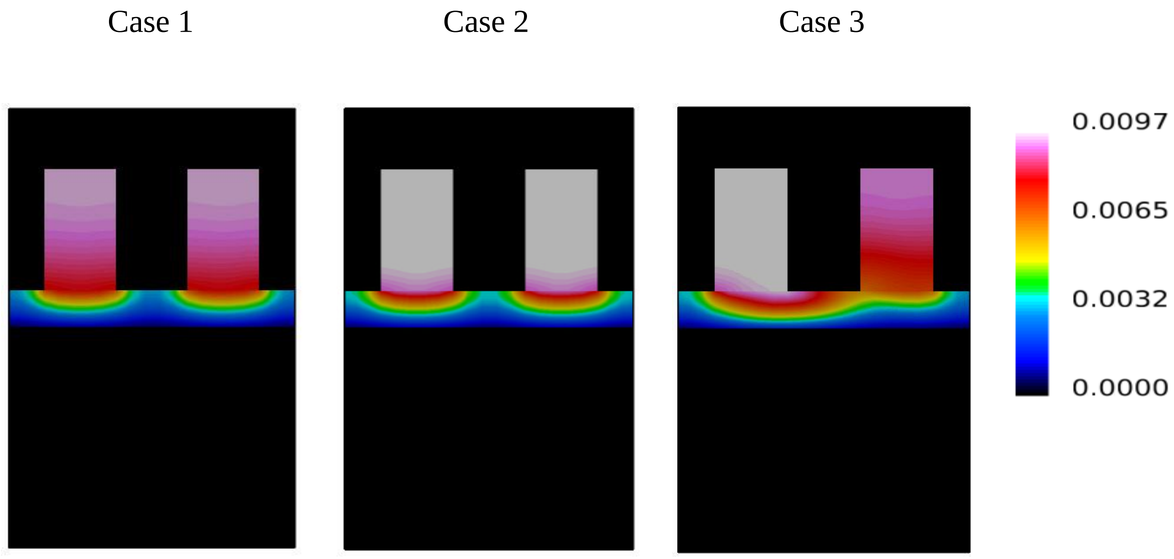

Fig. 4.9: The oxygen mass fraction distribution at the middle cross-section of the cell for Case 1, Case 2, and Case 3.

In Case 3, cross flow was induced in the parallel flow field by applying two different velocities in the adjacent channels. Because the differential pressure between adjacent channels causes a significant pressure gradient through the GDL, there was a large amount of flow crossover across the GDL.

For this reason, the current density under the rib increased because of cross flow. Finally, this cross flow between adjacent channels significantly changed the current density distribution over the entire reactive area. From Fig. 4.11, it is evident that the current density under the rib increased significantly for Case 3.

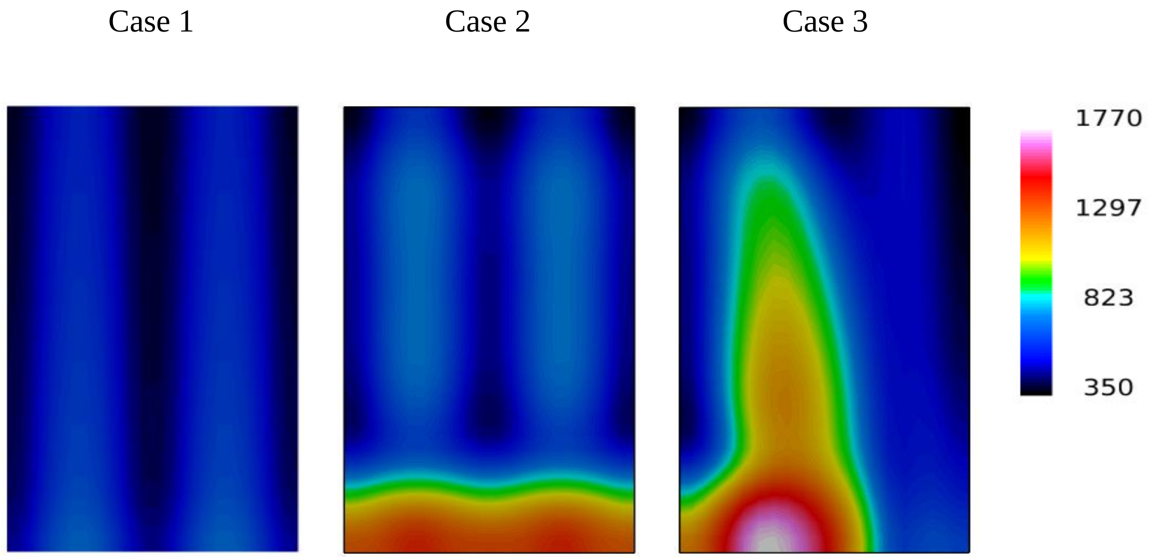

Fig. 4.10: The current density (A/m^2) distribution on the middle cross-section in the membrane for Case 1, Case 2, and Case 3

However, under the low pressure gas channel, the current density decreased slightly because oxygen could not move toward the catalyst layer owing to the transport of reactant gas through the GDL from the high-pressure to the low-pressure regions of the gas channel. In addition, simultaneous cross flow increased the overall degree of non-uniformity in the current density distribution.

4.3.2.4 Polarization curve by cross flow

The polarization curve of pitch length 0.5 mm is shown in Fig. 4.12 with Case 1, Case 2 and Case 3. In the previous section, it has already been discussed the performance enhancement from Case 1 to Case 2. The polarization curve provided that the performance increases in the mass transport region while cross flow is induced through the GDL and in between two channels by Case 3.

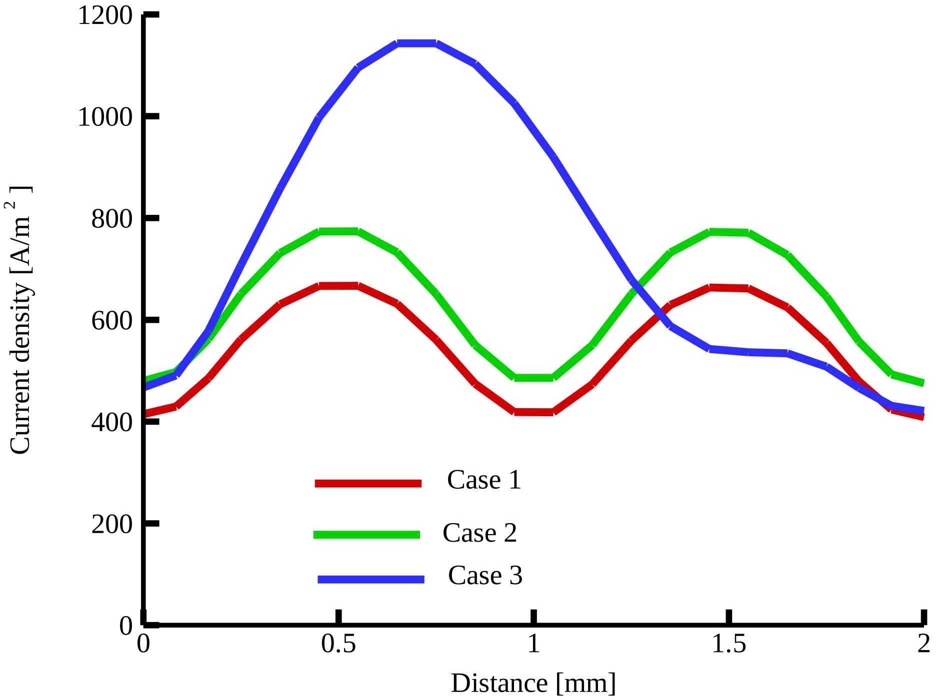

Fig. 4.11: The current density distribution along the in-plane direction in the mid-length of the cell for Case 1, Case 2, and Case 3

Since the cross flow through GDL facilitate the oxygen transport towards the catalyst layer (see Fig. 4.9), therefore the limiting current density increases when the cross flow is applied through the GDL under the rib by Case 3. The sharp declination appears in the mass transport region of polarization curve for all the cases. Because, in our present simulation the supplied oxygen was much lower, therefore further growth of current is not possible.

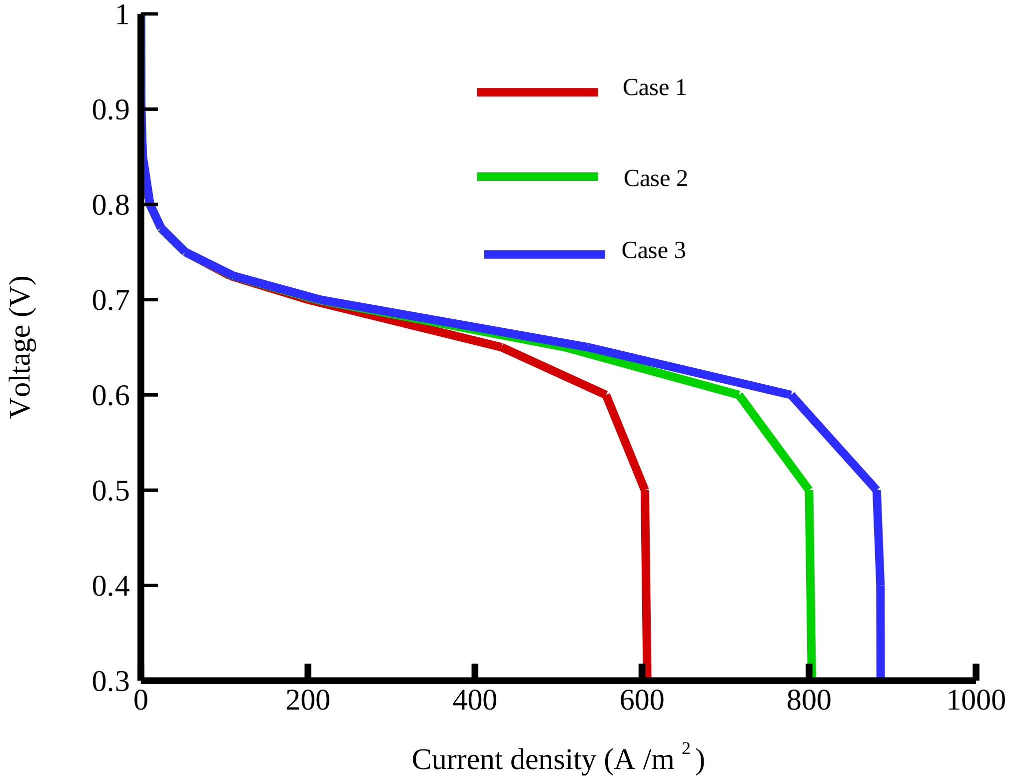

Fig. 4.12: The polarization curve for Case 1, Case 2 and Case 3 with a pitch length 0.5 mm

4.4 Conclusion

A three dimensional, single -phase, isothermal study of a polymer electrolyte fuel cell (PEFC) has been conducted and explained the mechanism of convective flow effect on the performance of fuel cell numerically. We identified the individual contributions to cross flow and clarified the influence of convective flow on current density and oxygen mass fraction distribution. We summarize our conclusions as follows:

1. The pitch length of the gas channel had a large effect on the performance of the fuel cell. We found that as the gas-channel pitch length decreased, the current density profile became more uniform. The improved performance can be achieved by using a gas channel with a smaller pitch length. The convection flow in the gas channel caused by the inlet gas velocity can also increase the performance in the mass transport region of polarization curve.

   In our present simulation the obtained polarization curves show the similar behavior like an optimized design although we used simplified geometry and very special conditions of oxygen transport. Therefore, the newly developed three dimensional single phase computational model was successfully applied to compute gas flow characteristics and to evaluate the performance of fuel cells.

2. The cross flow through the GDL under the rib significantly facilitate the oxygen transport towards the catalyst layer. This cross flow can increase the performance of fuel cell in the mass transport region of polarization curve by reducing the oxygen transport resistance, although this also increases the non-uniformity in local current

density. Therefore, it is possible to overcome the oxygen transport limitation by cross flow.

The present technique of using our simplified geometry could be a valuable tool for understanding the mechanism of cross flow and its effect on oxygen transport and current density distribution. This study of cross flow by inducing in the parallel channel layout may also help the manufacturer to design the flow field.

In the present study, in order to avoid the existence of liquid water in the cell, the contribution of cross flow has been evaluated on the performance of fuel cell under a very special condition (oxygen concentration 0.8%). Although having low concentration of oxygen and simplified geometry, the role of cross flow regarding the oxygen transport towards the catalyst layer has been evaluated successfully, consequently the PEM fuel cell performance improvement by cross flow. The effect of cross flow on the performance of PEM fuel cell also would be survived with high current density operation. However, the present simulation didn't treat operating PEM fuel cell with high current density as it induces liquid water in the cell. Therefore, for high current density operation two phase modeling is needed to predict the fuel cell performance improvement by cross flow. Furthermore, it is expected that cross flow may improve the performance of fuel cell by removing the liquid water from the cell which should be investigated under practical operation of PEM fuel cell.

4.5 References

[1] Xu C., Zhao T. S., A new flow field design for polymer electrolyte-based fuel cells, *Electrochemistry communications* ,9 2007, pp.497-503

[2] Li X., Sabir I., Review of bipolar plates in PEM fuel cells: Flow Field designs, *International Journal of Hydrogen Energy*, 30, 2005, pp. 359-371

[3] Li X., Sabir I., Park J., A flow channel design procedure for PEM fuel cells with effective water removal, *Journal of Power Sources*, 163, 2007, pp. 933-942

[4] Williams M. V., Kunz H. R., Fenton J., Influence of convection through Gas-diffusion layes on limiting current in PEM FCs using a serpentine Flow Field, *J. Electrochemical Society*, 151, 2004, pp. A1617-A1627

[5] Feser J. P., Prasad A. K., Advani S. G., On the relative influence of convection in serpentine flow fields of PEM Fuel cells, *Journal of Power Sources*, 161, 2006,pp 404-412

[6] Suresh P. V. and Jayanti S., Effect of air flow on liquid water transport through a hydrophobic gas diffusion layer of a polymer electrolyte membrane fuel cell, *International Journal of Hydrogen Energy*, 35, 2010, pp. 6872-6886

[7] Nishimura A., Shibuya K., Morimoto A., Tanaka S., Hirota M., Nakamura Y., Kojima M., Narita M., Investigattion on impact of separator structure on in-plane distribution of coupling phenomena in single cell of PEFC to realize uniform distribution, *Journal of Thermal Science and Technology*, 5 , 2010, pp, 319-341

[8] Spernjak D., Prasad A. K., Advani S. G., In situ comparison of water content and dynamics in parallel, single-serpentine and interdigitated flow fields of polymer

electrolyte membrane fuel cells, *Journal of Power Sources*, 195, 2010, pp. 3553-3568

[9] Jeon D. H., Greenway S., Shimpalee S., Zee J. W. V., The effect of serpentine flow-field designs on PEM fuel cell Performance, *International Journal of Hydrogen Energy*, 33, 2008, pp. 1052-1066

[10] Dutta S., Shimpalee S., Zee J. W. V., Three dimensional numerical simulation of straight channel PEM fuel cells, *Journal of Applied Electrochemistry,* 30, 2000, pp. 135-146

[11] Tabe Y., Kikuta K., Chikahisa T., Kozaki M., Basic evaluation of separator type specific phenomena of polymer electrolyte membrane fuel cell by the measurement of water condensation characteristics and current density distribution, *Journal of Power Sources,* 193, 2009, pp. 416-424

[12] Naing K. S. S., Tabe Y., Chikahisa T., Performance and liquid water distribution in PEFCs with different anisotropic fiber directions of the GDL, *Journal of Power Sources*, 196, 2011, pp. 2584-2594

[13] Nguyen T. V, A gas distributor for proton-exchange membrane fuel cells, *Journal of Electrochemical Society*, 143, 1996, pp. L103-L105

[14] Um S., Wang C. Y., Three dimensional analysis of transport and electrochemical reactions in polymer electrolyte fuel cells, *Journal of Power Sources*, 125, 2004, pp. 40-51

[15] Hu G., Fan J., Chen S., Liu Y., Cen K., Three-dimensional numerical analysis of proton exchange membrane fuel cells (PEMFCs) with conventional and interdigitated flow fields, *Journal of Power Sources*, 136, 2004, pp. 1-9

[16] Akhtar N., Kerkhof P. J. A. M., Effect of Channel and rib width on transport phenomena within the cathode of a proton exchange membrane fuel cell, *International Journal of Hydrogen Energy*, 36, 2011, pp. 5536-5549

[17] Kumar P. M., Kolar A. K., Effect of cathode channel dimensions on the performance of an air-breathing PEM fuel cell, *International Journal of Thermal Sciences*, 49, 2010, pp. 844-857

[18] Inoue G., Matasukuma Y., Minemoto M., Effect of gas channel depth on current density distribution of polymer electrolyte fuel cell by numerical analysis including gas flow through gas diffusion layer, *Journal of Power Sources*, 157, 2006, pp. 136-152

[19] Nishimura A., Shibuya K., Morimoto A., Tanak S., Hirota M., Nakamura Y., Kojima M., Narita M., Hu E., Dominant factor and mechanism of coupling phenomena in single cell of polymer electrolyte fuel cell, *Applied Energy*, 90, 2012, pp. 73-39

[20] Saha L. K., Oshima N., Prediction of flow crossover in the GDL of PEFC using serpentine flow channel, *The Journal of Mechanical Science and Technology*, 26, 2012, pp.1315-1320

[21] Williams M. V., Kunz H. R., Fenton J. M., Influence of Convection Through Gas-Diffusion Layers on Limiting Current in PEMFCs Using a Serpentine Flow Field, *Journal of the Electrochemical Society*, 151,2004, pp. A1617-A1627

[22] Pharoah J. G. On the permeability of gas diffusion media used in PEM fuel cells, *Journal of Power Sources*, 144, 2005, pp. 77-82

[23] Sun L., Oosthuizen P. H., McAuley K. B., A numerical study of channel-to-channel flow cross-over through the gas diffusion layer in a PEM-fuel cell flow system using a

serpentine channel with a trapezoidal cross-sectional shape, *International Journal of Thermal Sciences*, 45, 2006, pp. 1021-1026

[24] Kanezaki T., Li X., Baschuk J. J., Cross leakage flow between adjacent channels in PEM fuel cells, *Journal of Power sources*, 162, 2006, pp. 415-425

[25] Shi Z., Wang X., A numerical study of flow crossover between adjacent channels in a proton exchange membrane fuel cell with serpentine flow field, *Journal of Power Sources*, 185, 2008, pp. 985–992

[26] Prasad K. B. S., Jayanti S., Effect of channel-to-channel cross flow on local flooding in serpentine flow fields, *Journal of Power Sources*, 180, 2008, pp. 227-231

[27] Park J., Li X., An experimental and numerical investigation on the cross flow through gas diffusion layer in a PEM fuel cell with a serpentine flow channel, *Journal of Power Sources*, 163, 2007, pp. 853-863

[28] Jiao K., Park J., Li X., Experimental investigations on liquid water removal from the gas diffusion layer by reactant flow in a PEMFC fuel cell, *Applied Energy*, 87, 2010, pp. 2770-2777

[29] Suresh P. V., Jayanti S., Deshpande A. P., Haridoss P., An Improved flow field with enhanced cross flow for fuel cell applications, *International Journal of Hydrogen Energy*, 35, 2011, pp. 6067-6072

[30] Choi K. S., Kim H. M., Moon S. M., An experimental study on the enhancement of the water balance, electrochemical reaction and power density of the polymer electrolyte fuel cell by under-rib convection, *Electrochemistry Communications*, 13, 2011, pp. 1387-1390

[31] Nam J. H. , Lee K. J., Sohn S., Kim C. H., Multi-pass serpentine flow fields to enhance under rib convection in polymer electrolyte membrane fuel cells: design and geometrical characterization, *Journal of Power Sources*, 188, 2009, pp. 14-23

[32] Xu C., Zhao T. S., A new flow field design for polymer electrolyte-based fuel cells, *Electrochemistry Communications*, 9, 2007, pp. 497-503

[33] Mazumder S., Cole J, V., Rigorous 3-D mathematical modeling of PEM fuel cells" I. Model predictions without liquid water transport, Journal of the Electrochemical Society, 150, 2003a, pp. 1503-1509

[34] Mazumder S., Cole J. V., Rigorous 3-D mathematical modeling of PEM fuel cells I. Model predictions with liquid water transport, Journal of the Electrochemical Society, 150, 2003 b pp. 1510-1517

[35] Meng H., Wang C. Y., Electron Transport in PEFCs, Journal of the Electrochemical Society, 151, 2004, pp. A358-A367

[36] Berning T., Lu D. M., Djilali N., Three dimensional computational analysis of transport phenomena in a PEM fuel cell, Journal of Power Sources, 106, 2002, pp. 284-294

[37] http://www.ciss.iis.u-tokyo.ac.jp/english/dl/

[38] Tsubokura M., Kobayashi T., Nakashima T., Nouzawa T., Nakamura T., Zhang H., Onishi K., Oshima N., Computational visualization of unsteady flow around vehicles using high performance computing, *Computers & Fluids*, 38, 2009, pp. 981-990

[39] Tsubokura M., Nakamshima T., Kitoh K., Sasaki Y., Oshima N., Kobayashi T., SAE Int. J. Passenger Cars; Mech. Syst. 2 (2009) 168-178

[40] Saha L. K., Kurihara E., Oshima N., Comparative Studies of Time-stepping Schemes

for the Treatment of the Darcy Drag Term of the momentum Equation, *Journal of Fluid Science and Technology*, 5, 2010, pp. 259-269

[41] Saha L. K., Tabe Y., Oshima N., Effect of GDL deformation on the pressure drop of polymer electrolyte fuel cell separator channel, *Journal of Power Sources*, 202, 2012, pp. 100-107

CHAPTER FIVE

Water Transport through the Membrane

5.1 Introduction

Because of its high power density and low operating temperature, the PEM fuel cell is thought to be a promising candidate for mobile and vehicle applications and for use in distributed power systems. However, some technical problems remain to be solved in achieving practicability and commercialization. One technical challenge is that of maintaining an optimal level of water within the cell by managing the transport of water into the cell and its removal from the cell. On the one hand, sufficient water is needed to maintain the proton conductivity of the PEM but, on the other hand, the accumulation of too much liquid water in the cathode can cause flooding, obstructing transport of the oxygen reactant from the gas channel to the reaction sites of the catalyst layer.

This chapter will focus on the transport of water in the membrane of a polymer electrolyte fuel cell. A key element in ensuring optimal performance of a PEM fuel cell is the proper management of water. There is a complex relationship between the water content of a PEM fuel cell and the cell's performance. The water content, which has a close relationship to the proton conductivity, directly controls the performance of a

PEM fuel cell (Springer et al., 1991). Failing to manage water properly results in either flooding or drying out in the membrane of the cell.

There are four basic modes for water transport across the PEM.

1. **Back diffusion**: Water transport as a result of the concentration gradient-driven flow from the cathode side to the anode side.

2. **Electro osmotic drag**: Water transport from the anode side to the cathode side through the membrane as a result of proton transporting through the membrane.

3. **Hydraulic permeation**: Water transport through the membrane as a result of gas or capillary pressure gradient between anode and cathode side.

4. **Thermo osmosis flux:** Thermo osmosis water flux is caused by the temperature-gradient.

Electro osmotic drag and back diffusion are basic mechanisms for water transport in the PEM fuel cell. These two phenomena are strongly interrelated and ultimately determine the overall water flux in the membrane. Water transportation in the membrane by electroosmosis and back diffusion has been extensively studied by several authors. The effect of hydraulic permeation is generally negligible compared with the effects of electroosmotic and back diffusion because the hydraulic permeability is very low (Dai et al. 2009). Recently, Kim and Mench (2009) described temperature-driven water transport in the membrane by a process known as thermo-osmosis.

In recent decades, a great deal of research effort has been devoted to transport phenomena of individual components; this work includes one-dimensional studies

[Springer et al. (1991, 1993), Okada et al. (1996)], two-dimensional studies [Fuller and Newman (1993), Nguyen and White (1993)], and several three-dimensional models.

Okada et al. (1996) proposed a one-dimensional mathematical model of the water-content profile of the membrane. Their studies showed that the water content in the membrane is greatly influenced by the electrical current density and by the water transfer coefficient. Springer et al. (1991, 1993) developed a one-dimensional model that describes water transport in the membrane and they measured the diffusion coefficient, the electroosmotic drag coefficient, and the membrane proton conductivity experimentally as functions of the water content. Fitted curves were incorporated into their one-dimensional model to capture the water-transport phenomena in the membrane. Fuller and Newman (1993) developed a quasi-two-dimensional mathematical model of transport in the PEM fuel cell to address water management, heat management, and fuel utilization. The model developed by Nguyen and White (1993) is identical to the model developed by Fuller and Newman, except that it incorporates variable hydration of the polymer electrolyte membrane, as proposed by Springer et al. (1991, 1993).

In the current study, a three-dimensional, single-phase water transport model is proposed based on that of Springer et al. (1991, 1993). In the modeling, the catalyst layer is treated as a very thin layer, so that it is not considered directly as a computational domain. However, all the variables and their gradients are computed in the line of the catalyst by an averaging model, as discussed in detail below.

One aim of this study was to validate our newly developed water-transport model and to compare the results with those of the environmental magnetic resonance imaging

(EMRI) studies of Tsushima et al. (2010). Another aim was to explain the effects of relative humidity and current density on the water content profile in the membrane.

5.2 Water transport modeling

5.2.1 Definitions of the three types of water present in the PEM fuel cell

The protonic conductivity of the membrane, which has a marked effect on the performance of the cell, depends on the level of hydration of the membrane. Therefore, to develop a model of the fuel cell it is important to understand the physics of water transport in the cell and how this affects the cell's performance, and to develop a modeling framework that incorporates these factors.

First, we need to understand the nature of the three phases of water (liquid-phase water, gas-phase water, and solid-phase water) that are transported in the fuel cell and to confirm the definitions of these phases.

In the PEM fuel cell, water can be present as three phases: the solid phase, the gas phase, and the liquid phase. Each of these states of water is not necessarily present in every domain of the cell. For example, water vapor (gas phase) is always present in the gas diffusion layer but not in the membrane, whereas solid-phase water is present only in the membrane and the catalyst layer, where ionomers are present (i.e., within polymers). The PEM is a solid that contains no voids and which can chemically incorporate water in the form of the hydronium ion (H_3O^+). Water in this form in the auxiliary PEM is responsible for proton transport. Water molecules that are transported through the PEM from the anode to the cathode along with protons (H^+) will be referred to as water content λ transport in the PEM, where λ is the dimensionless quantity defined as follows:

$$\lambda = \frac{EW.V_{ex}\,C_w}{\rho_m^{dry}}$$

where ρ_m^{dry} (kg/m^3) is the dry density of the PEM, *EW* is the equivalent weight (mass) of the PEM (kg/mol), C_w is the water vapor concentration (mol/m^3), and V_{ex} is the coefficient of expansion of the PEM.

The liquid-phase (saturation) water *s*, expressed as a percentage of the volume of liquid water that is present in the void volume, is expressed by the following equation:

$$s = \frac{V_l}{V_V}$$

where V_l is the volume of liquid water (m^3) and V_v is the volume of voids (m^3). The water saturation *s* is therefore a dimensionless quantity with a value of between 0 and 1. Furthermore, the expression is defined only in cases where there a void space is present. These consist, basically, of the catalyst layer and the gas diffusion layer, although the gap in the flow path must also be considered, and *s* is also defined there in a broad sense. No value of *s* is defined in the membrane, because there are no pores in the PEM.

Finally, water in the gas phase is represented by using the gas mass fraction Y_w. This is expressed as the mass of water vapor per unit volume, (the ratio of the total weight of the mass of all the species), represented by the following equation:

$$Y_w = \frac{M_w}{\sum_j M_j}$$

Here, M_w is the mass of water vapor per unit (kg/m^3). Because it is defined as existing only in locations where gaps are present (the channel, the gas diffusion layer, and the catalyst layer), water vapor is not defined in the case of the PEM.

Figure 5.1 summarizes the range and the presence of the three state of water in a fuel cell. A mark ○ in the figure shows that the corresponding phase of water is present within that region of the cell.

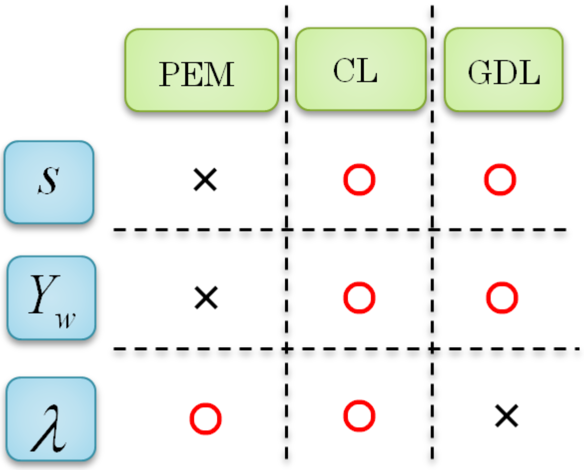

	PEM	CL	GDL
s	×	○	○
Y_w	×	○	○
λ	○	○	×

Fig. 5.1. Relationship between three kind of water and the materials of a PEM fuel cell (PEM = polymer electrolyte membrane, CL = catalyst layer, GDL = gas diffusion layer)

5.2.2 Basic water-transport equations

In general, the transport of gases in channels and porous media is driven by both convection and diffusion. Convection is induced by the consumption or production of materials in the electrochemical reaction. Convective flow through the porous media can also depend on the nature of the flow field that is used, especially in the case of a serpentine channel. Therefore, the current model will consider both diffusion and convection as means of gas-phase transport.

5.2.3 Water transport in the membrane region

Transport of water in the membrane is generally described in terms of two major mechanisms: (1) back diffusion as a result of the presence of a water concentration gradient between the anode side and the cathode side, and (2) the electro-osmotic drag caused by migration of water as protons are transported through the membrane. The diffusivity of dissolved water is strongly dependent on the temperature and the water content of the membrane, which is a function of the temperature and the water activity. The water content λ can be calculated from the ratio of the number of water molecules to the number of charged (SO_3H^+) sites.

$$\frac{\partial}{\partial t}\left(\frac{\rho_m^{dry}}{EW \cdot V_{ex}}\lambda\right)=\nabla\cdot\left(D_{wl}\nabla\frac{\rho_m^{dry}}{EW \cdot V_{ex}}\lambda\right)-\nabla\cdot\left(n_d\,\frac{\vec{\mathrm{i}}}{F}\right) \tag{5.1}$$

where n_d is the electroosmotic drag coefficient and is defined as the number of water molecules carried by per proton when a current is passed. Furthermore, both the electroosmotic drag coefficient n_d and the diffusivity D_{wl} are generally functions of the water content of the membrane. According to the model of Springer et al. (1991), n_d is given by the following expression:

$$n_d = \frac{2.5}{22}\lambda \tag{5.2}$$

and the diffusivity D_{wl} is given by the following relationship:

$$D_{wl} = \begin{cases} 3.10\times 10^{-7}\lambda\left[-1.0+\exp(0.28\lambda)\right]\exp\left(-\dfrac{2436}{T}\right) & 0\le\lambda<3 \\ 4.17\times 10^{-8}\lambda\left[1.0+161.0\exp(-\lambda)\right]\exp\left(-\dfrac{2436}{T}\right) & 3\le\lambda\le 16.8 \end{cases} \tag{5.3}$$

5.2.4 Water transport in the region of the gas diffusion layer

The gas diffusion layer is a porous medium made from carbon fiber or carbon cloth, which permit gas to flow readily in the pores of gas diffusion layer. The water that is produced can condense or evaporate in the gas diffusion layer, depending on the environment. To describe the distribution of liquid water and gas-phase transport of water vapor in our current model, we need to solve the two set of equations that are discussed below.

The governing equation for the transport and formation of liquid water can be written as follows:

$$\frac{\partial}{\partial t}(\varepsilon_d \rho_l s)+\nabla\cdot(\varepsilon_d \rho_l \,\mathrm{u}\, f_l)=\nabla\cdot(\varepsilon_d \rho_l D_c \nabla s)-\nabla\cdot\left(\frac{f_l f_g k(\rho_l-\rho_g)}{\nu}\mathrm{g}\right)+\dot{m} \tag{5.4}$$

where s is the degree of saturation by liquid water (defined as the ratio of the volume of water to the volume occupied by pores), ε_d is the dry state of porosity (defined as $\varepsilon=\varepsilon_d(1-s)$, where ε is the porosity of the porous medium), ρ_l is the density of liquid water, and ρ_g is the density of the gas mixture. The density of the two-phase mixture is defined as follows:

$$\rho=\rho_l\, s+\rho_g\,(1-s) \tag{5.5}$$

The first term in Equation 5.2 represents stored liquid water and the second term represents water transported through pressure-driven advection. The first term in the right-hand side of the equation represents the effect of surface tension in the porous medium, derived by using the capillary diffusion approximation. The second term represents the gravity-induced migrating flux in the porous medium. The terms f_l and f_g represent the relative mobilities of liquid and gas in the gas phase and liquid phase, respectively.

$$f_l = s(2-s) \tag{5.6}$$

$$f_g = 1 - f_l \tag{5.7}$$

The capillary diffusion coefficient D_c is defined as follows:

$$D_c = -\frac{s^3 K f_g}{\mu_l}\left[\frac{dP_c}{ds}\right] \tag{5.8}$$

The Leverett function is generally used to express the relationship between capillary pressure and liquid saturation in porous media:

$$P_c = P_l - P_g = \sigma\cos(\theta_c)\left(\frac{\varepsilon}{\kappa}\right)^{1/2} J(s) \tag{5.9}$$

Here, σ is the surface tension and $J(s)$ is given by the following expression:

$$J(s) = \begin{cases} 1.417(1-s) - 2.12(1-s)^2 + 1.263(1-s)^3 & (\theta_c < 90^0) \\ 1.417s - 2.12s^2 + 1.263s^3 & (\theta_c > 90^0) \end{cases} \tag{5.10}$$

The last term in Equation 5.4 can be written as follows:

$$\dot{m} = \begin{cases} M_l k_c \dfrac{\varepsilon X_w}{RT}\left(X_w P - P_{sat}\right) & if\,(X_w P > P_{sat} \\ \\ M_l k_e \dfrac{\varepsilon s \rho_l}{M_l}(X_w P - P_{sat}) & if\,(X_w P < P_{sat} \end{cases} \tag{5.11}$$

where k_c and k_e represent the rates of condensation and evaporation, respectively; $x_w P$ is the partial pressure of water vapor; and x_w is the mole fraction of water vapor. The saturation pressure of water is denoted by P_{sat}, and it can be computed by using the curve-fitted expressions provided by Springer et al. (1991).

$$\log_{10} P_{sat} = -2.1794 + 0.02953\left(T - 273.15\right) - 9.1837\times10^{-5}\left(T - 273.15\right)^2 \\ +1.4454\times10^{-7}\left(T - 273.15\right)^3 \tag{5.12}$$

The gas transport inside the gas diffusion layer is modeled by the following equation.

$$\frac{\partial}{\partial t}\left(\varepsilon\rho Y_i\right) + \nabla\cdot\left(\varepsilon\rho\,\mathbf{u}Y_i\right) = \nabla\cdot\mathbf{J}_i + \omega_i \tag{5.13}$$

The diffusion flux of species is given by the Stefan–Maxwell equation:

$$\mathbf{J}_i = \rho D_i^{eff}\nabla Y_i + \frac{\rho Y_i}{M}D_i^{eff}\nabla M - \rho Y_i\sum_j D_i^{eff}\nabla Y_j - \frac{\rho\nabla M_i}{M}\sum_j D_i^{eff} Y_j \tag{5.14}$$

Here, M is the molecular weight of the mixture and D_i^{eff} is the effective mass diffusivity given by the following expression (Meng and Wang (2004b)):

$$D_i^{eff} = \left[\varepsilon_d\left(1-s\right)\right]^{1.5} D_i \tag{5.15}$$

The last term in Equation 5.13 represents the generation or consumption of species resulting from electrochemical reactions:

$$\omega_i = -\frac{M_i\, m_i}{n\,F}\, j \tag{5.16}$$

Here, m_i and n are the stoichiometric coefficient and the number of electrons transferred in the electrochemical reactions, respectively (Meng and Wang (2004b)), which can be expressed as follows:

$$\sum_i m_i\, X_i = n\, e^-$$

Here, x_i denotes the chemical formula for species i.

5.2.5 Water transport in the catalyst layer region

In this model, the catalyst layer is considered to be a very thin layer and is therefore not considered directly as a computational domain. However, all the variables and their gradients are calculated in the line of the catalyst layer and the thickness of the catalyst layer is also taken into account in a special way. For the water content in the catalyst layer, the average profile of water content is used. In the catalyst layer, the water content in the polymer electrolyte is related to the activity of water in adjacent pores by using an experimentally derived relationship for Nafion:

$$\lambda = \left(0.043 + 17.81 a_w - 39.85 a_w^2 + 36.0 a_w^3\right)\left(1 - s\right) + 16.8\, s \tag{5.17}$$

In Equation 5.9, the activity is given in terms of the partial pressure, saturation pressure, and mole fraction of water vapor.

$$a_w = \frac{\bar{x}_w P}{P_w^{sat}} \tag{5.18}$$

Here a_w is the water activity and $\bar{x}_w$ is the average mole fraction of water vapor.

The basic equation for water transport together with the boundary conditions at every interface are listed in Table 5.1. The thin-layer modeling approach was used in our model.

Table 5.1: Details of the water transport model

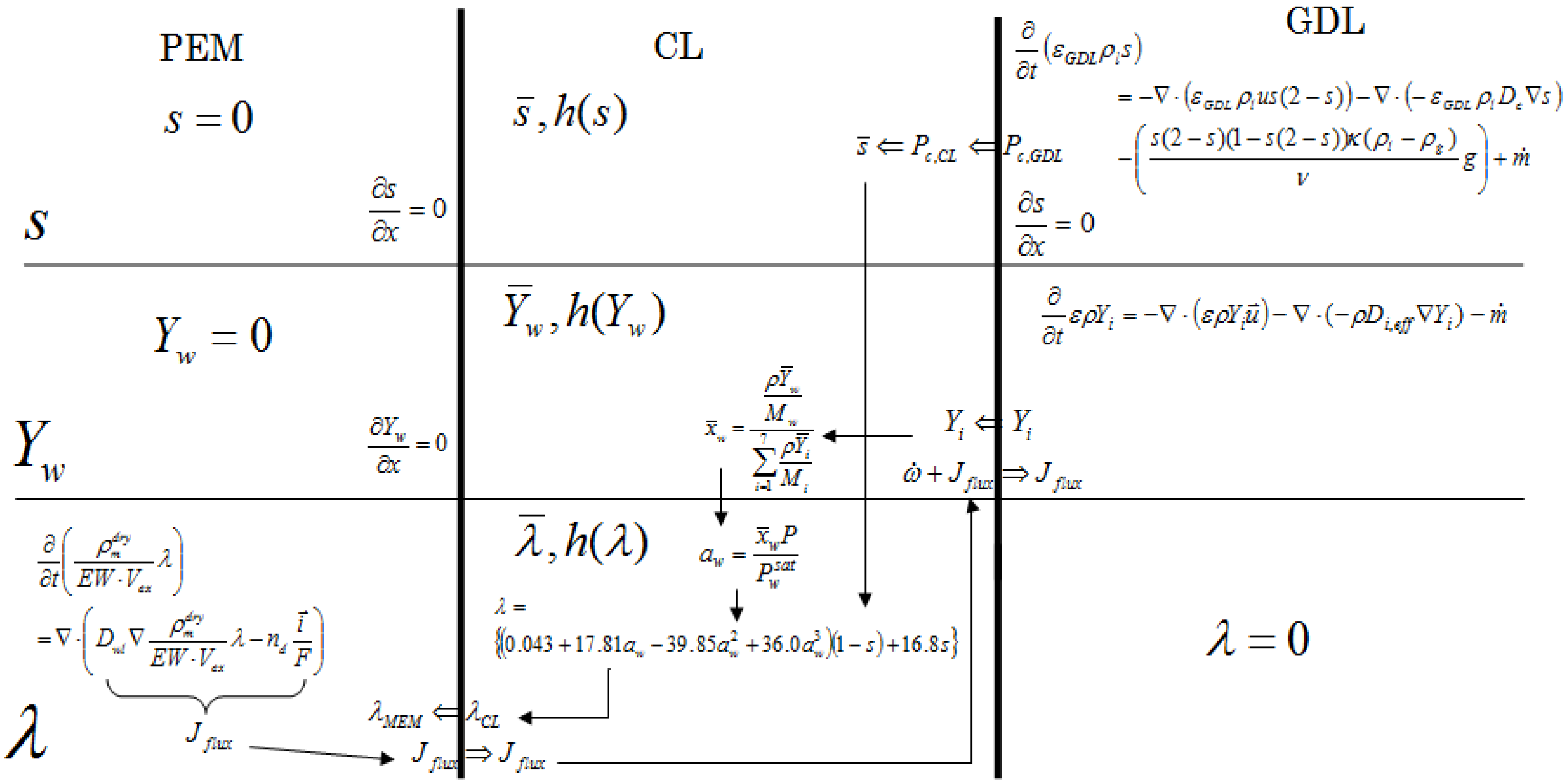

The above figure presents basic equations and boundary conditions for liquid water saturation (s), the mass fraction of water vapor (Y_w) and the water content in the polymer electrolyte (λ) in the membrane (PEM), catalyst layer (CL), and gas diffusion layer (GDL) regions.

5.2.6 Model Assumptions

1. The water produced in the cell is assumed to be water vapor and there is no condensation or evaporation.

2. Flow is incompressible and laminar.

3. Porous media are assumed to be isotropic and homogeneous.

4. The temperature regime is assumed to be isothermal (no variations in the temperature).

5. Gas and liquids (hydrogen, oxygen, or water vapor) do not penetrate into membrane.

6. Contact resistance between any two parts of the fuel cell is negligible.

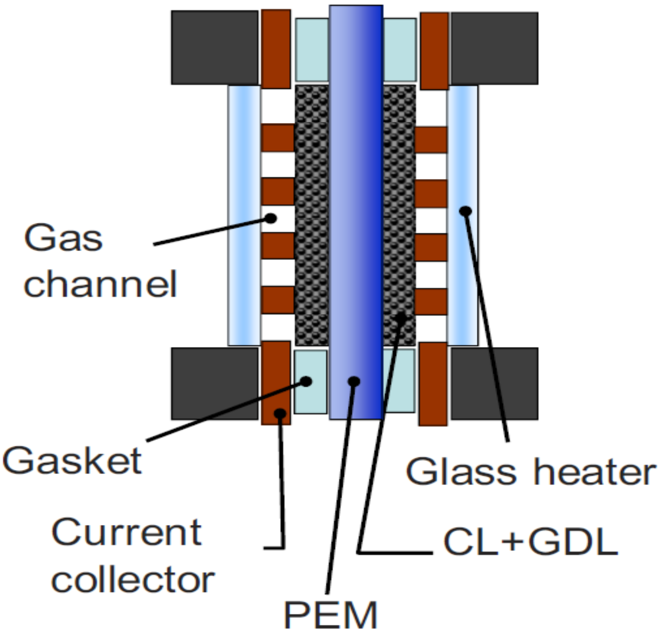

(a)

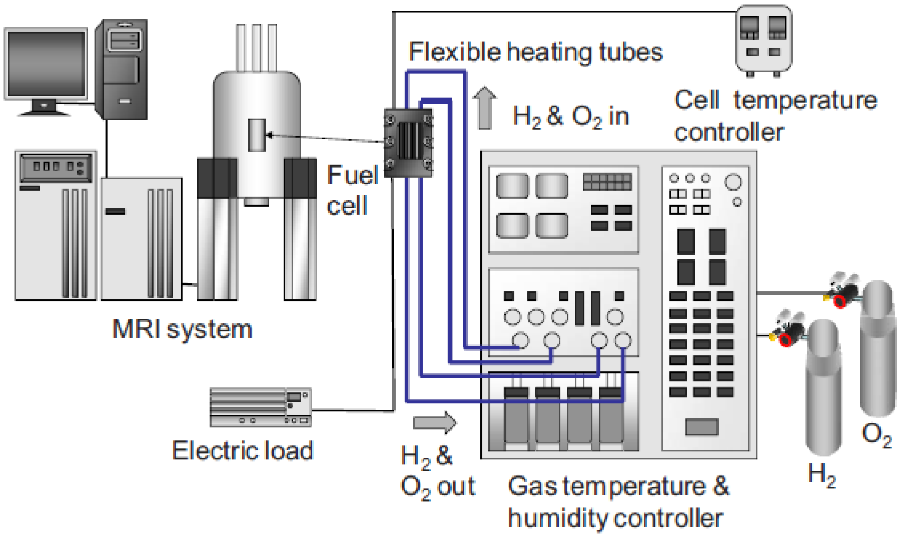

(b)

Fig. 5.2. (a) Schematic of a cross-sectional view of a PEM fuel cell for EMRI experiments (b) EMRI system for PEM fuel cell visualization (Tsushima et al., 2010)

5.3 Computational Domain

In the experiments performed by Tsushima et al. (2010), magnetic resonance imaging (MRI) was used to investigate the distribution of water in the membrane of an operational PEM fuel cell, and the effects of relative humidity and current density on the through-plane water-content distribution in the membrane were examined. The experimental setup and the MRI visualization system are shown in Fig. 5.2. In the experiments, five parallel channels were used as flow channels. The design of the computational domain used in the present simulation is based on the geometry used in the experiments. However, to reduce the computational load and costs, only a single channel with half a rib region on both sides is considered.

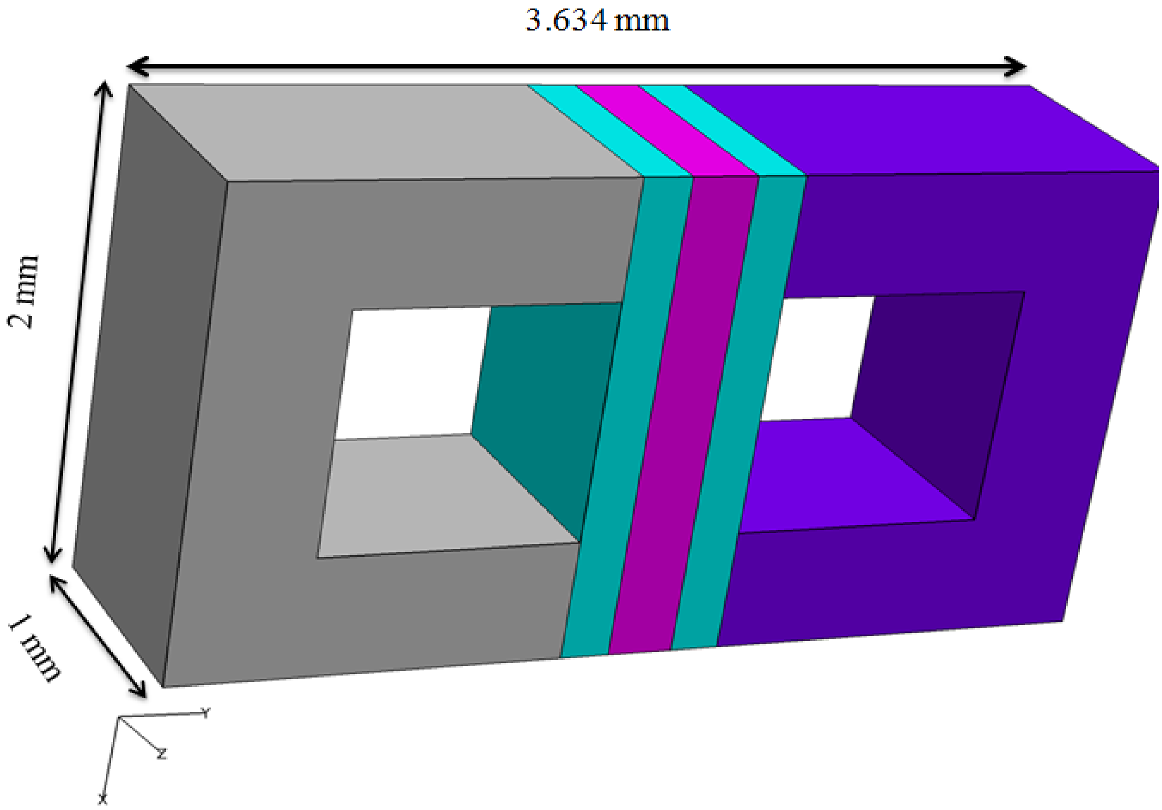

(a)

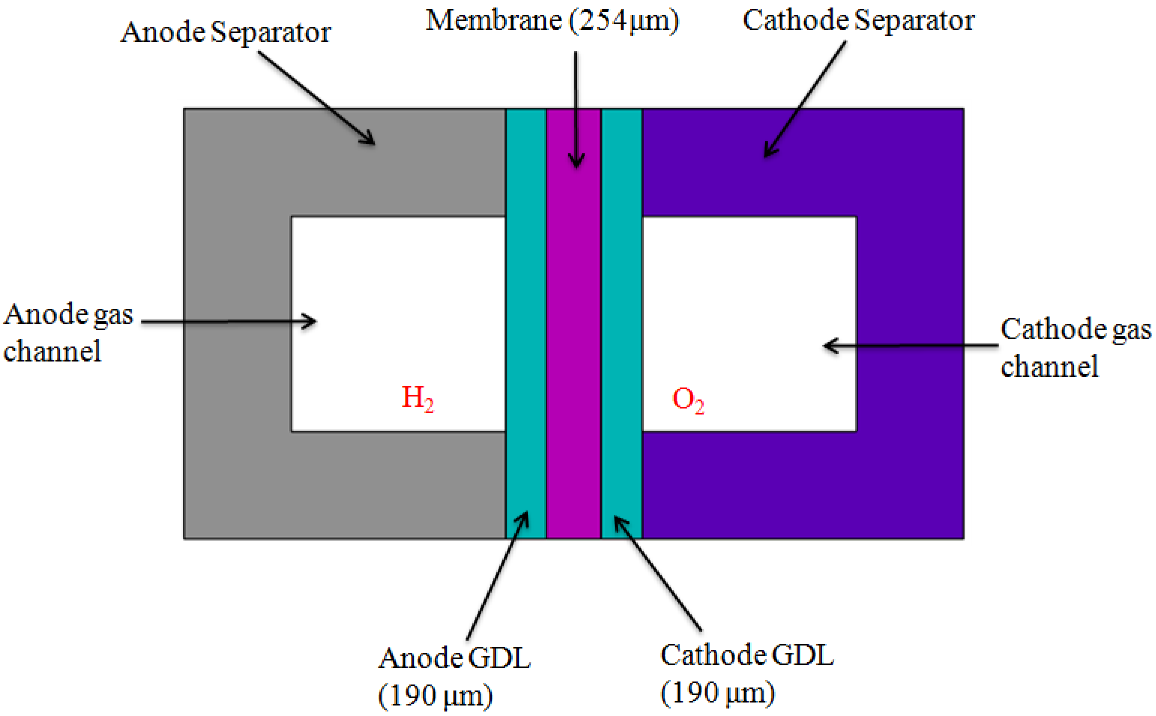

(b)

Fig. 5.3. (a) Computational domain and (b) cross-sectional view of the calculation domain.

To allow for the effects of the other channels, symmetry had been taken into account. The length of channel was also shortened. The three-dimensional computational domain used in this study is shown in Fig. 5.3; it consists of straight channels in the cathode and anode sides as gas channels.

The cathode side consists of the cathode gas channel, the cathode gas diffusion layer, and the cathode bipolar plate. The anode side consists of the corresponding components. The membrane is located between the anode side and the cathode side. As we discussed earlier, the catalyst layer in our model is considered as an interface between the membrane and the gas diffusion layer; therefore, the catalyst layer is absent from the computational domain. However, in our computational code, the thickness of the catalyst layer is taken into consideration, and all the variables and their gradients are calculated in the line of the catalyst layer by a special technique.

5.4 Solution Strategy

Equations for continuity, momentum, species, electrons, and protons, along with the equations for water transport through the membrane and for electrochemical reactions were solved simultaneously to obtain the results. The time-dependent conservation equations were discretized by the finite-volume method and solved by using the software FrontFlow/Red (Advance Soft Co. Ltd., Tokyo), which takes into account the porous nature of the computational domain.

Table 5.2: Details of the geometric design for the present simulation

Dimension	**Value**
Channel width	1.0 mm
Channel length	1 mm
Channel height	1 mm
Gas diffusion layer thickness	190 µm
Membrane thickness	254 µm
Bipolar plate thickness	0.5 mm

Table 5.3: Operating conditions

Relative humidity	**Current density**
Cathode/anode relative humidity = 40%	Current density = 0.1 A/cm^2
	Current density = 0.2 A/cm^2
Cathode/anode relative humidity = 80%	Current density = 0.1 A/cm^2
	Current density = 0.2 A/cm^2

Table 5.4: Physicochemical parameters

Reference hydrogen concentration, C_{H_2} (mol m^{-3})	40
Reference oxygen concentration, C_{O_2} (mol m^{-3})	40
Anode transfer coefficient	$\alpha_c = 1$
Cathode transfer coefficient	$\alpha_c = 1$
Faraday constant (F) (C mol^{-1})	96487
Gas diffusion layer porosity	0.8
Gas diffusion layer permeability (m^2)	1.76×10^{-11}
Equivalent weight of polymer (kg mol^{-1})	1.1
Dry membrane density (kg m^{-3})	1100
Operating pressure (atm)	1

5.5 Results and discussion

The numerical scheme described above and the physical and operating parameters listed in Tables 5.3 and 5.4 were used to obtain the numerical results that are discussed below.

5.5.1 Effects of low relative humidity

5.5.1.1 Convergence history

Convergence and steady-state simulation are very important for analyzing real physics, because unsteady solutions can entail a great deal of variation; this is sometimes very impractical, as the results are dependent on the choice of initial conditions, algorithm, and grid. We therefore first needed to confirm that our simulations attained a steady state. In the simulation, we assumed that the membrane was initially hydrated at the appropriate level of humidity corresponding to each set of operating conditions. The initial level of hydration within the membrane was assumed to be uniform.

Figure 5.4 shows the convergence history for the current density. The current density profile took a long time (about five hours) to achieve a steady state.

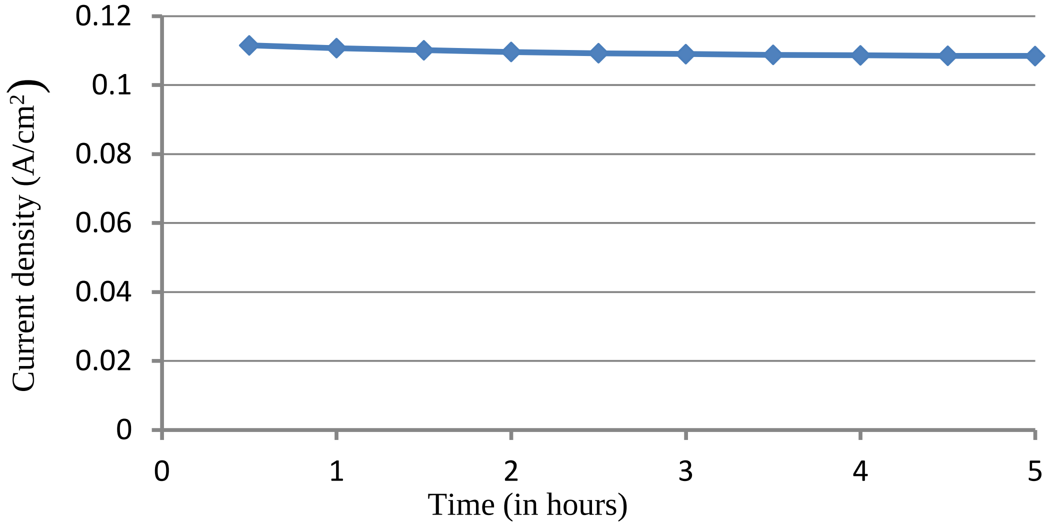

Fig. 5.4. Convergence history of the current density

The convergence history of the water content profile in the polymer membrane under the channel/rib is shown in Fig. 5.5.

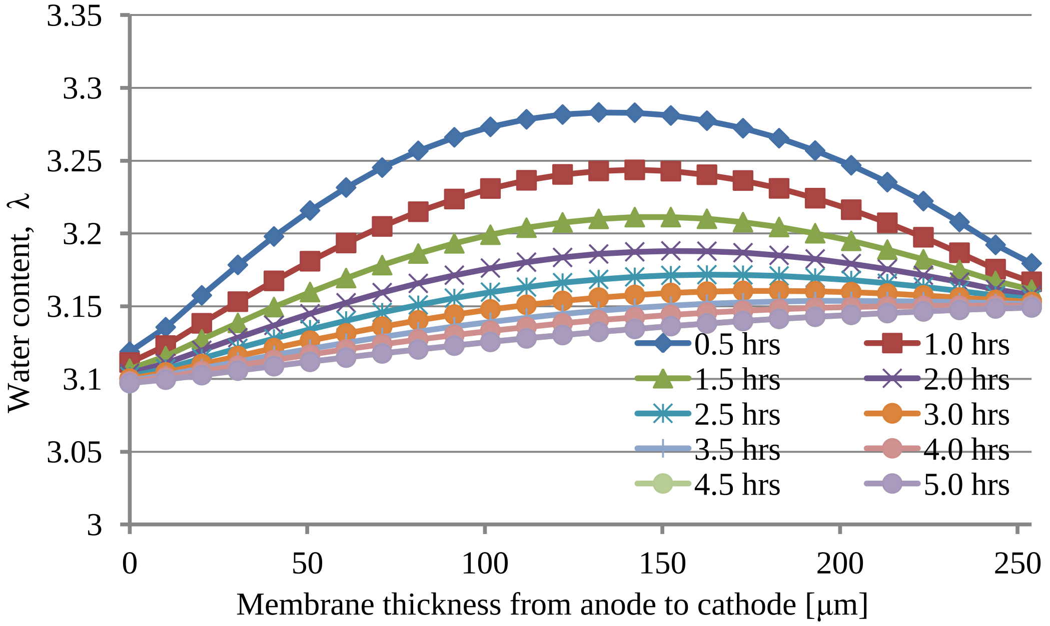

(a)

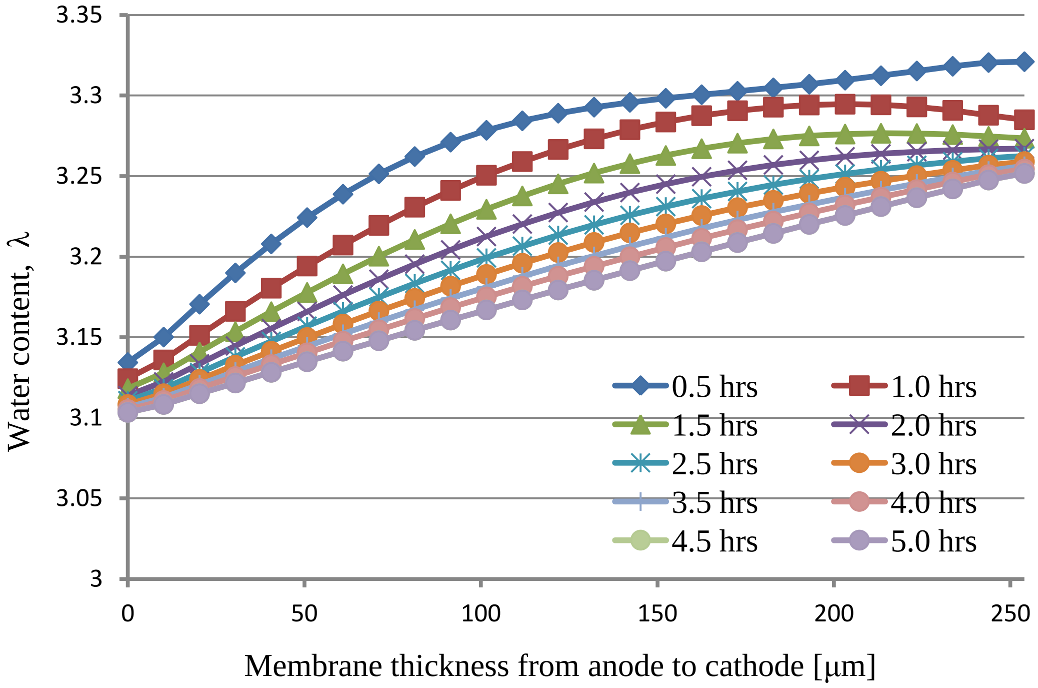

(b)

Fig. 5.5. The unsteady water content distribution through the membrane (a) under the channel and (b) and under the rib of a PEM fuel cell

5.5.1.2 Current density distribution

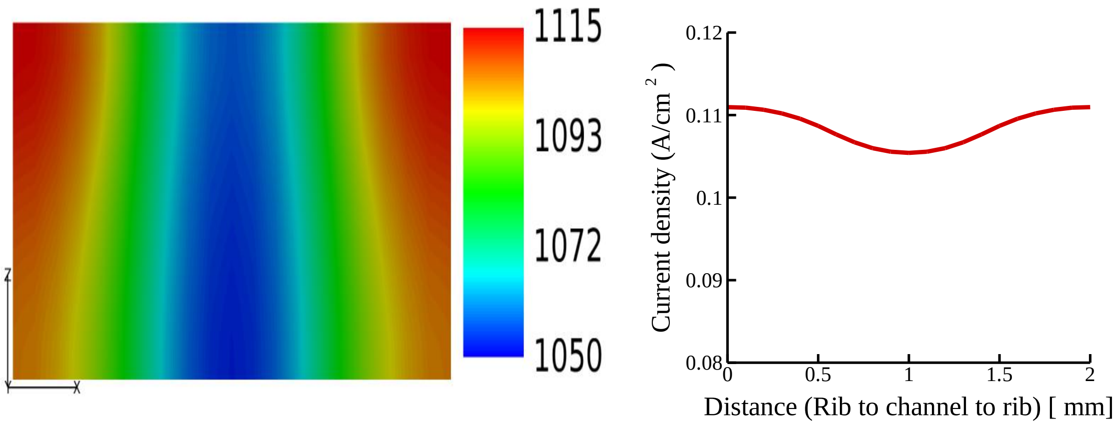

(a)

(b)

Fig. 5.6. (a) Local current-density distribution in the middle of the membrane; (b) current-density distribution along the center line of (a) in the direction from the rib to the channel

Fig. 5.6 shows the local current-density distribution in the middle of the membrane. The current density distribution in the membrane under the rib is higher than that under the channel. Therefore, amount of water produced under the rib is greater than that under the channel.

The water-concentration distribution in the gas channel and in the gas diffusion layer on both the anode and cathode sides is shown in Fig. 5.7 for a relative humidity of 40% and current densities of 0.1 and 0.2 A/cm^2. The formation of water on the cathode side depends on the relative humidity of the supplied gas and on the production of water by the electrochemical reaction. Generation of a high current density in the fuel cell produces more water in the cell, so that the water concentration on the cathode side increases at higher current densities. As we have already discussed with respect to Fig.

5.6, the current density under the rib is higher than that under the channel; therefore, more water is generally produced under the rib than under the channel.

5.5.1.3 Water concentration distribution

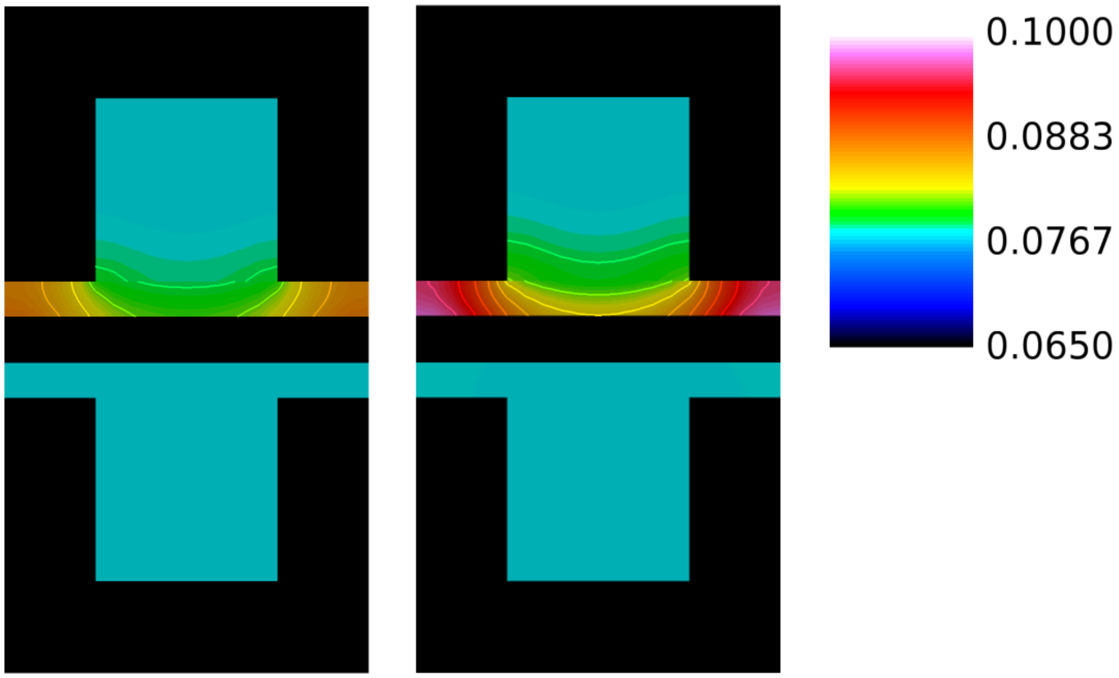

(a) (b)

Fig. 5.7. Water concentration distribution in the gas channel and the gas diffusion layer (both anode and cathode sides) at a relative humidity of 40% and current densities of (a) 0.1 A/cm^2 and (b) 0.2 A/cm^2

The removal of water from under the rib is less efficient than that under the channel, and this contributes to the accumulation of water under the rib. From Fig. 5.7 one can easily see that the water-concentration gradient through the membrane is steeper under the rib than under the channel. However, the water concentration gradient when the fuel cell is operated at the lower current density (0.1 A/cm^2) is less than that when it is operated at the higher current density (0.2 A/cm^2).

The water content distributions for various operating current densities and a relative humidity of 40% are shown in Fig. 5.8. The water content in the membrane increases when the PEM fuel cell is operated at a higher current density. However, the increase of water content in the membrane is small and it is most pronounced in the section of the membrane underneath the rib.

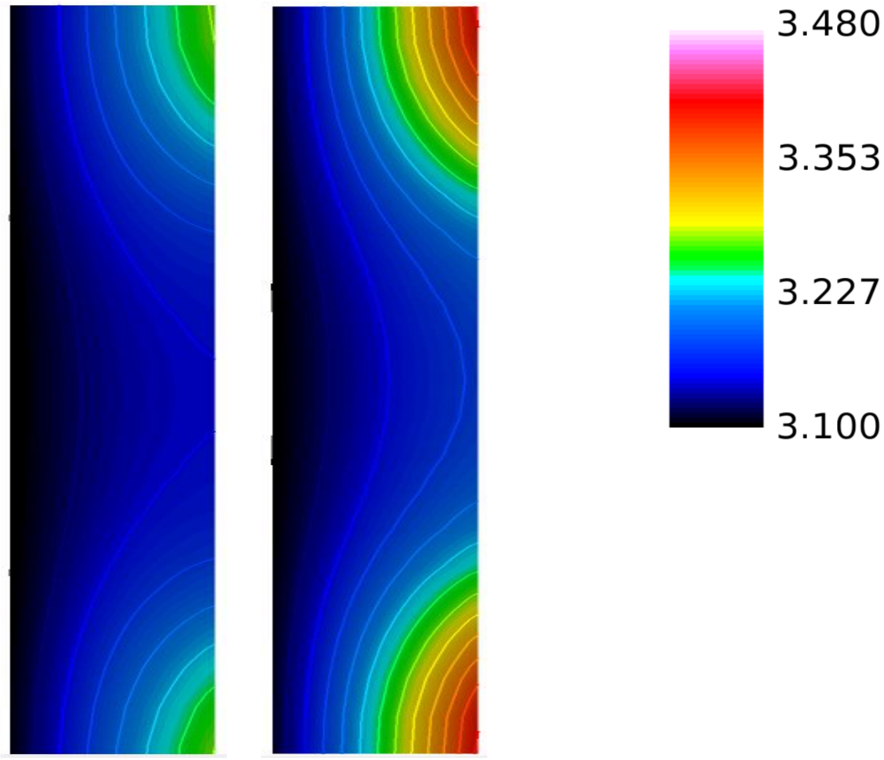

Fig. 5.8. Water content distribution in the membrane (anode and cathode sides) at a relative humidity of 40% and current densities of (a) 0.1 and (b) 0.2 A/cm^2

Figure 5.9 show the water content distributions in the membrane for a relative humidity of 40% and a current density of 0.2 A/cm^2. The water content distribution under the channel is lower than that under the rib, as the water concentration in the gas diffusion layer under the channel is lower than that under the rib. On the other hand, the water content under the rib is higher than that under the channel.

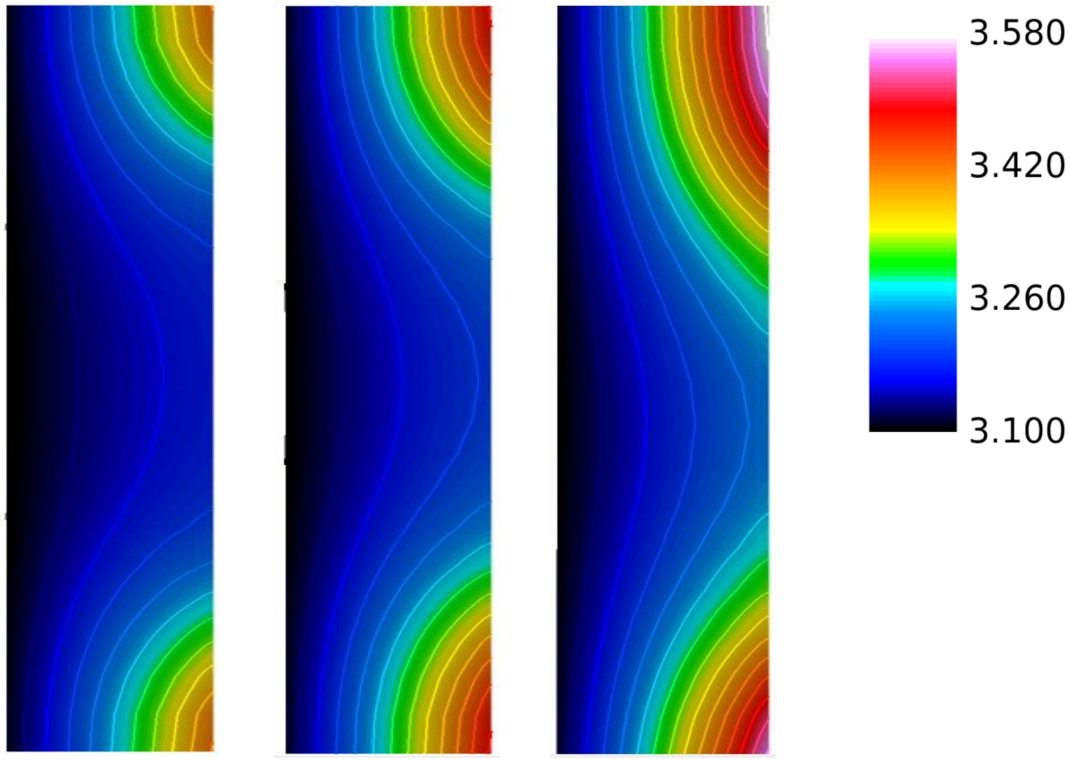

(a) (b) (c)

Fig. 5.9. Water content distribution (a) near to the inlet region, (b) at the middle of the cell, and (c) near the outlet region for a relative humidity of 40% and a current density of 0.2 A/cm^2

Fig. 5.9(a) shows the water content distribution in the membrane near the channel inlet. The water content near the channel inlet is lower than that at other positions [Figs. 5.9(b) and 5.9(c)] and it increases gradually from the inlet position to the outlet position.

This suggests that membrane dehydration can occur near the inlet position and flooding can occur near the outlet region of the gas channel.

5.5.1.4 Numerical validation of the developed model at a low humidity

To validate our computational model, we carried a numerical simulation using the same conditions as those used in the experimental study of Tsushima et al. (2010).

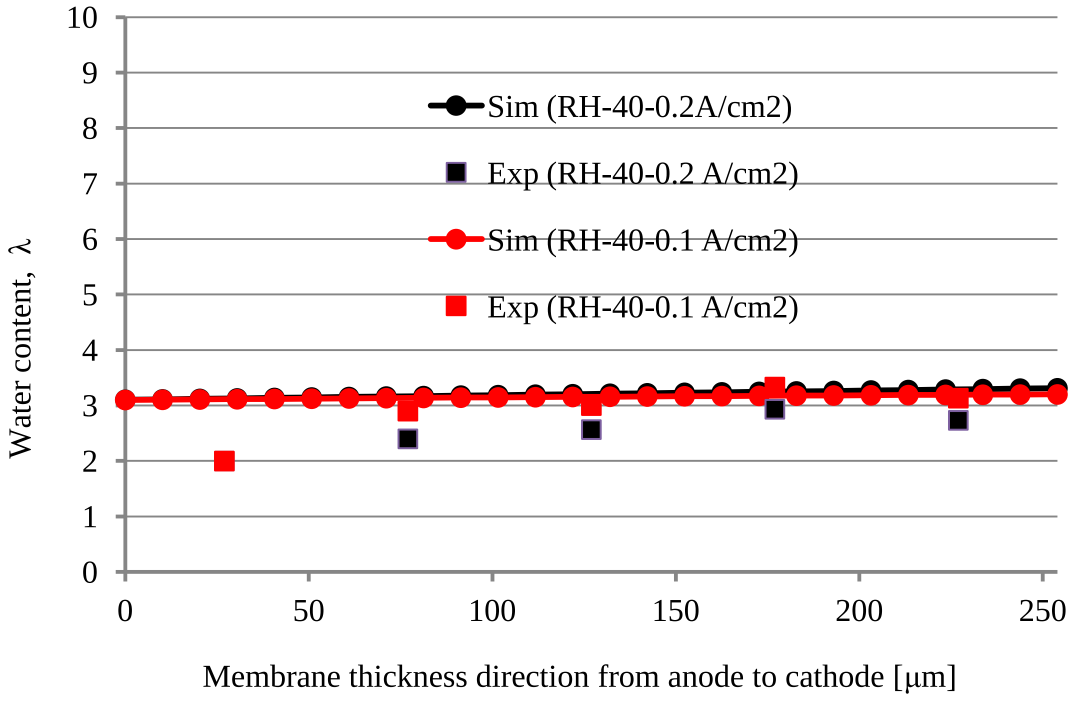

Fig. 5.10. Comparison of simulation (Sim) results with experimental ones (Exp)

Calculated and experimental through-plane water-content profiles are presented in Figure 5.10 for various fuel-cell operating conditions; the results were obtained by averaging the profile of water content in the membrane under the channel with that in the membrane under the rib. The results of the numerical simulations with our model agreed well with the experimental measurements. When the relative humidity was 40%, the water content profile in the membrane calculated by numerical simulation was flat and unaffected by the current density, in a similar manner to that shown by experiment. For a current density of 0.2 A/cm^2, the calculated water content profile was also very close to the experimental profile. The results in Fig. 5.10 show that molecular diffusion in the membrane plays a major role in water transport in the membrane at a low relative humidity. Near the edge, however, there was a significant difference between the results of the simulation and the experimental results. This may be the result of experimental error. The magnetic resonance imaging (MRI) system used in the experiment was capable of capturing the physics very accurately, but because of the resolution of the MRI system, measurements in the edge area might have been affected by both the nearby catalyst layer and membrane, so that measurements of the water content in the membrane near the edge are not reliable.

5.5.2 Effects of high relative humidity

The water contents and water concentration distributions in the membrane, the gas channel, and the gas diffusion layer were also predicted at a high relative humidity in a similar manner to that described above.

5.5.2.1 Convergence history

The convergence history for the current density for a cell operating at a relative humidity of 80% is presented in Fig. 5.11. The current density attained a relatively steady state within a short time and became completely steady after about five hours.

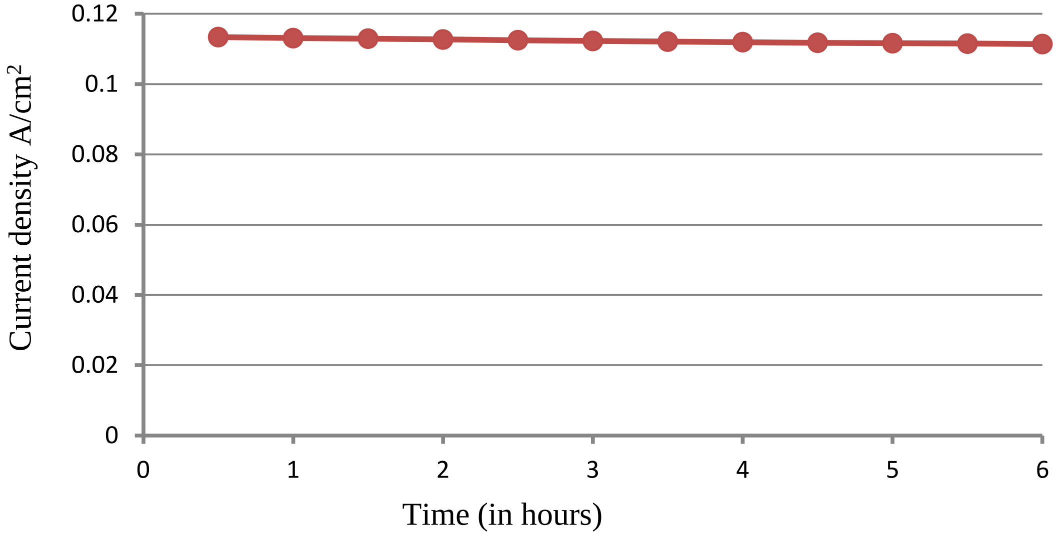

Fig 5.11. Convergence history of the current density for a relative humidity of 80%

Figures 5.12(a)–(b) show the steadiness of the water content profiles in the membrane underneath the channel and underneath the rib.

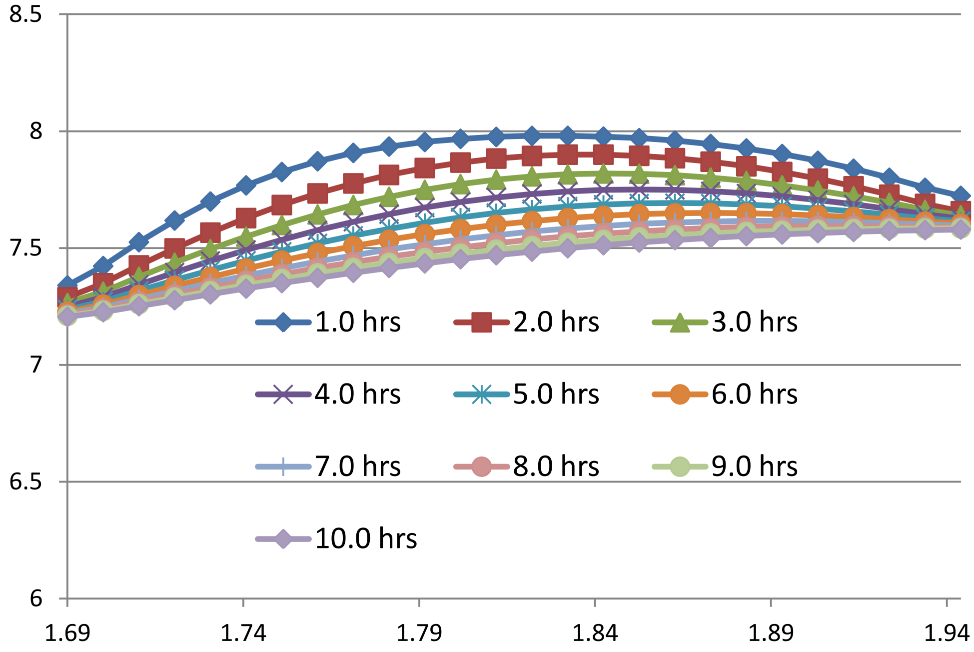

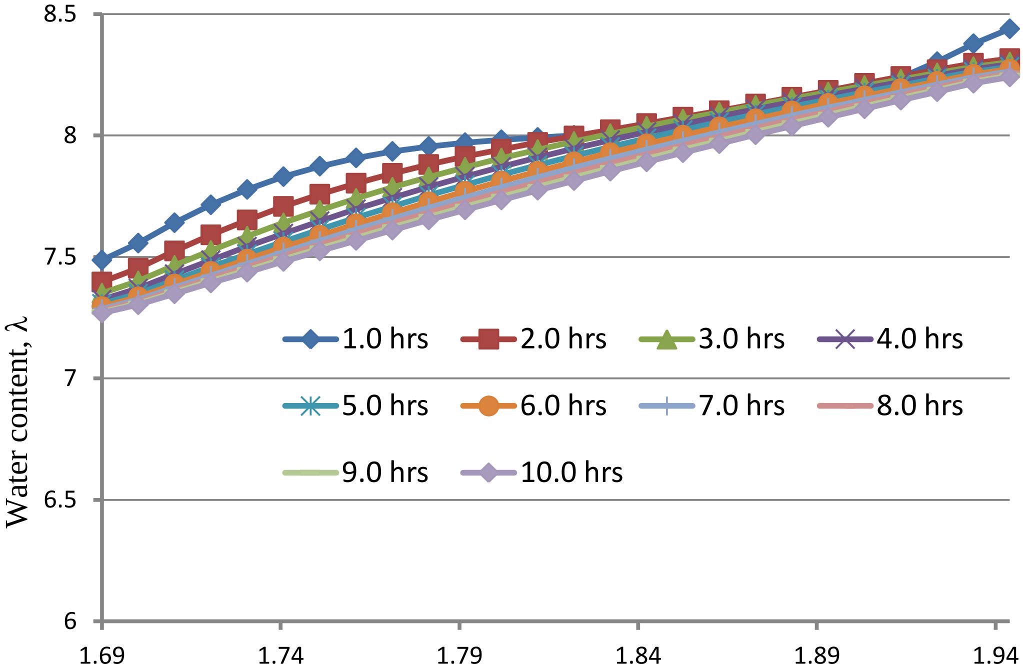

Fig. 5.12. Convergence history of water content through the membrane (a) under the channel and (b) under the rib at a high humidity (80%) and a current density of 0.1 A/cm^2

Although the current density attains a steady state very quickly, the water content distribution inside the membrane takes a long time (of the order of hours) to reach a steady state. As we know, variations in water content can also affect the current density; therefore, a complete steady water-content profile is important for achieving accurate predictions of the current density distribution.

5.5.2.2 Water concentration

The water vapor concentration in the gas channel and gas diffusion layer for a high relative humidity at a current density 0.1 A/cm^2 is presented in Fig. 5.13. The water vapor concentration in the gas diffusion layer in the direction from the channel inlet to the outlet gradually increases as water is produced by electrochemical reaction and moves towards the outlet position as a result of convective flow. Therefore, the water concentration at the outlet region is higher than that at other positions in the cell.

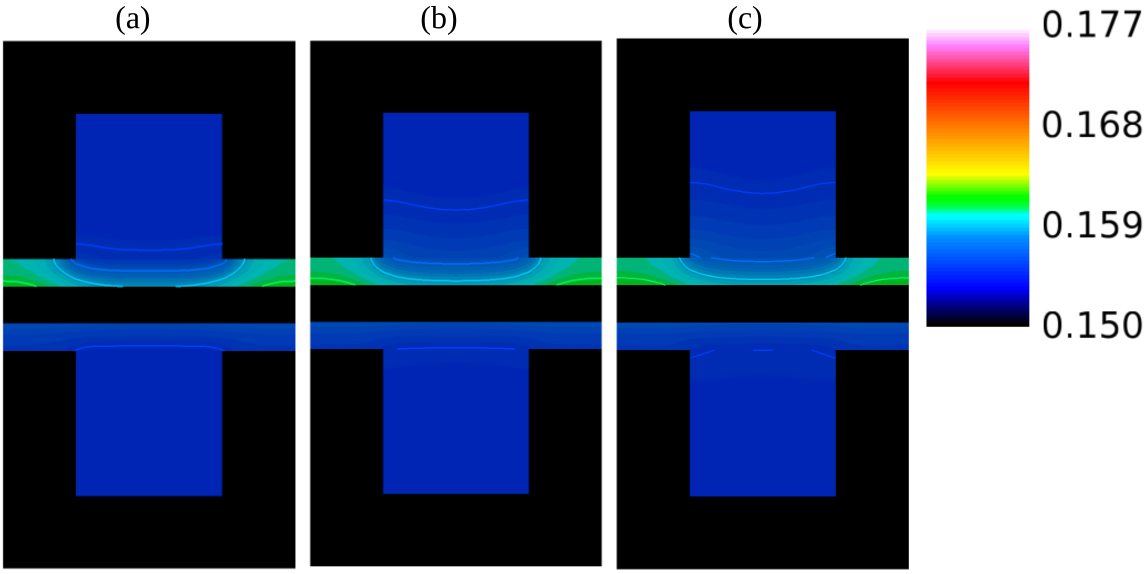

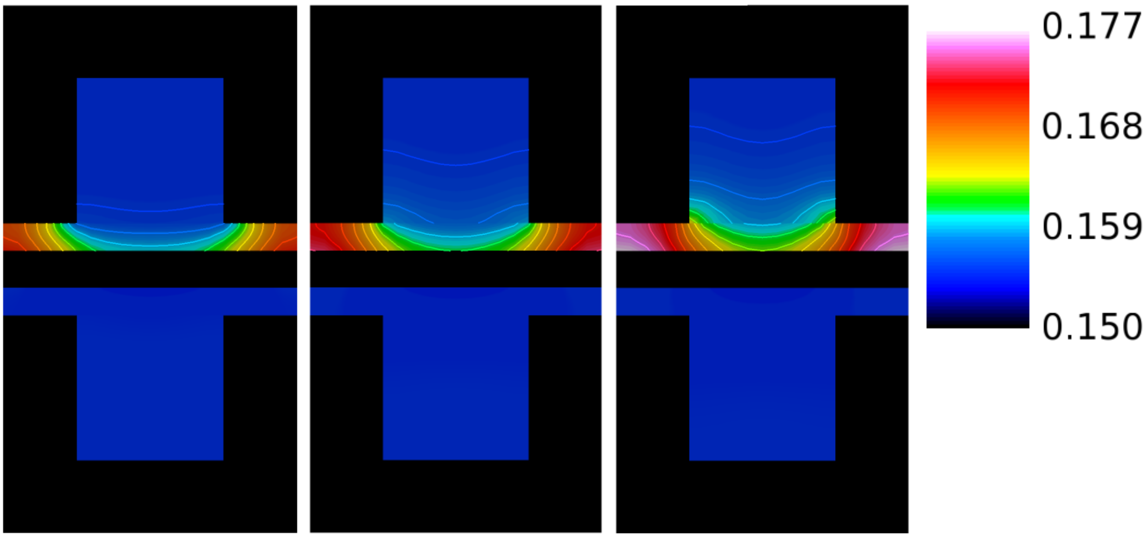

Fig. 5.13. Water concentration distributions (a) near to the inlet region (b) in the middle of the cell, and (c) near the outlet region for a high relative humidity (80%) and a current density of 0.1 A/cm^2.

The water concentration near the inlet region is lower, which contributes to a reduction in the water concentration gradient across the membrane.

Figures 5.14(a)–(c) show the water content distributions in the membrane at various positions in the cell for various current densities and a high humidity. The water content distribution in the membrane is not uniform because the water vapor concentration on the cathode side is not uniform. The figures clearly show that the water content distribution in the membrane varies, not only from the anode side to the cathode side, but also in the in-plane direction, so that the water content under the rib is higher than that under the channel. The water content through the membrane under the rib is higher than that under the channel. On increasing the current density, the water content in the membrane increases as more water is generated at the cathode side and, therefore, the amount of water transported through the membrane by back diffusion increases.

5.5.2.3 Numerical validation of the developed model at a high humidity

Finally, Figures 5.15(a)–(b) show a comparisons between the predicted and experimental water contents in the membrane for a high relative humidity and current densities of 0.1 A/cm^2 and 0.2 A/cm^2.

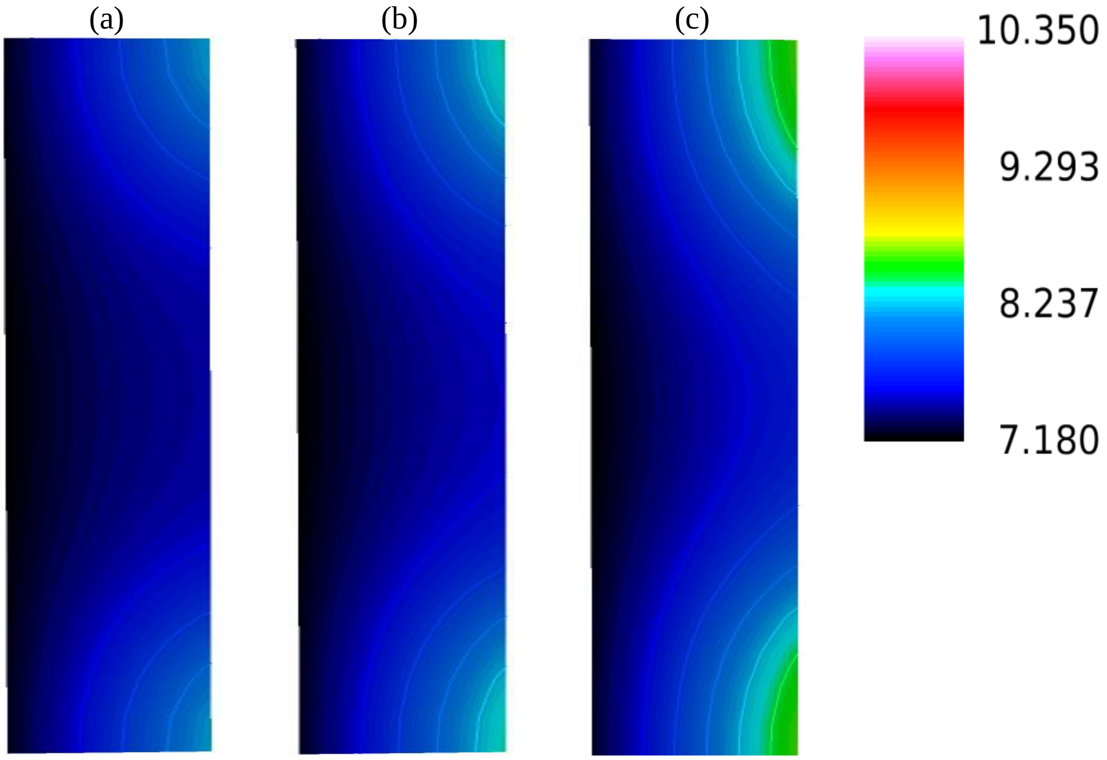

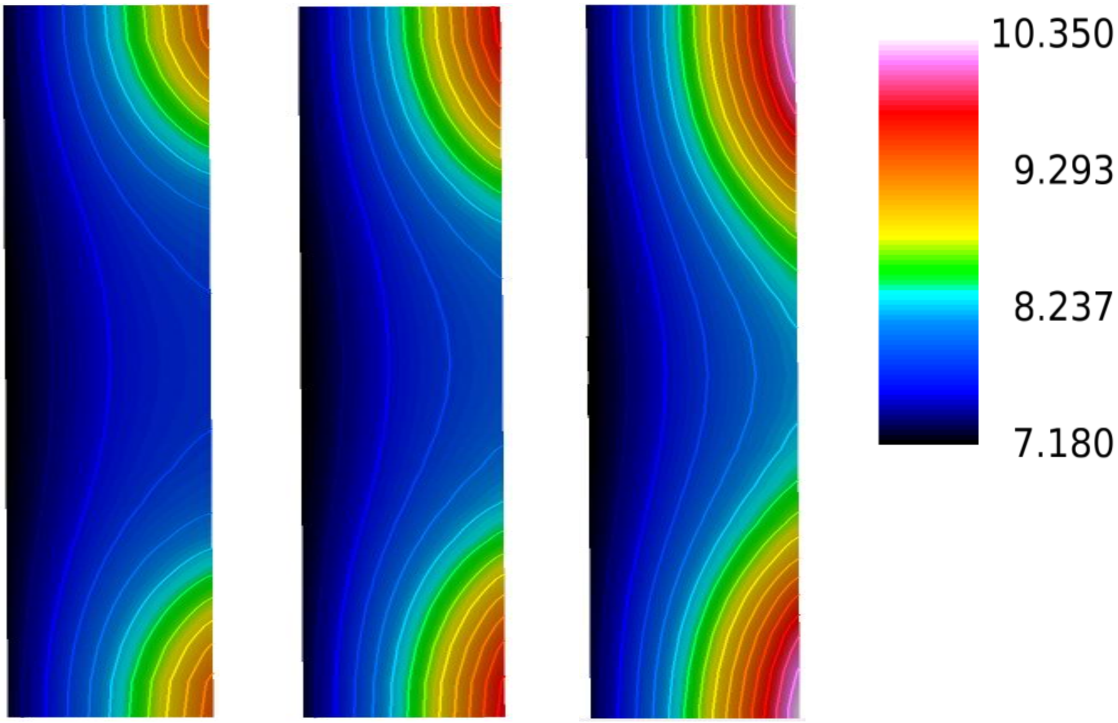

Fig. 5.14. Water content distributions (a) near the inlet region, (b) in the middle of the cell, and (c) near the outlet region for a high humidity (80%) and current densities of 0.1 and 0.2 A/cm^2

The water content profiles obtained by numerical simulation at various current densities agreed well with the experimental measurements. In the case of a high relative humidity (80%), increasing the current density shifted the water content profile because operation at a higher current density causes more water to be generated at the cathode side. The water content through the membrane under the rib is higher than under the channel. This trend in the water content of the membrane becomes more pronounced on increasing the current density. The trend in the water content distribution through the membrane with changing current density is captured well and is similar to the experimental measurements. However, there is a discrepancy in the water content on the anode side of the membrane, because the effect of electroosmotic drag is not obvious. This may be the result of the choice of the approximation for the interfacial boundary conditions.

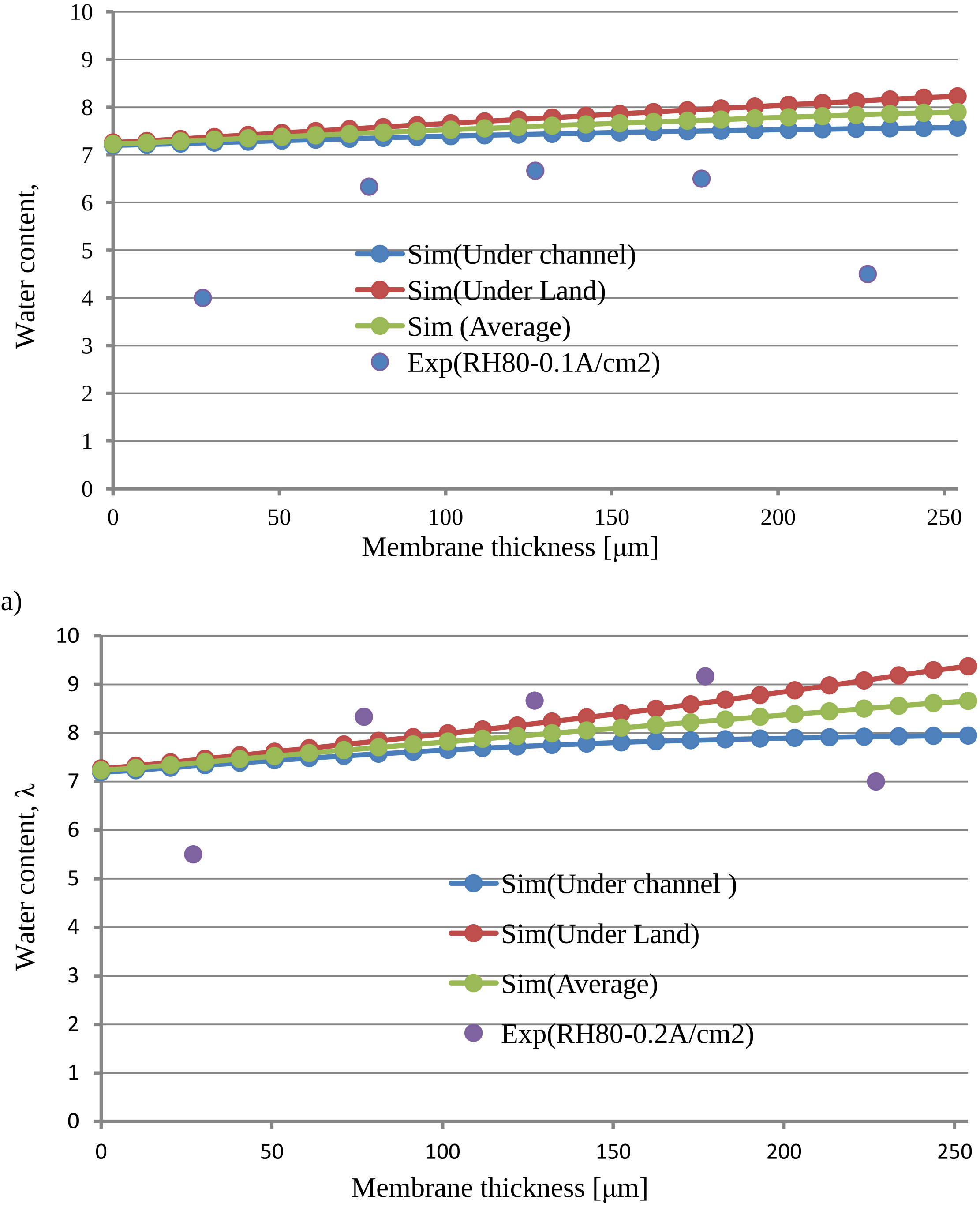

(a)

(b)

Fig. 5.15. Comparison of the experimental (Exp) and simulated (Sim) water content profiles in the membrane for a relative humidity of 80% and current densities of (a) 0.1 A/cm^2 and (b) 0.2 A/cm^2

Therefore, more-accurate approximation is needed especially with regard to the interfacial resistance between the catalyst layer and membrane.

5.6 Conclusions

We have developed a complete three-dimensional isothermal single-phase model that we successfully applied to an actual operating PEM fuel cell. This newly developed computational model has been validated by comparing the results of the simulation with those of the experimental study of Tsushima et al. (2010). The water content profile was accurately predicted by our model, which showed a very good agreement with the experimental measurements at a low relative humidity. The water content profile observed through the membrane under the rib is higher than that under the channel, and this effect is particularly strong at a high humidity. At a low relative humidity (40%), the water content profile in the membrane is flat. The water content in the membrane remained almost unaltered on increasing the operating current density from 0.1 A/cm^2 to 0.2 A/cm^2 at a relative humidity of 40%.

In the case of a high relative humidity (80%), changing the current density was clearly seen to affect the water content profile inside the membrane. The trend in the water content profile through the membrane with changing current density was similar to that observed in the experiment; the water content in the membrane increases with increasing current density. In the case of a high relative humidity, the newly developed model was qualitatively validated by comparing numerical predictions of the water content profile with experimental measurements. However, in the case of a high relative humidity (80%), there was a discrepancy in the water content on the anode side of the membrane, because the influence of electro osmotic drag was not obvious. This may be the result of the choice of approximation of the interfacial boundary conditions. Therefore, a more accurate approximation is needed, especially in relation to modeling the interfacial resistance between the catalyst layer and the membrane.

This short report shows our current water transport model can provide desirable information on water transport phenomena in the membrane of a PEM fuel cell.

References

Dai W., Wang H., Yuan X. Z., Martin J. J., Yang D., Qiao J., Ma J. (2009), A review on water balance in the membrane electrode assembly of proton exchange membrane fuel cells. *Int. J. Hydrogen Energy*, **34** 9461–9478.

Fuller T. F., Newman J. (1993), Water and thermal management in solid-polymer-electrolyte fuel cells. *J. Electrochem. Soc.* **140**, 1218–1225.

Kim S., Mench M. M. (2009), Investigation of temperature-driven water transport in polymer electrolyte fuel cell: Thermo-osmosis in membranes. *J. Membr. Sci.* **328**, 113–120

Meng H., Wang C. Y. (2004b), Electron Transport in PEFCs, *J. Electrochem. Soc.* **151**, A358–A367.

Nguyen T. V., White R. E. (1993), A water and heat management model for proton exchange-membrane fuel cells. *J. Electrochem. Soc.* **140**, 2178–2186.

Okada T., Xie G., Tanabe Y. (1996), Theory of water management at the anode of polymer electrolyte fuel cell membranes, *J. Electroanal. Chem.* **413**, 49–65.

Springer T. E., Wilson M. S., Gottesfeld S. (1993), Modeling and experimental diagnostics in polymer electrolyte fuel cells. *J. Electrochem. Soc.* **140**, (1993) 3513–3526.

Springer T. E., Zawodzinski T. A., Gottesfeld S. (1991), Polymer electrolyte fuel cell model. *J. Electrochem. Soc.* **138**, 2334–2342.

Tsushima S., Ikeda T., Koido T., Hirai S. (2010), Investigation of water in a membrane in an operating PEMFC by environmental MRI. I. Effects of operating conditions. *J. Electrochem. Soc.* **157**, B1814–B1818.

Um S., Wang C. Y. (2004), Three-dimensional analysis of transport and electrochemical reactions in polymer electrolyte fuel cells. *J. Power Sources* **125**, 40–51.

CHAPTER SIX

Summary of Concluding Remarks and Directions for Further Research

To achieve the aim of this thesis, a comprehensive three-dimensional single-phase isothermal model of the PEM fuel cell has been developed and numerical simulations have been carried out to analyze the gas flow behavior in a serpentine channel, to analyze the contribution of cross convection flow to the performance of the fuel cell, and to analyze the mechanism of water transport across the membrane. The various concluding remarks that appear at the ends of each chapter are summarized below and directions for further research are discussed.

6.1 Summary of the concluding remarks

At the beginning of this dissertation, a three-dimensional single-phase isothermal model was used to investigate the gas-flow behavior in the separator channel and the gas diffusion layer of a PEM fuel cell. In the numerical simulation, we investigated the gas flow in the absence of an electrochemical reaction to predict the dependence of cross flow on the shape of the serpentine channel and on the thickness of the porous medium for a wide range of permeabilities and porosities. With the serpentine flow channel, it is found that reactant gases flow through the gas diffusion layer as a result of pressure differences between adjoining channels. It was observed that the pressure gradient through the gas diffusion layer under the channel is lower than that under the rib. The pressure characteristics in the gas channel of a PEM fuel cell have been identified and shown to be controlled mainly by the effects of friction on the fluid flow in the gas channel, by cross flow, and by the bend area of the serpentine channel. Cross flow reduces the pressure gradient in the straight part of the serpentine channel, and the pressure gradient is maximal in the bend areas of the serpentine channel. The rate of cross flow through the gas diffusion layer is comparable to the total inlet flow rate. The rate of cross flow through the gas diffusion layer increases with decreasing gas channel pitch length. Therefore, cross flow through the gas diffusion layer can be enhanced by decreasing the pitch length of the gas channel.

Having achieved an understanding of the behavior of gas flowing in the serpentine channel and porous media, we designed a parallel flow field so that cross flow through the gas diffusion layer and between the two channels was induced; this is described in Chapter

4. In Chapter 4, a three-dimensional, single-phase, isothermal model was developed in which the electrochemical reaction occurring in cell was taken into account. However, to avoid complicated two-phase flow phenomena, the level of hydration in the membrane was taken to be constant. The resulting model was applied to an operating fuel cell to investigate the coupled flow, species transport, and current density distribution. The effect of the gas channel pitch length on the performance was evaluated by using the new model. The results showed that it can capture all the physical phenomena that occur in a fuel cell. The applicability of the model was verified by its ability to simulate accurately such phenomena as the activation overpotential, the ohmic overpotential, and the mass-transport overpotential. The pitch of the gas channel has a marked effect on the performance of the fuel cell, and decreasing the gas channel pitch improves the performance of the cell. When cross flow through the gas diffusion layer and in between two channels is present, the performance of fuel cell improves in the mass-transport region of the polarization curve. Cross flow can enhance oxygen transport through the gas diffusion layer to the catalyst layer. More electrochemical reaction then occurs and, as a result, the performance of the fuel cell is improved.

Finally, in Chapter 5, a complete three-dimensional isothermal single-phase model of the PEM fuel cell is developed that takes into account variations in the state of hydration of the membrane. The developed model is capable of predicting the hydration and dehydration of the membrane at the cathode side and the anode side. This newly developed computational model was validated by comparison with experimental work. Calculated results from the model agreed closely with experimental measurements. The developed model is particularly useful in cases of low relative humidity because it does not take condensation and evaporation into account. Obtaining a steady state profile for the water content in the membrane takes around five hours of computational time, which is almost the same as that required in the experiment. Under conditions of low relative humidity (40%) and a current density of 0.1 or 0.2 A/cm^2, the water content profile in the membrane is flat. We also observed that the water content in the membrane under the rib is higher than that under the channel; this effect is particularly marked for the case of a high relative humidity. The newly developed water-transport model was qualitatively validated by comparing the calculated water content profile with experimental measurements. Trends in the water content profile with current density are well captured and are generally similar to those observed in the experiments. However, there was a discrepancy in the water content profile on the anode side of the membrane because the influence of osmotic drag was not obvious. This might have been the result of the choice of approximation for the interfacial boundary conditions. Therefore, a more accurate approximation with respect to the resistance at the interface between catalyst and membrane is required.

6.2 Directions for further research

We have mainly considered single-phase gas-flow behavior in a separator channel with a porous medium in a PEM fuel cell. In the three-dimensional study of gas-flow behavior through the porous medium, it was assumed that the medium is isotropic. However, the porous media that are used in actual PEM fuel cells are generally made from carbon cloth or carbon fiber paper, which inherently show anisotropic behaviors. As a result, the physical properties of real gas diffusion layers are anisotropic whereas, as a result of simplifications in the modeling and numerical calculations, the gas diffusion layer was treated as isotropic and homogeneous in the present study. Therefore, further research is required in which the real characteristics of anisotropic gas diffusion layers are examined. The three-dimensional single-phase model, which has been implemented and validated, offers opportunities for carrying this research forward.

The cross flow characteristics and its contribution to the performance of PEM cell has been examined in this study. The cross flow have been investigated regarding the oxygen transport and PEM fuel cell performance under special condition of oxygen concentration so that single phase flow was maintained in the cell. However, with high current density operation of PEM fuel cell the liquid water existence is obvious. It is expected that cross flow may also improve the performance of PEM fuel cell by removing the liquid water from the cell which should be investigated under practical operation of PEM fuel cell.

Furthermore, in deriving the model the PEM fuel cell has been considered as isothermal. In the practical situation, the PEM fuel cell is not isothermal. There is a significant temperature gradient inside the catalyst layer that affects condensation and evaporation processes in the catalyst layer and the gas diffusion layer. It will therefore be necessary to incorporate a heat equation into the three-dimensional model. Furthermore, in deriving the model, liquid water saturation at the gas diffusion layer, the channel, and at the interface between the gas diffusion layer and the channel was considered to be negligible.

In the practical situation of a fuel cell, however, water is produced by the electrochemical reaction and, moreover, it can vaporize or condense as the temperature changes. Therefore, to predict the real physics of a PEM fuel cell, a sophisticated model is required that can capture liquid water saturation, phase-change behavior, and the temperature distribution in the cell. Despite these limitations, however, our present developed three-dimensional single-phase model can be used to provide adequate predictions of the performance of a PEM fuel cell stack.

APPENDIX

The details list of parameters used in the simulation is presented in this section.

The parameters lists are described in each chapter. Since, a huge parameters was used in the chapter 5, so therefore, the physical parameters are listed here together with front flow control file name in the table below:

Table A: Physical parameters

Physical name	Control file name	Value
Equivalent weight of membrane	EW	1.1
Volume expansion in the membrane	Vex	1.62
Dry membrane density	Rho_dry_mem	1100
Anode/cathode catalyst layer thickness	A_catalyst_thick/C_catalyst_thick	50μm
Ionic conductivity of the membrane	ion_cond (use -1 for formula)	$\sigma_f = (0.514\lambda - 0.326)$ $\exp\left(1268\left(\frac{1}{303} - \frac{1}{T}\right)\right)$

Water diffusivity in the membrane	- (directly set in the source code)	$D_{wl} = \begin{cases} 3.10\times10^{-7}\lambda\left[-1.0+\exp(0.28\lambda)\right] \\ \exp\left(-\frac{2436}{T}\right) \quad 0\le\lambda<3 \\ 4.17\times10^{-8}\lambda\left[1.0+161.0\exp(-\lambda)\right] \\ \exp\left(-\frac{2436}{T}\right) \quad 3\le\lambda\le16.8 \end{cases}$

Table B: Operating conditions:

Name	Control file name	Value
Pressure	P=101325	1 atm
Temperature	t=343.15	343.15 K
Relative humidity=80% (With 0.8% O_2 and N_2 at the cathode side)	ys=0.7423,0.2577,0,0,0,0,0 (Anode side)	ys=0.7423,0.2577,0,0,0,0,0 (Anode side)
	ys=0.1705,0,0.1,0,0,0.8195,0 (Cathode side)	ys=0.1705,0,0.1,0,0,0.8195,0 (Cathode side)
Relative humidity=40% (With 0.8% O_2 and N_2 at the cathode side)	ys = 0.5538,0.4462,0,0,0,0,0 (Anode side)	ys = 0.5538,0.4462,0,0,0,0,0 (Anode side)
	ys= 0.0813,0,0.0095,0,0,0.9092,0 (Cathode side)	ys= 0.0813,0,0.0095,0,0,0.9092,0 (Cathode side)

Note: In order to start the calculation of water content profile (λ) in the membrane, it is necessary to set some value of λ initially. One can set the value of λ in the control file. For example, aks=0, 1

The meaning of aks is either saturation value or water content or both. Here first digit '0' means there is no saturation initially and '1' means the initial value of λ is 1.